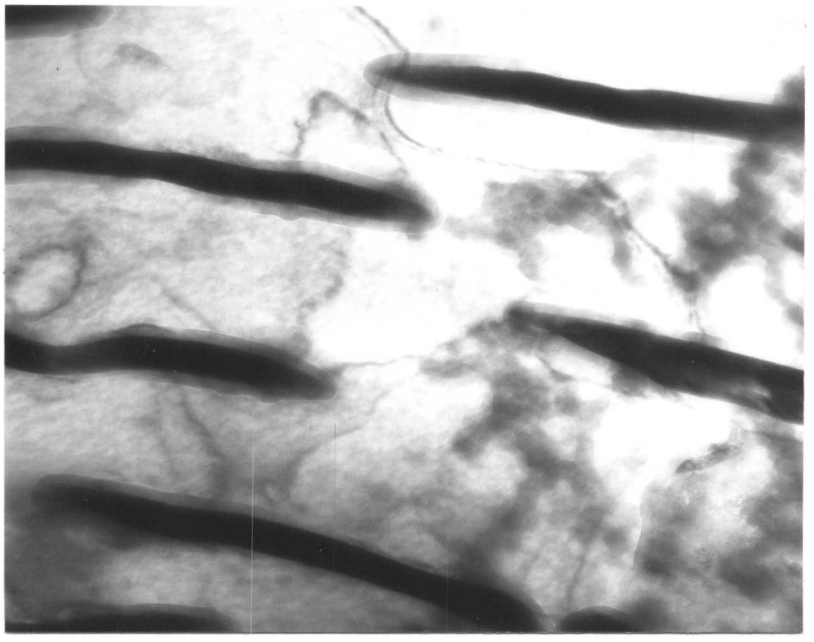

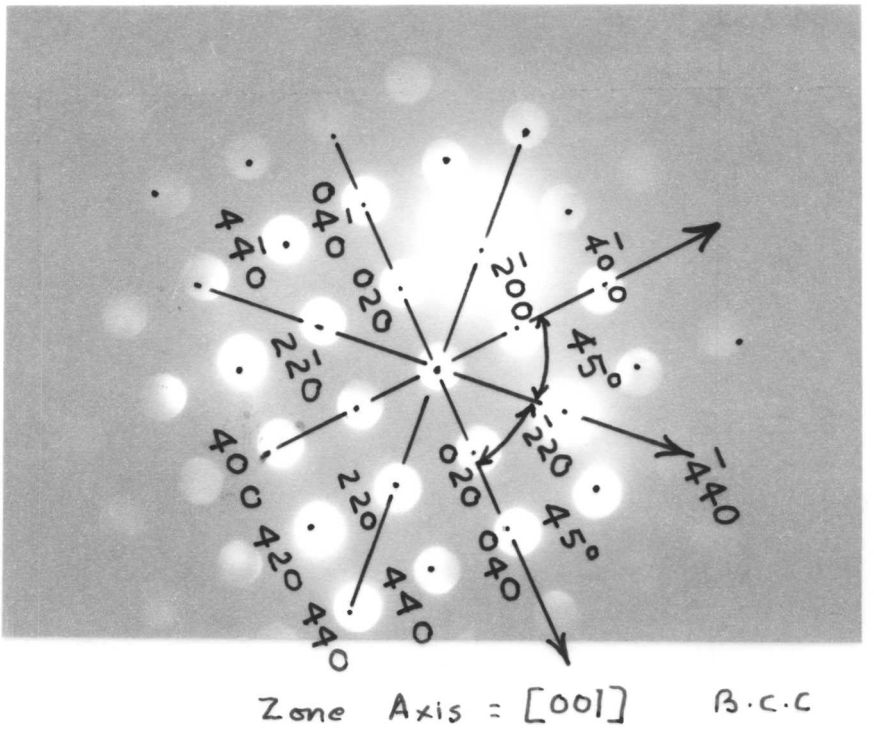

Figure 5.7(a): Transmission electron micrograph showing rod-shaped morphology of the tungsten carbide.

(b) Convergent beam diffraction pattern.

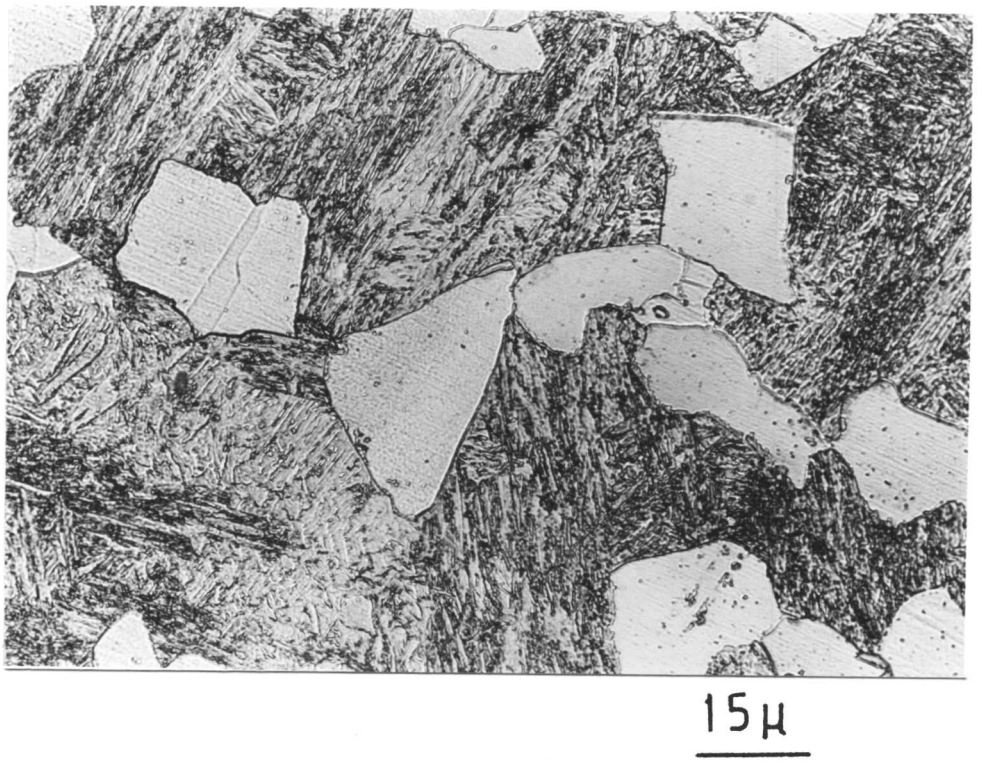

Figure 5.9a: Microstructure developed within 2.5 minutes at 850°C in Fe-5W-0.23C (wt%).

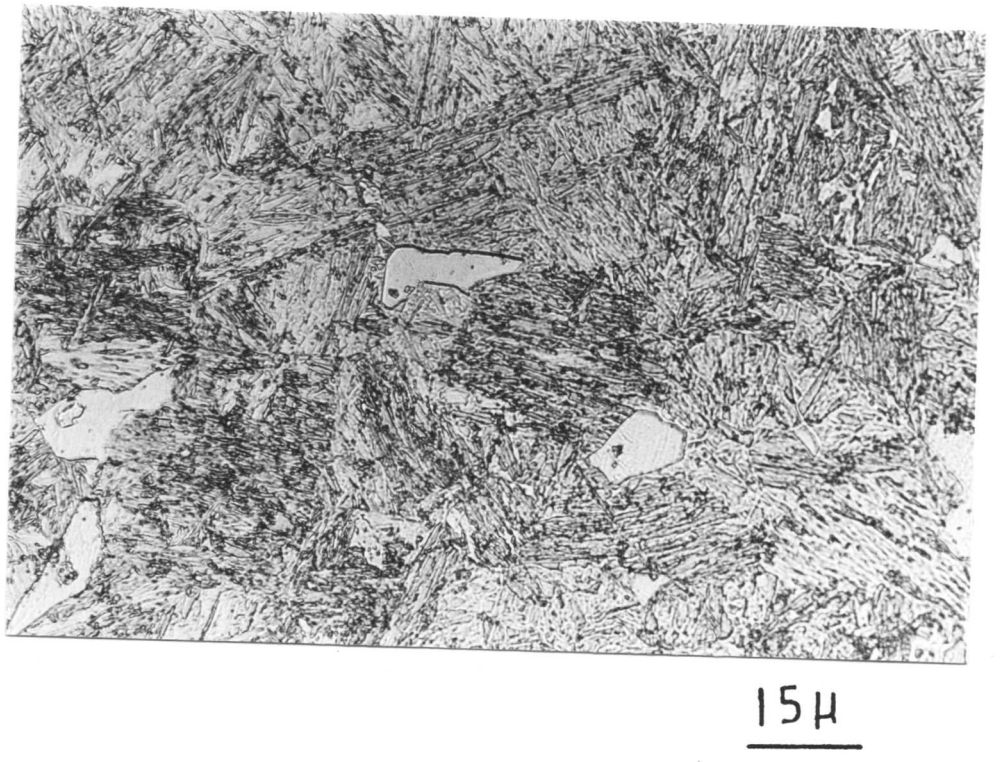

Figure 5.10a: Microstructure developed after same heat treatment as above in Fe-5.9W-0.14Ti-0.21C (wt%) alloy.

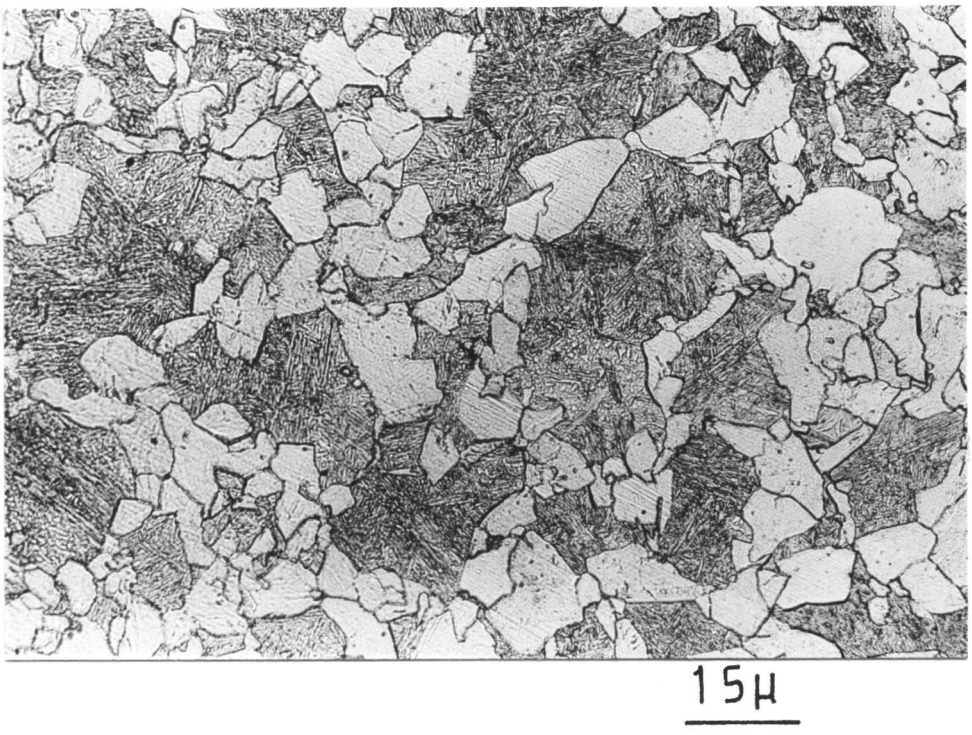

Figure 5.9b: Microstructure developed at 750°C within 5 minutes in Fe-W-C alloy.

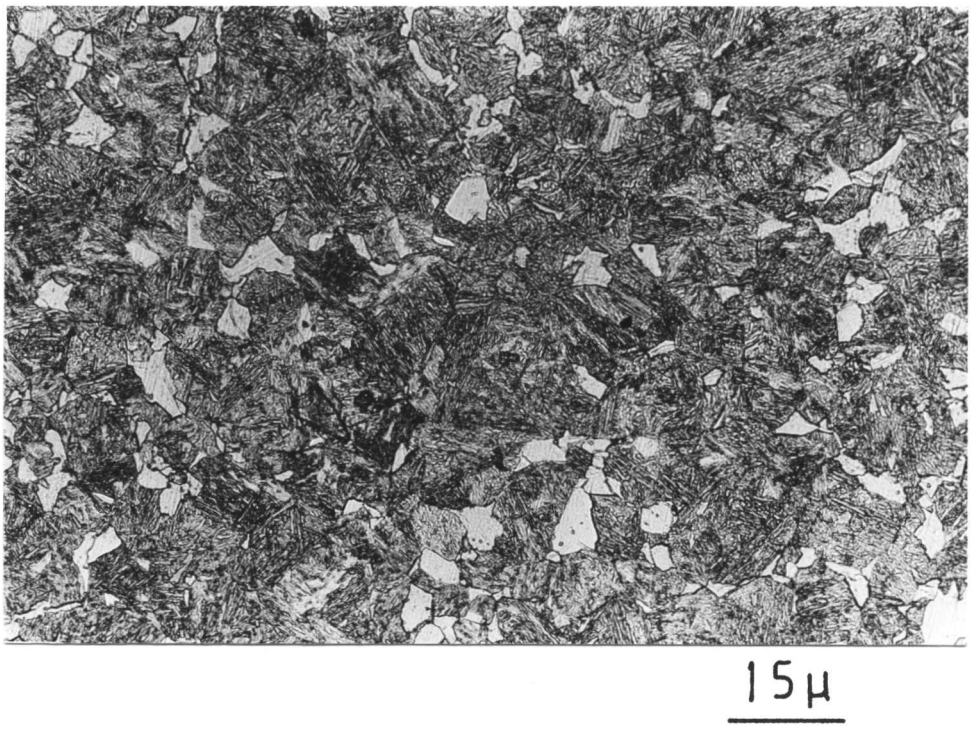

Figure 5.10b: Microstructure developed after the same heat-treatment in Fe-W-Ti-C alloy.

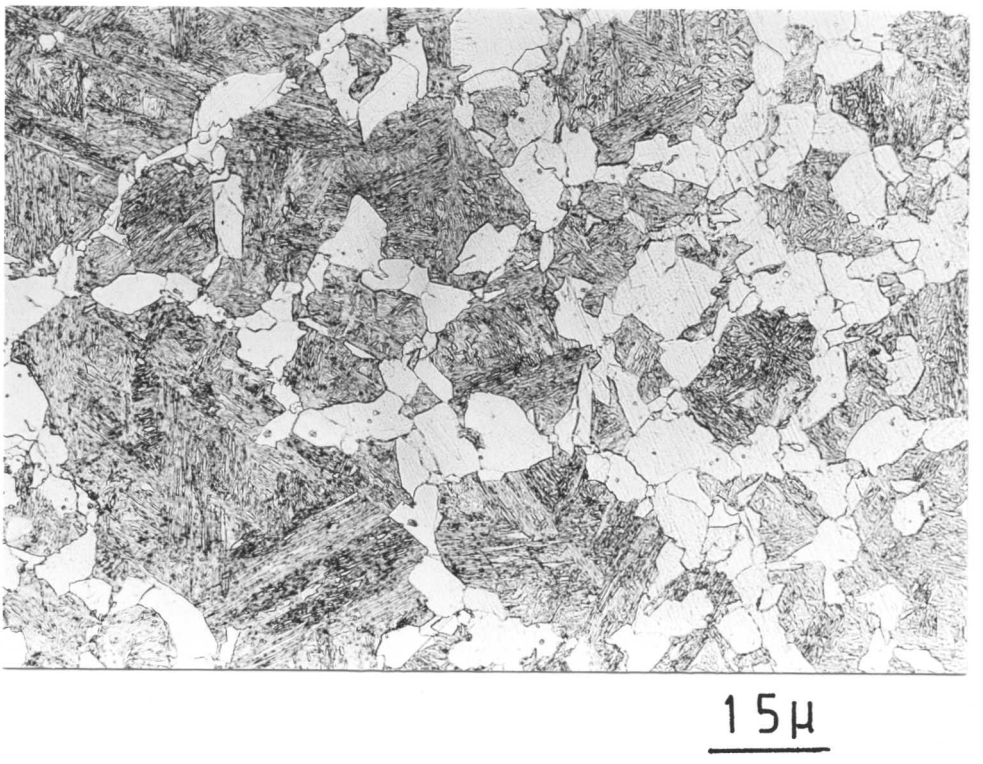

Figure 5.9c: Microstructure obtained at 700°C/10 Min in Fe-W-C alloy.

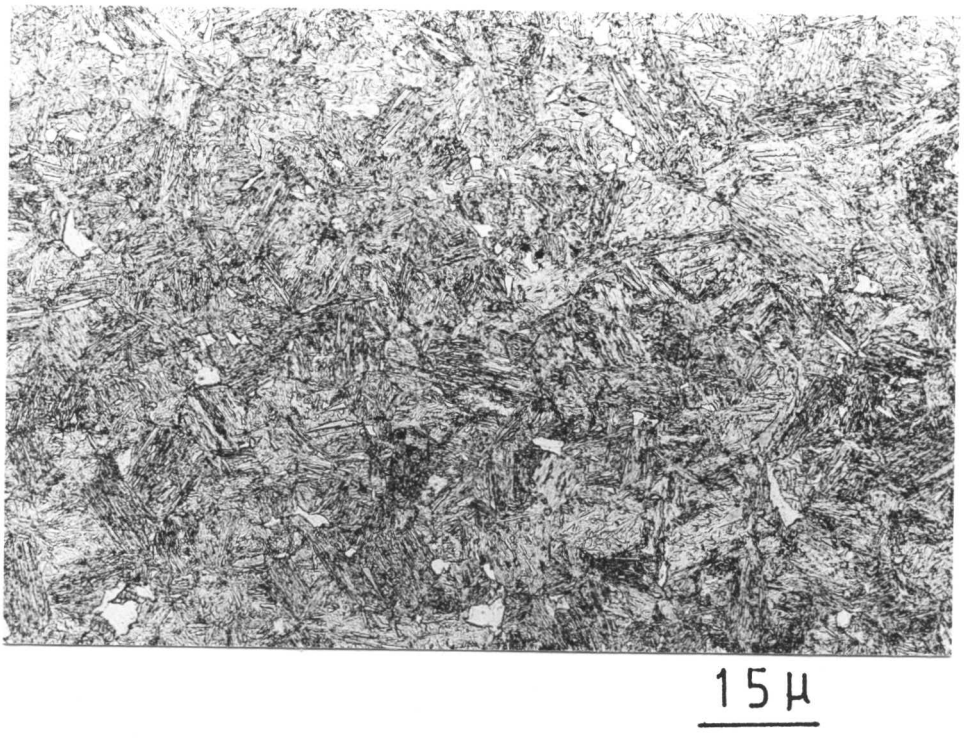

Figure 5.10c: Microstructure developed after same heat-treatment as Fe-W-Ti-C alloy.

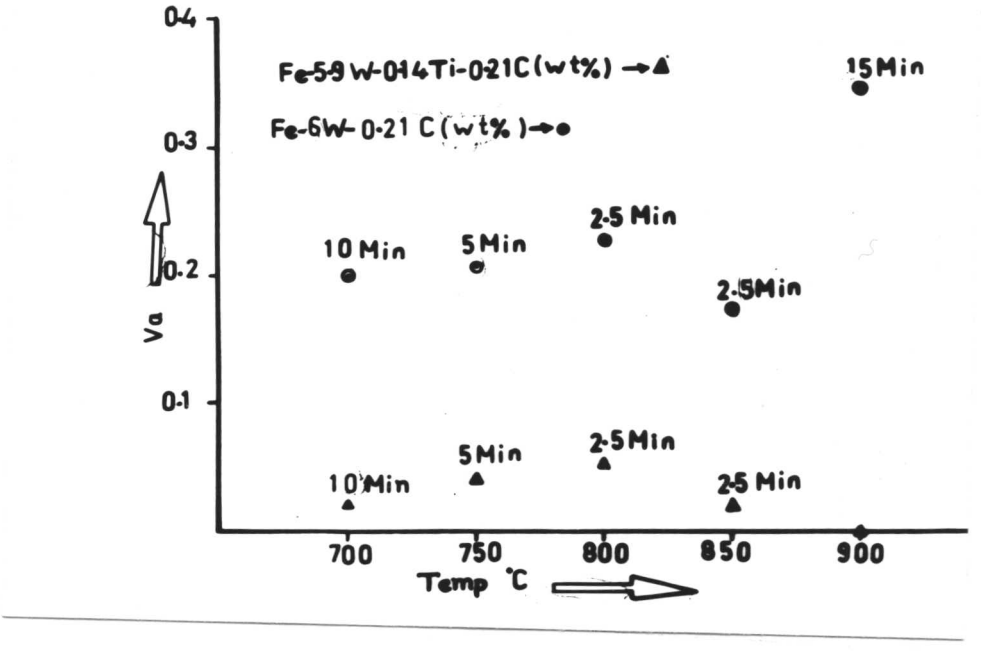

Figure 5.11: Quantitative measurement of volume fraction (Vα) at different isothermal temperature in alloy with and without titanium. It clearly shows that titanium is effective in retarding the $\gamma \rightarrow \alpha$ transformation.

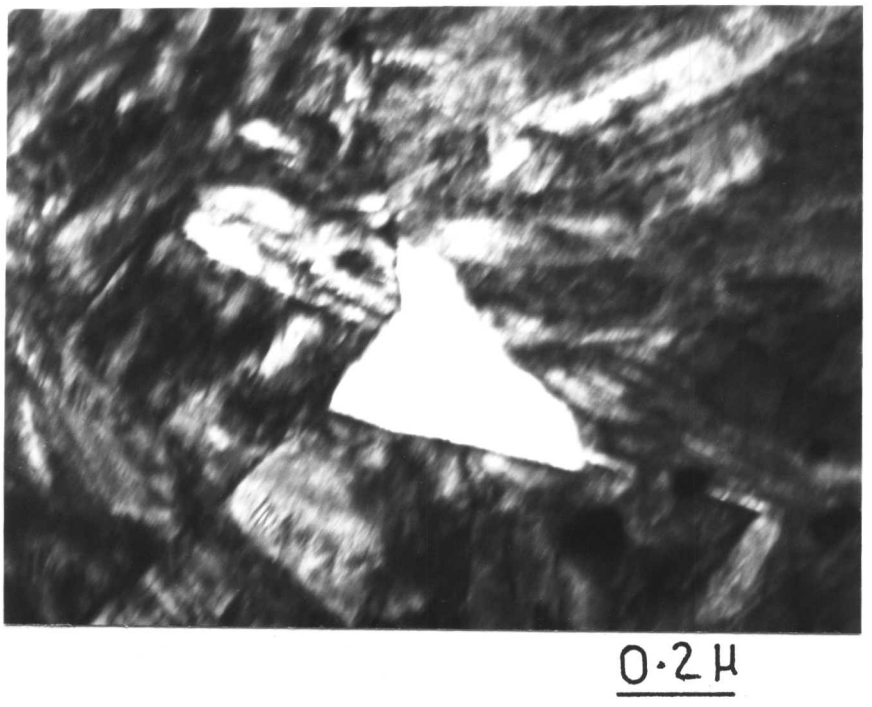

Figure 5.12: Transmission electron microscope showing carbide free ferrite formed during early stages of transformation.

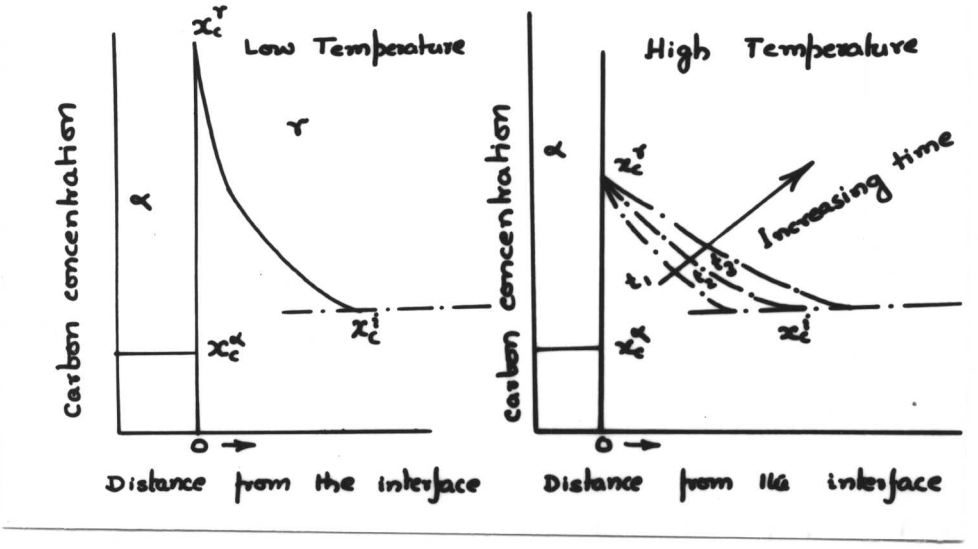

Figure 5.13: Schematic diagram showing carbon concentration profile near the moving interface under two different circumstances.

CHAPTER VI

The $\gamma \rightarrow \alpha$ transformation in Fe-5W-2.3Si-0.15C (wt%) alloy.

6.1 Introduction: To achieve the best combination of strength and toughness in alloy steels, an alternate approach of direct transformation is gaining importance. Small additions of strong carbide forming elements such as Nb, V, Ti etc, have been shown to increase the strength and toughness of low carbon low alloy steels at room temperature by forming a fine dispersion of carbides through the process of interphase precipitation as well as by grain refinement[1,2,3]. Detailed structural studies have revealed that these carbides are nucleated at the semicoherent γ/α interface and appear as bands representing successive stages of the transformation front[4]. The size and spacing of the carbide precipitation depend on the isothermal transformation temperature, the alloy composition, the volume fraction of carbide and the rate at which the decomposition of austenite takes place[5]. In addition to interphase precipitation, there is another kind of carbide morphology which forms at relatively lower temperatures. This carbide appears as fibres[6]. These fibrous carbides nucleate on the incoherent γ/α interface and grow normal to the interphase-boundary as fine fibers often only 500Å diameter. These two types of carbide morphology are competitive, often occurring together in the same specimen and even in the same original austenite grain. However, variation in heat-treatment or alloy composition can markedly alter the proportion of two morphologies observed. At sufficiently high undercooling these two modes of carbide precipitation are superseded by formation of supersaturated ferrite. The carbides are precipitated on dislocations by aging process from these supersaturated ferrites. Dislocations are generated during the transformation and act as a preferential nucleation sites. The pioneering work by Honeycombe and his students[7-16] led to important advances in our understanding of these microstructures which develop during the $\gamma \rightarrow \alpha$ transformation. They presented convincing evidence to elucidate the various mechanisms of carbide precipitation by performing extensive series of well conceived experiments.

The present investigation aimed to characterize and if possible, elucidate the transformation behaviour of Fe-5W-2.3Si-0.15C (wt%) alloy in the temperature range 850°C to 700°C. This alloy is similar in composition to that used in chaper V except that it contains Si and slightly less amount of carbon. This particular composition was selected to examine the effect of silicon on the transformation characteristics. To our surprise, the microstructure in this particular alloy is quite different from that obtained at

in Fe-5W-0.23C (wt%) alloy. This change in microstructure is attributed to the presence of silicon.

6.2 Experimental Results:

6.2.1 Isothermal Transformation at 700°C: The $\gamma \rightarrow \alpha$ transformation at this temperature was much faster than in the similar alloy without Si . Isothermal transformation at 700°C for 5 minutes showed approximately 15 vol.% transformation. The $\gamma \rightarrow \alpha$ transformation started predominatly at austenite grain-boundaries to form grain-boundary allotriomorphs (Figure 6.1a). The rate of thickening appeared low compared with that of lengthening, leading to high aspect ratio for those allotriomorphs. In the majority of cases, the interface appeared planar and facetted. Occasionally interface pinning was noticed (Figure 6.1b). Fine carbides were also detected within the austenite grain.

Many interesting features appeared when the time of transformation was increased to 10 minutes at 700°C. The $\gamma \rightarrow \alpha$ transformation achieved its equilibrium value within 10 minutes whereas the alloy without Si showed only 10 vol.% transformation. Grain-boundary allotriomorphs developed rapidly to form equiaxed ferrite. A fine dispersion of alloy carbides (tungsten carbide, M_6C/W_2C) was noticed within these ferrite grains in contrast to those formed in Fe-W-C alloy. More interesting is that these carbides were enveloped by a precipitate free zone (PFZ) (Figure 6.2a). The width of the PFZ appeared constant (6 to 8μm) in the majority of cases, although sectioning effects are not taken into account. However, no PFZ was observed near the α/α interface (Figure 6.2a arrowed). A dark grey rim appeared along the γ/α interface which grew in the austenite. The thickness of the rim was not uniform, indicating that the rate of growth varied even within the same grain. The interface of this growing grey rim occasionally showed the presence of ledges (Figure 6.2c). The interface of the growing rim showed evidence of pinning (Figure 6.2b).

With further increase in time to 40 minutes at 700°C, the fine dispersion of carbides within the ferrite grew in size and became more apparent using optical microscopy (Figure 6.3a). These carbides appeared to be of the Widmanstätten type (Figure 6.3b). The width of PFZ remained almost constant. The dark grey rim grew in thickness (Figure 6.3c,).

With further increase in time to 80 minutes at 700°C, the dark grey region grew in thickness and finally consumed the whole austenite grain (Figure 6.4a). However, in some cases, a dark etched region appeared ahead of this growing rim during the latter stage. No such microstructural features were observed in Fe-5W-0.23C (wt%) alloy.

Electron microscopy was employed to get microstructural details of this growing rim. The rim was found to contain dense distribution of carbides in different morphologies. Most of these carbides are very fine but some of them are relatively coarse and elongated (Fig. 6.5a). In certain areas it was observed that these carbides are arranged in rows (Fig. 6.5b). Probably these rims have formed by a discontinuous reaction. With increasing time of transformation, the coarse carbides grew rapidly in dimension - whereas the fine carbides appeared to resist growth (Fig. 6.5a and b). After long ageing treatments (i.e. at 700°C for 40 to 80 minutes), the resulting microstructure show two interfaces at some places. The primary interface of the discontinuous reaction was followed by a secondary discontinuous reaction (Fig. 6.5c). The second discontinuous coarsening reaction appeared to have the same two phase, but during this step carbide dispersion is much finer. The region containing finer dispersion of carbides was bounded on one side by previously existing grain-boundary (Fig. 6.5c). The carbides formed from supersaturated ferrite are shown in (Fig. 6.5d). Non-uniform distribution of carbides is apparent in this micrograph. Widmanstätten type of carbides were also observed in certain areas of ferrite (Fig. 6.5e).

6.2.2 Isothermal Transformation at 800°C was much faster as expected. Within 1.5 minutes about 50 volume % transformation occurred. The incubation period appeared to be minimum at this temperature. Grain boundary allotriomorphs formed at this temperature showed a tendency towards facetting. (Fig. 6.6a). Frequent evidence of ledges was also recorded. The height of the ledge appeared to vary even at the same interface. Close optical microscopy observations indicated the presence of carbides at the γ/α interface.

Fine carbides were also noticed within the austenite as well as inside the ferrite. At high magnification, fibrous carbides were noticed (Figure 6.6b-c). These fibrous carbides appeared to grow in association with low energy facets which have moved by a ledge mechanism.

6.2.3 Clear evidence of interphase precipitation was obtained when the specimen was transformed at 850°C (Figure 6.7a). The band spacing varied even within the same grain. Occasionally, fibrous carbides were observed (Figure 6.7b). Random or irregular dispersions of alloy carbides were also noticed frequently along with banded dispersions.

SEM taken from these specimens are shown in (Fig 6.8a-h). Figure 6.8a-d show sheets of precipitates. It suggests that the precipitation has occurred on a semi-coherent interface which moves by a ledge mechanism. However, in certain areas the precipitates are not arranged perfectly in rows (Fig. 6.8e-h).

Probably these carbides have formed on an incoherent interface. It is also apparent from these micrographs that the band spacing is not uniform. The variation in band spacing is about an order of magnitude.

TEM studies were done to examine the γ/α interface responsible for banded dispersion of carbides. Fig. 6.9 shows that the ledge mechanism operating during formation of banded carbide dispersion. The variable band spacing is shown in Fig. 6.9.

6.2.4 Step Quenching.

Step quenching was tried in order to ascertain the effect of transformation temperature on the transformation product. The specimen was first held at 700°C for 20 minutes followed by upquenching at 800°C for 3.5 minutes. Figure 6.10 shows that one side of the interface contains a dark etched region while the fine dispersion of alloy carbide was noticed on the other side of the interface. The dark etched region consisted of a fine dispersion of carbides rather than fibrous carbides.

6.3 Discussion: At all temperatures, the reaction was much faster compared to Fe-5W-0.23C (wt%) alloy.

The $\gamma \rightarrow \alpha$ transformation started predominantly at austenite grain-boundaries to form allotriomorphs. The aspect ratio of these allotriomorphs was high at 700°C. It indicates that the rate of thickening is very slow compared to lengthening at this temperature. The interface appeared planar in the majority of cases. Planar interfaces are taken as evidence of low energy facets on a macroscopic scale. Evidence of ledges implies that the ledge mechanism plays a dominant role in determining the transformation kinetics over a wide range of temperatures. The high proportion of planar interfaces observed over a wide range of temperature, implies that partial coherency can exist at the majority of interface orientations and that a truly incoherent structure is rare[17].

It was also observed that interfaces were pinned by carbides. The pinning occurred mainly due to the carbides already present in the austenite. The protuberances were developed as the interface moved across the carbide particles already present in austenite.

At high transformation temperatures (850°C), the carbide precipitation occurred predominantly by an interphase mechanism. In contrast, complete absence of carbide precipitation by an interphase mechanism was observed in Fe-5W-0.23C alloy (Chapter V) at this temperature. It is believed that the presence of silicon causes a significant drop in solid-solubility of carbides in ferrite. Consequently these carbides are precipitated during the $\gamma \rightarrow \alpha$ transformation

by a ledge mechanism and the resultant carbides are generally aligned (Fig. 6.7 to 6.9). Two distinct modes of carbide precipitation were noticed at 700°C. A fine dispersion of carbides was noticed within each ferrite grain. These carbides have formed from supersaturated ferrite by an ageing process. However, there was another kind of precipitation phenomenon noticed at this temperature. A grey rim appeared to form along the γ/α interface. The formation of rim is analogous to that of the discontinuous precipitation.

In discontinuous precipitation the heterogeneous nucleation of grain-boundary precipitates takes place with concurrent boundary migration. The reaction product is a two-phase lamellar cell which consumes the supersaturated matrix. The reaction is discontinuous in so far as there are discrete changes in crystallographic orientation and chemical composition at the advancing reaction front. The discontinous precipitation reaction is expressed as:

$$\gamma \rightarrow \gamma^1 + \beta$$

where the depleted matrix γ^1 phase has the same structure as the initial supersaturated solid solution γ, differing from it only in composition. The precipitating phase β can be an intermetallic phase[18], a solid solution of another lattice structure[19] or a solid solution of the same lattice structure[20].

The initiation of the discontinuous reaction has been the subject of many investigations and there are two proposed mechanisms for the initial migration of boundaries leading to discontinuous precipitation.Tu and Turnbull[21] have proposed the so called pucker mechanism in which facetted nuclei of the precipitating phase form at the grain-boundary with a low energy interface with one of the grains. The system then reduces its energy by a puckering of the grain bounday. The boundary then migrates to regain its minimum length and also leaves both sides of the precipitate with a low energy relationship with the one grain. It is believed that during migration further precipitation occurs because of favourable orientation of the boundary. Hence the process is self sustaining. The pucker mechanism has been unequivocally demonstrated to operate in many discontinuous reaction.

Fournelle and Clark[22] on the other hand suggested that boundary migration occurs due to its curvature in the direction required for grain growth. Allotriomorphs on grain-boundary act as a pinning centres and lead to cell formation. The process is not auto-catalytic in any respect and is self-sustaining almost immediately, due to the establishment of a chemical free energy difference across the advancing interface. Precipitate/matrix orientation habit plane is of little importance in this mechanism. This

mechanism was first established in Cu-In[22].

Optical metallographic observations followed by TEM showed that the rim nucleated along the γ/α interface. As the ageing continues, the precipitation reaction proceeds through the formation of duplex cells containing α matrix and the carbides. During the growth of cells, the multiplication of the cells occurs mainly by the nucleation of new lamellae at the cell boundary (Fig. 6.5a), the progressive development of the microstructure for different periods of time at 700°C is displayed in Figs. 6.1 to 6.4. After a long ageing time, two interfaces in the discontinuous cells were observed. Such two step coarsening of the discontinuous product in the duplex cell has been frequently reported in the past. A recent observation is due to Fournelle[23] in Fe-10%Ni-6% Ti wt% alloy.

Definite conclusions regarding the mechanism of nucleation of the discontinuous cells in this alloy are not possible. However, it is anticipated that the mechanism of nucleation suggested by Fournelle and Clark is operative in this alloy. This is further supported by the fact that the carbides observed at the γ/α interface are non-facetted rather than facetted as required in Tu and Turnbull's model.

Precipitate free zones (PFZ) surrounding the ferrite grains were observed at 700°C width of the PFZ remained constant during the latter period of transformation. Precipitate free zones are often observed adjacent to grain-boundaries in age hardening alloys. Originally these zones were attributed to localized depletion of solute because of preferential precipitation at the grain-boundaries[24]. Depletion of vacancies during the nucleation of matrix precipitate might control the formation of PFZ[25,26]. Microanalysis results have confirmed that the PFZ in this particular alloy have developed due to solute depletion rather than depletion of vacancies. This solute depletion is believed to occur by partioning of carbon and alloying element (i.e. C, W and Si) to the growing rim.

6.4 Conclusions:

1. At high transformation temperatures (850°C), banded carbide dispersions appeared. The band spacing was not uniform. This reflects the tendency towards variable ledge height responsible for such dispersion.
2. Random dispersions of alloy carbides were also noticed along with the banded structure.
3. In the majority of cases, the interface appeared planar.
4. At lower transformation temperatures (700°C) the mechanism of interphase precipitation was completely suppressed. A random dispersion alloy carbides formed from supersaturated ferrite during the later stages of transformation

and not by a ledge mechanism.

5. PFZ's surrounding ferrite grains were also noticed. Formation of PFZ's was attributed to localized depletion of solute because of preferential precipitation at the grain-boundaries.

6. Dark grey rims appeared to form at the γ/α interfaces but grew in the austenite. Finally all the austenite grains were replaced by these grey constituents. It is believed that these grey rims are formed by a discontinuous precipitation reaction.

7. The presence of silicon in the alloy accelerated the $\gamma \rightarrow \alpha$ transformation. It also enhanced the tendency towards developing banded structures at the highest transformation temperatures, possibly by decreasing the solid solubility of alloy carbide in austenite at that temperature. However, its precise role in inducing the discontinuous reaction at lower temperatures is not well understood.

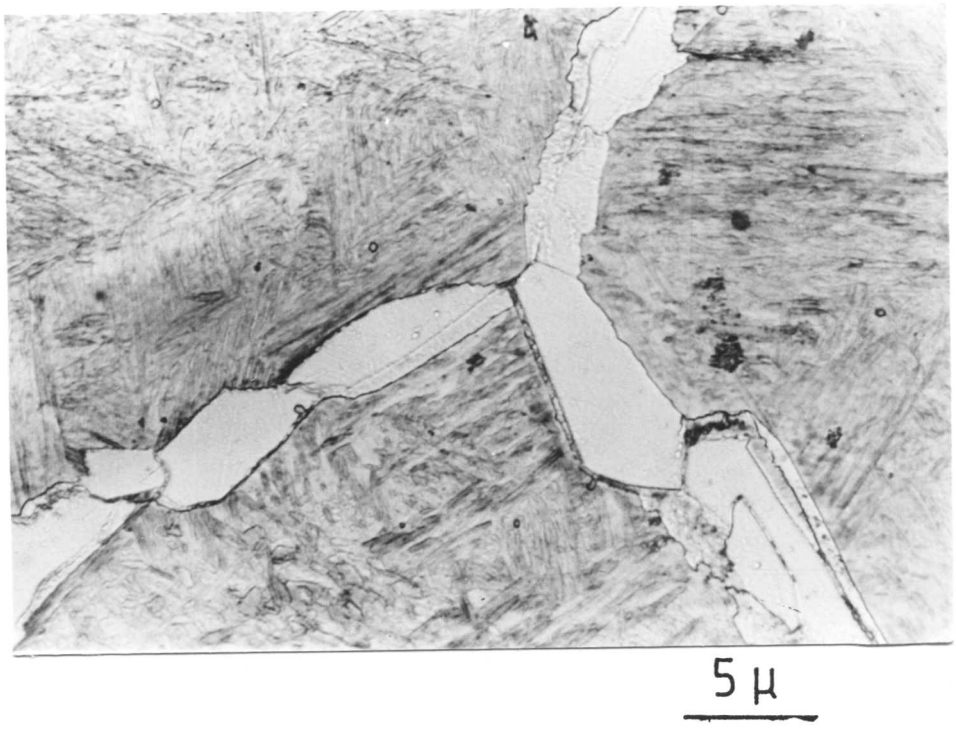

Figure 6.1a - Showing grain-boundary allotriomorphs.
(Isothermal transformation at 700°C for 5 minutes.)

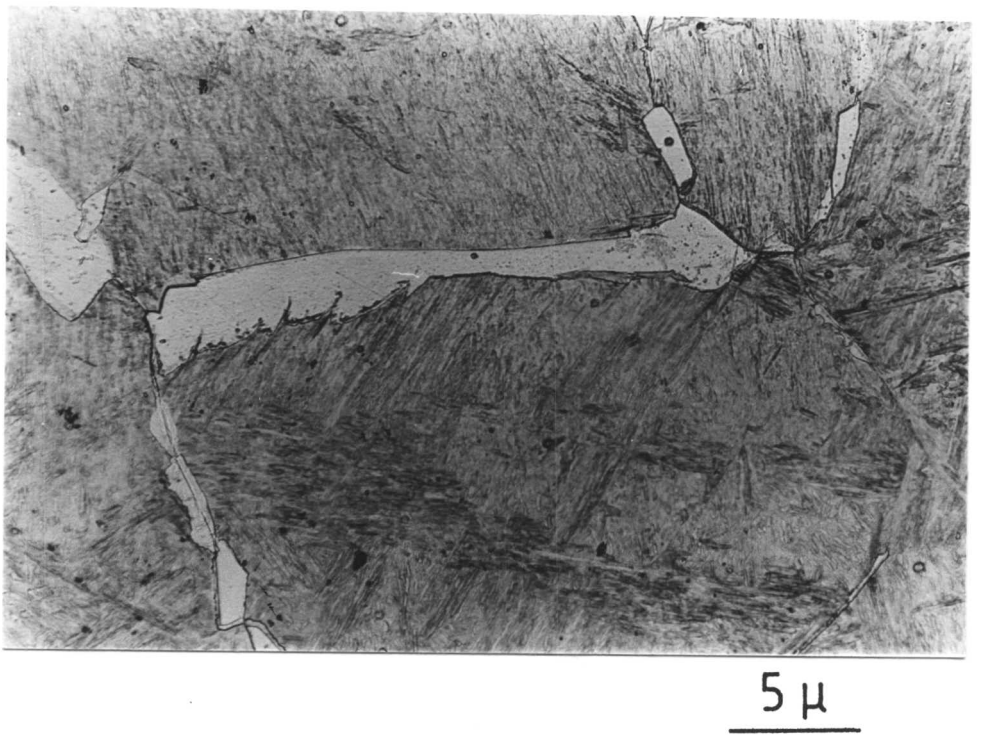

Figure 6.1b - Showing evidence of interface pinning by tungsten carbide. (Isothermal transformation at 700°C for 5 minutes.)

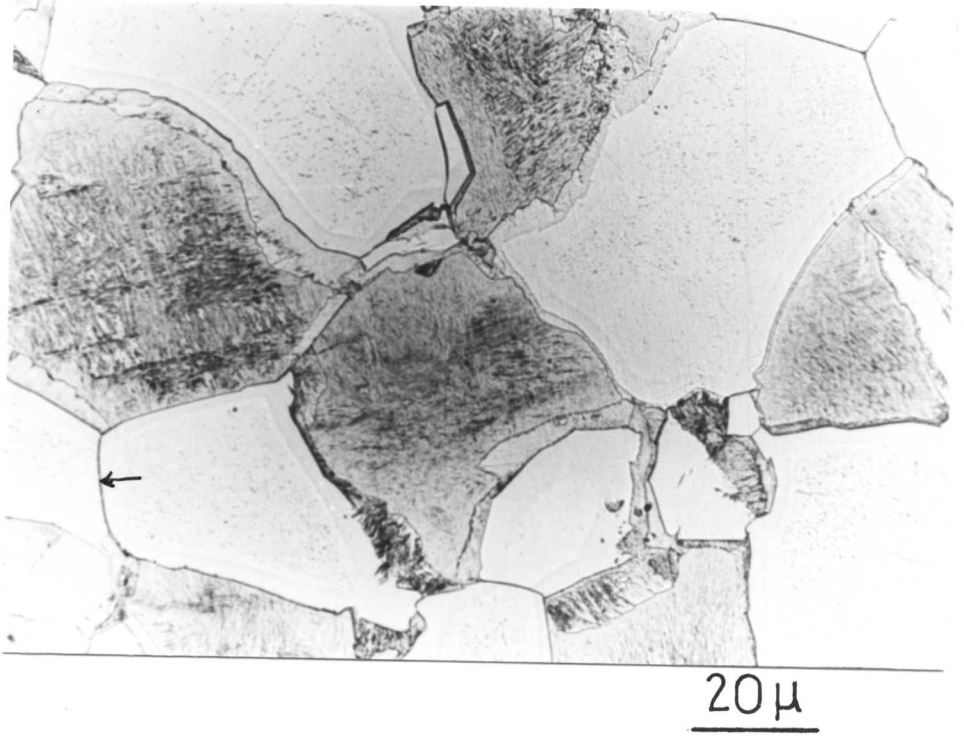

Figure 6.2a - Showing fine dispersion of carbides within the ferrite, surrounded by PFZ. A dark grey rim appeared to grow inside the austenite from the γ/α interface. (Isothermal transformation at 700°C for 10 minutes.)

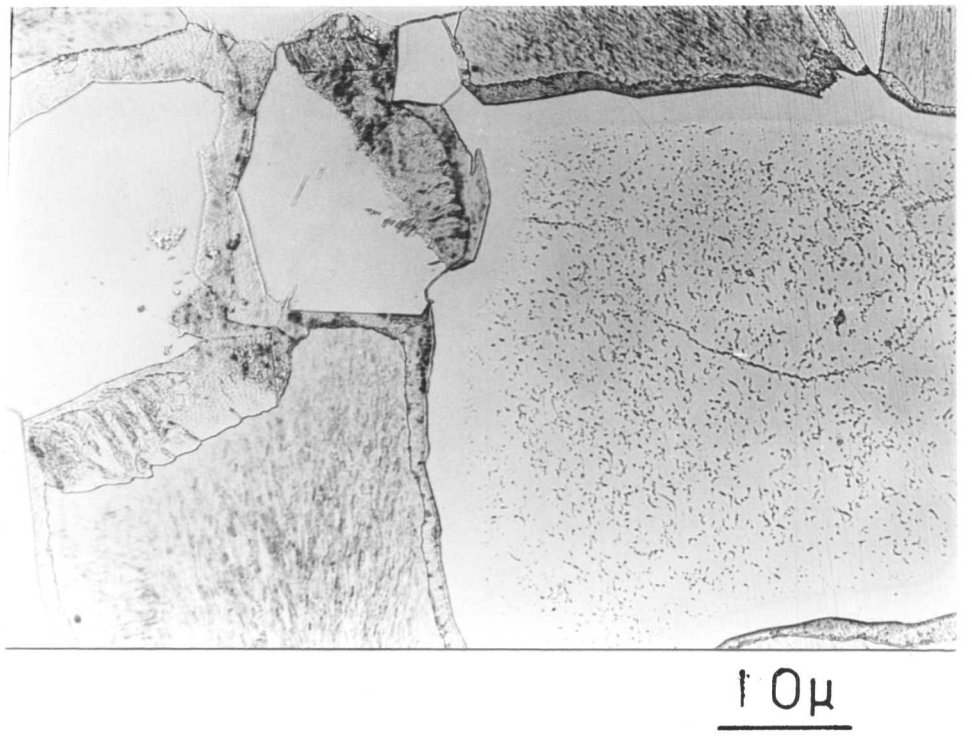

Figure 6.2b - Showing evidence of pinning at the interface of growing rim. (Isothermal transformation at 700°C for 10 minutes.)

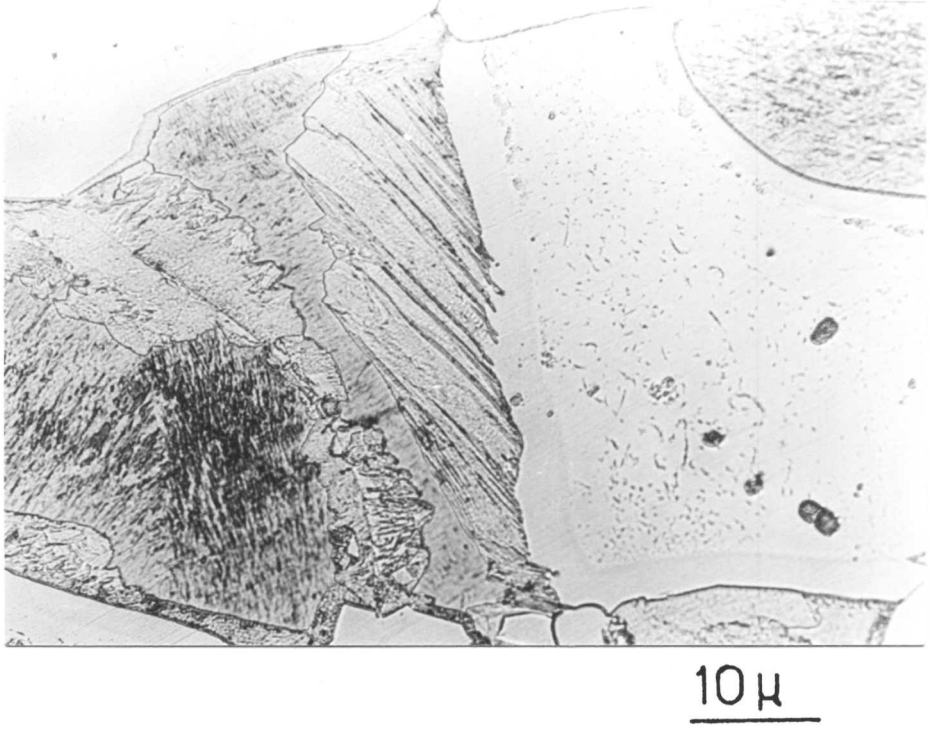

Figure 6.2c - Showing presence of ledges ahead of the growing dark grey rim. (Isothermal transformation at 700°C for 10 minutes.)

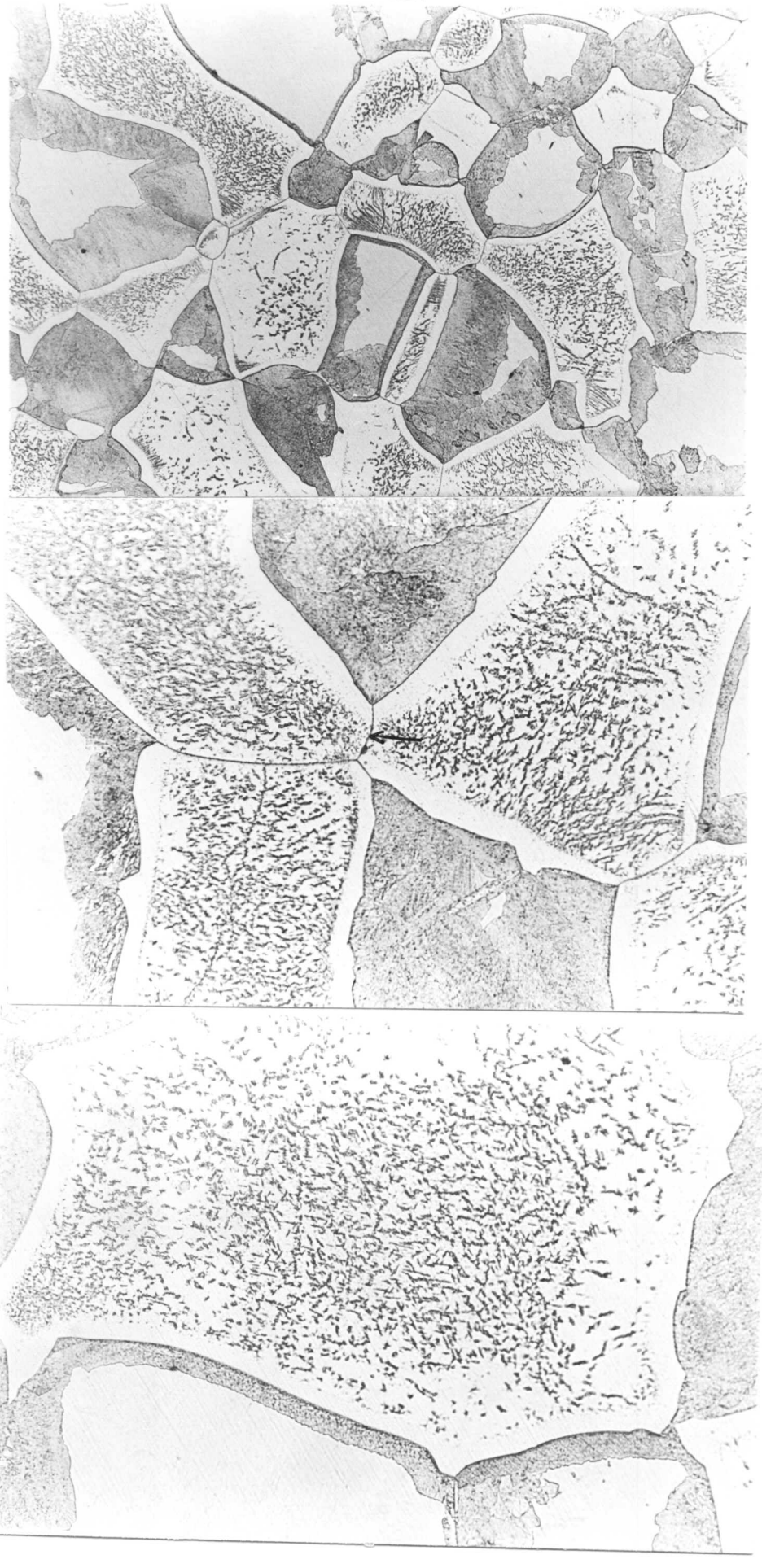

Figures 6.3a,b,c - Showing fine dispersions of carbide within the ferrite grain. The rim also grew in thickness with increasing time. (Isothermal transformation at 700°C for 40 minutes.)

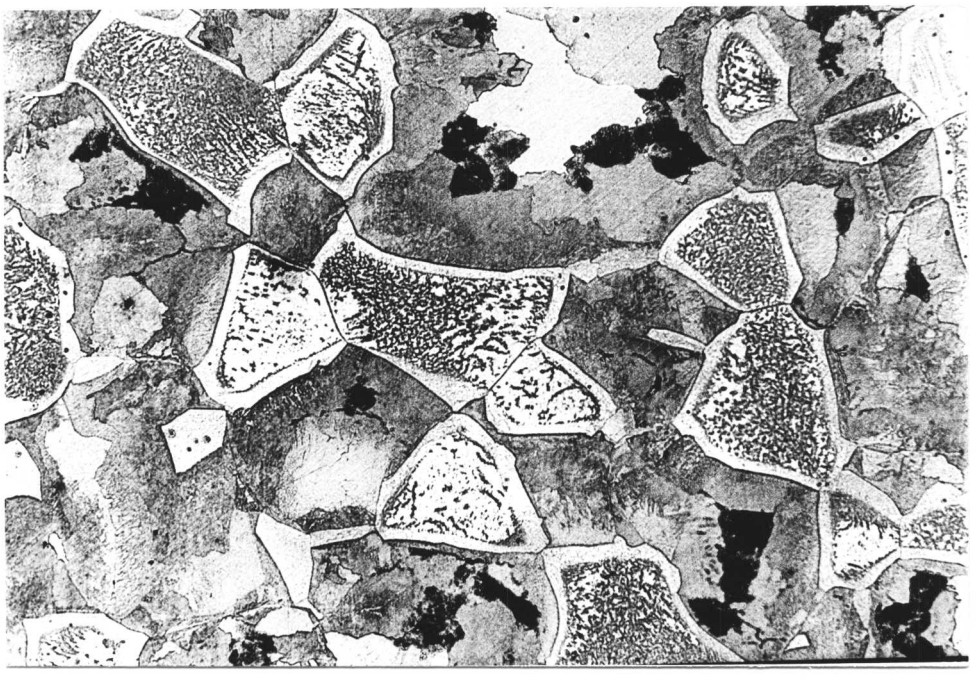

Figure 6.4 - Isothermal transformation at 700°C for 80 minutes. The dark grey rim grew further in size.

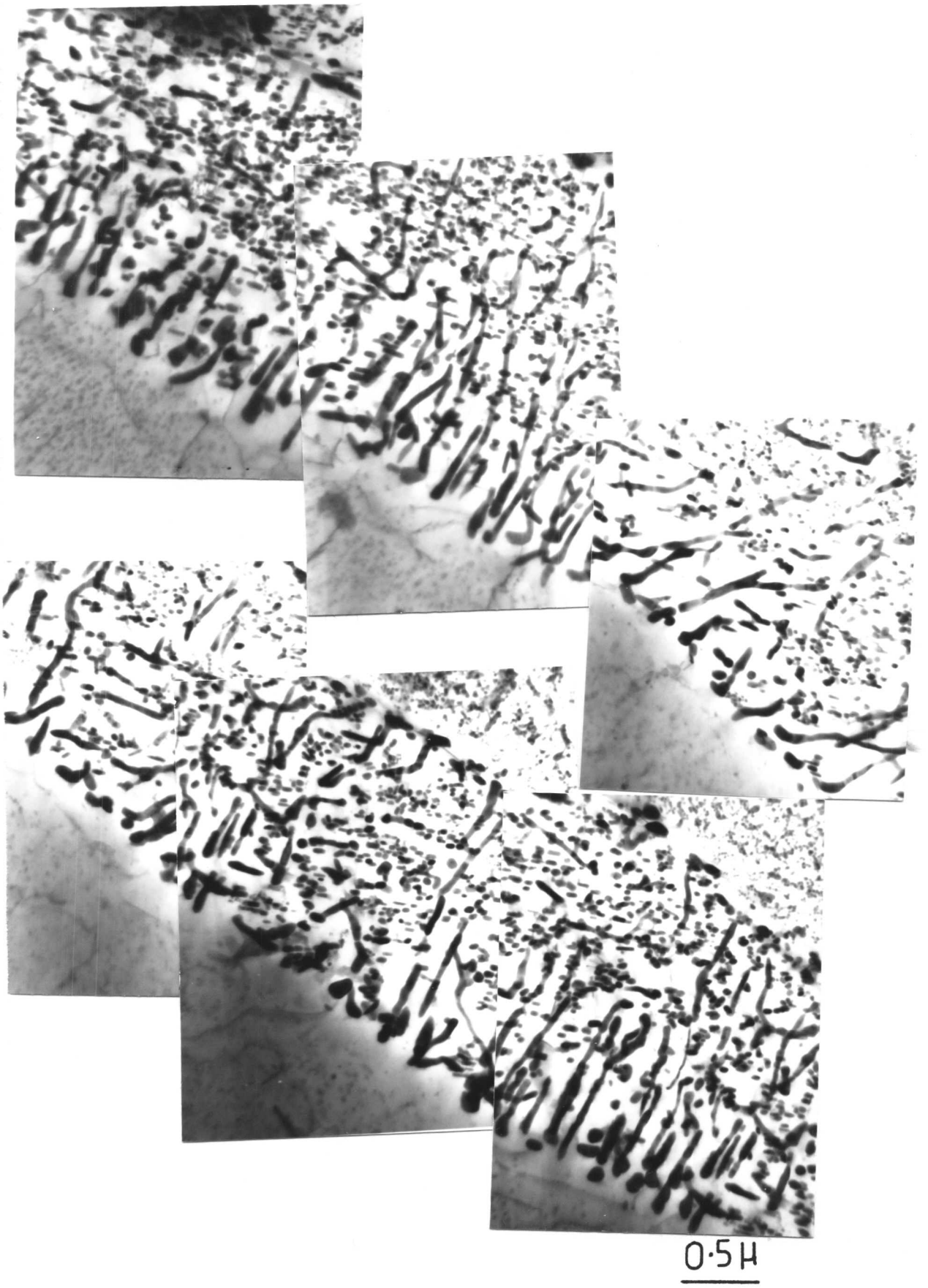

Figure 6.5a - Microstructure of the rim. It consists of fine dispersions of carbides in α. Some coarse carbides are also visible.

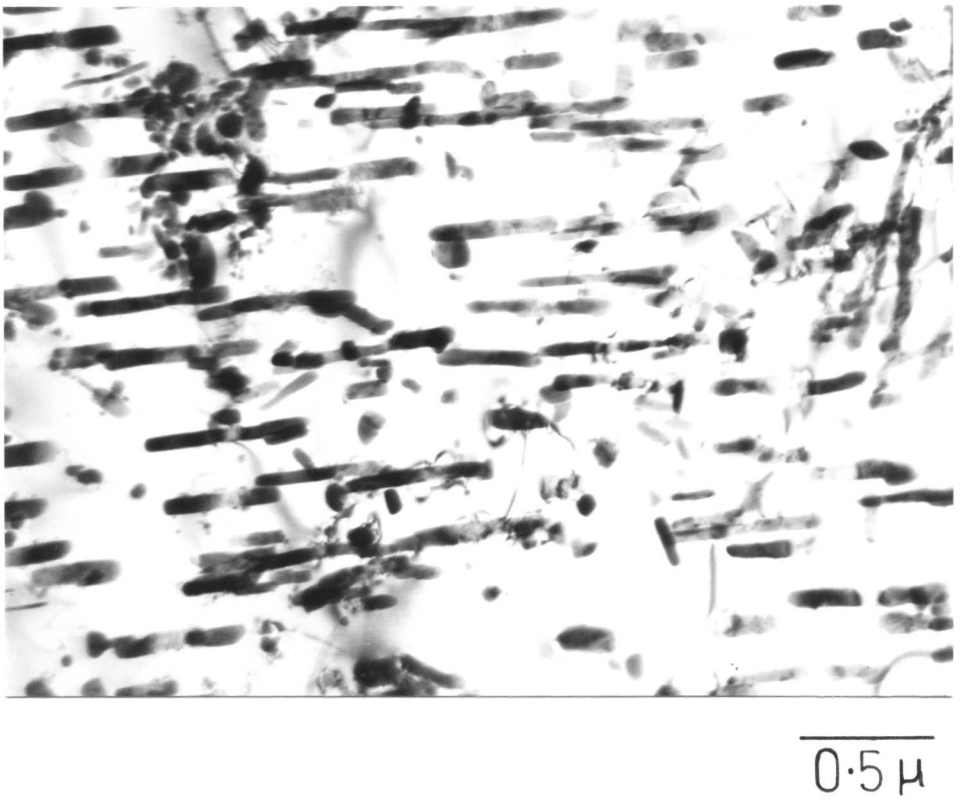

Figure 6.5b - Carbides arranged in one particular direction.

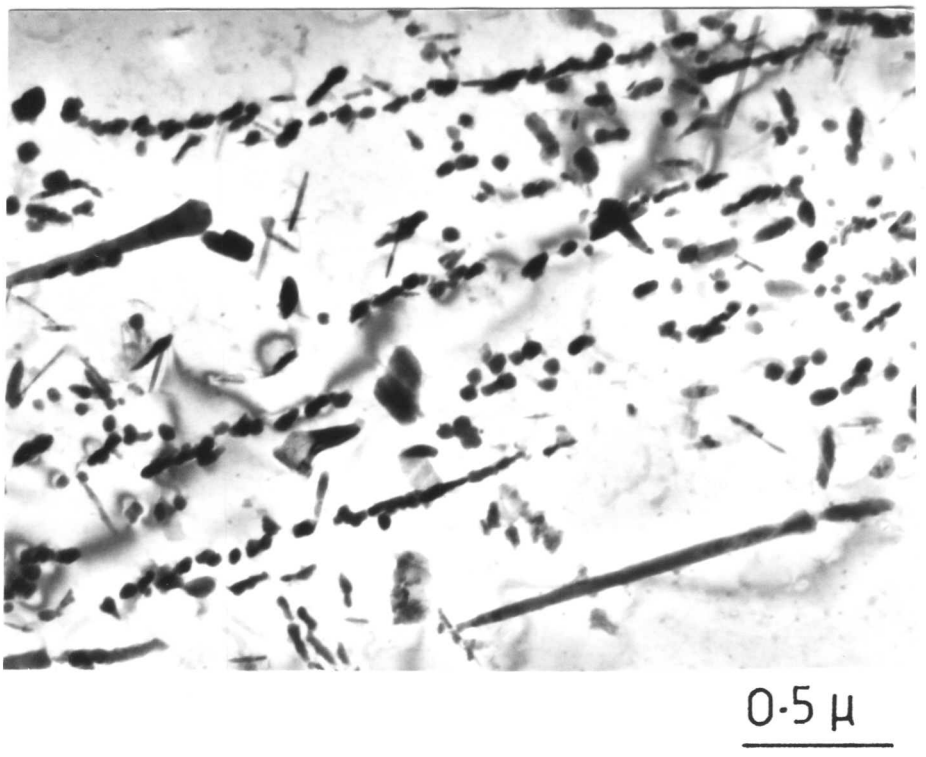

Figure 6.5d - Carbide formed from supersaturated ferrite are less dense and non-uniform in distribution.

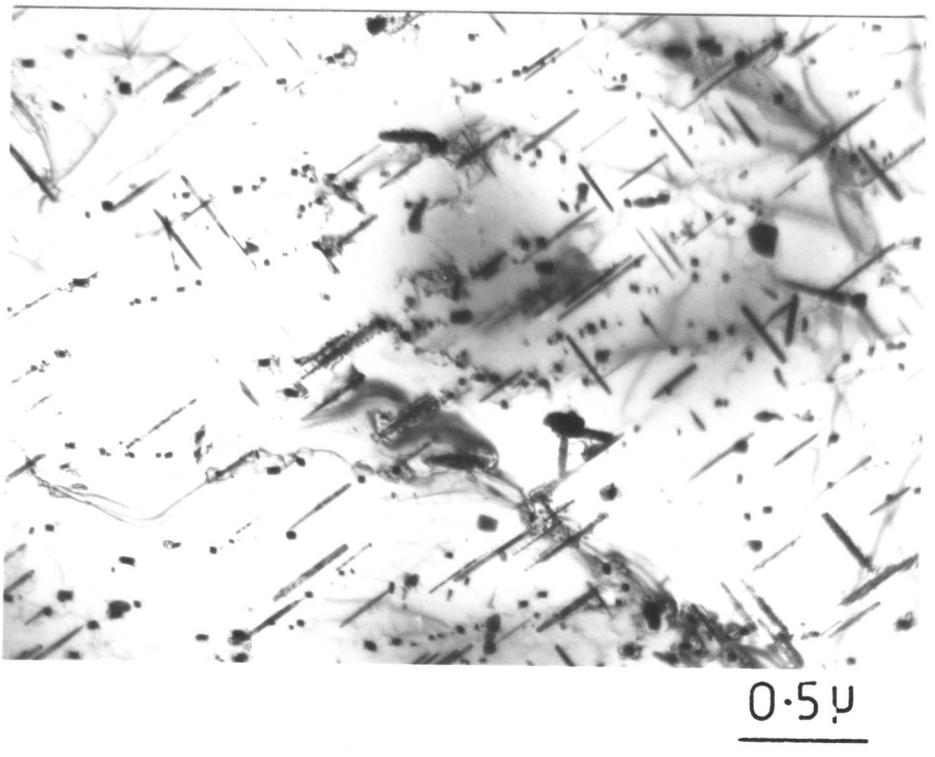

Figure 6.5e - Formation of Widmanstätten type of carbide in α.

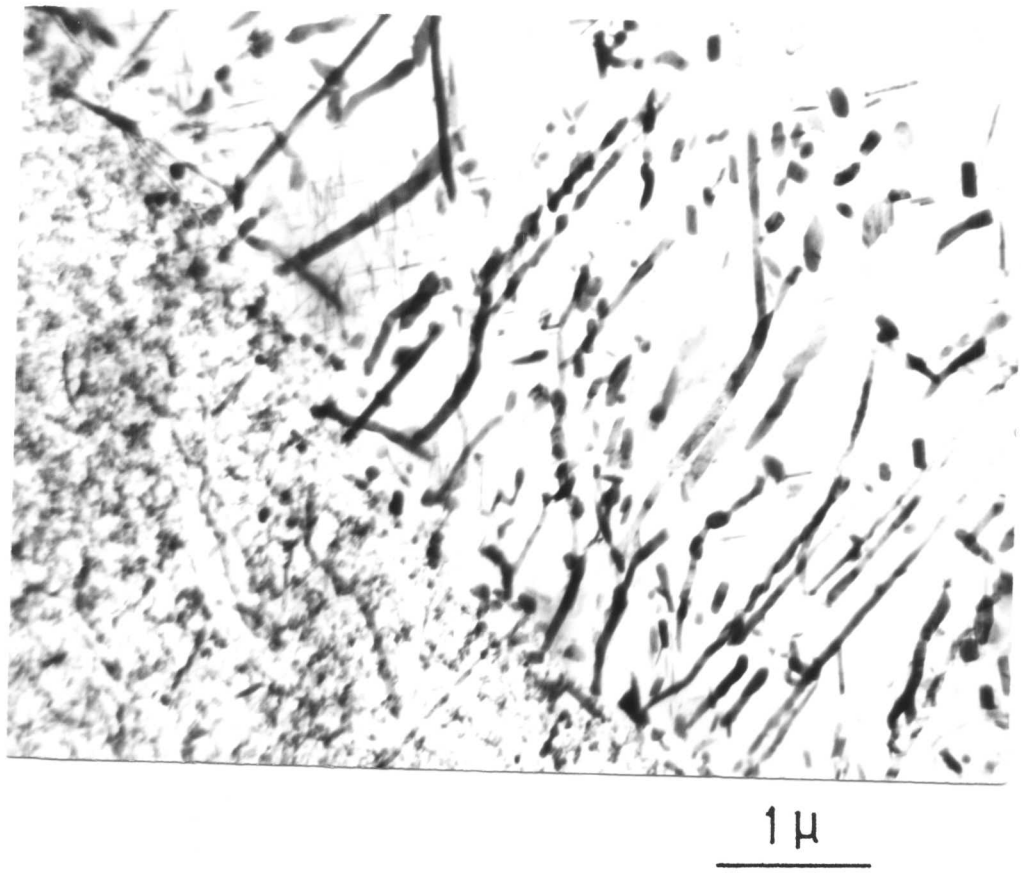

Figure 6.5c - Microstructure showing two step coarsening of the discontinuous precipitations.

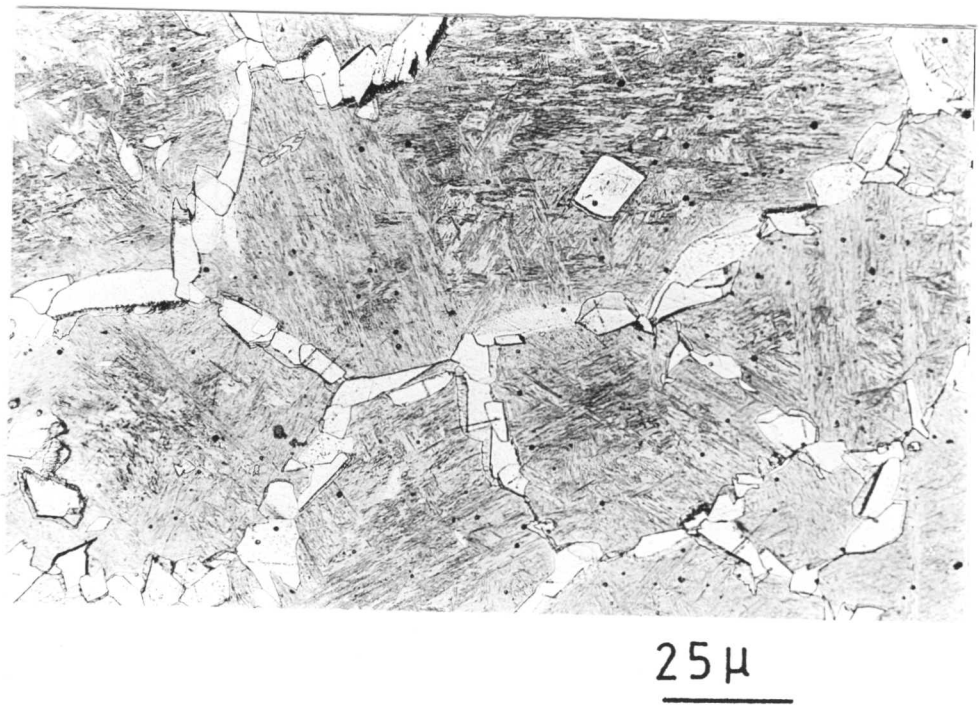

Figure 6.6a - Showing grain-boundary allotriomorphs occasionally containing ledges. (Isothermally transformed at 800°C for 1.5 minutes.)

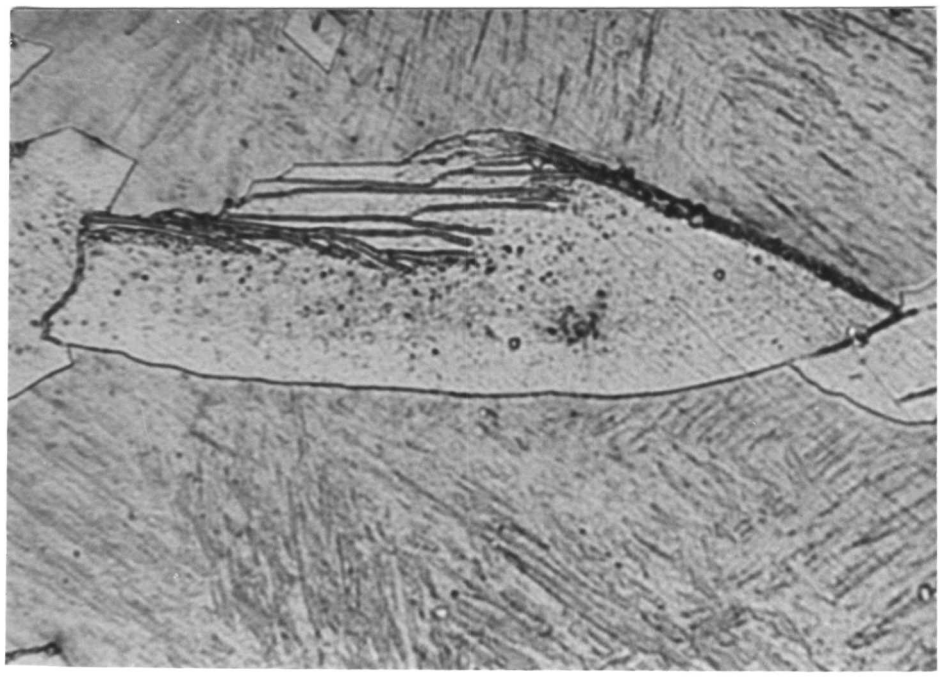

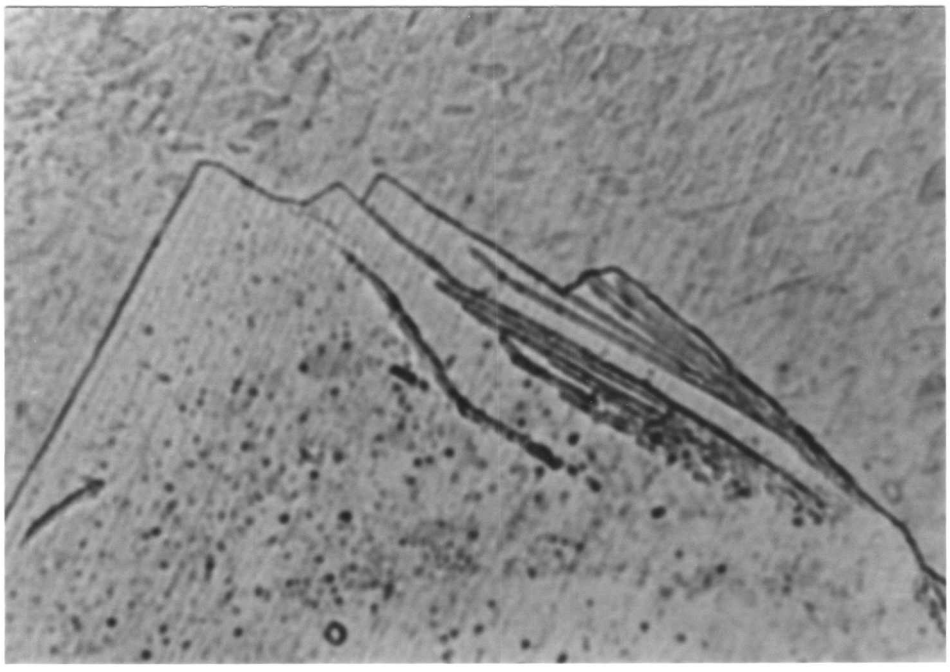

Figures 6.6b-c - Showing fibrous carbides in association with low energy interface which has moved by ledge mechanism. (Isothermal transformation at 800°C for 1.5 minutes.)

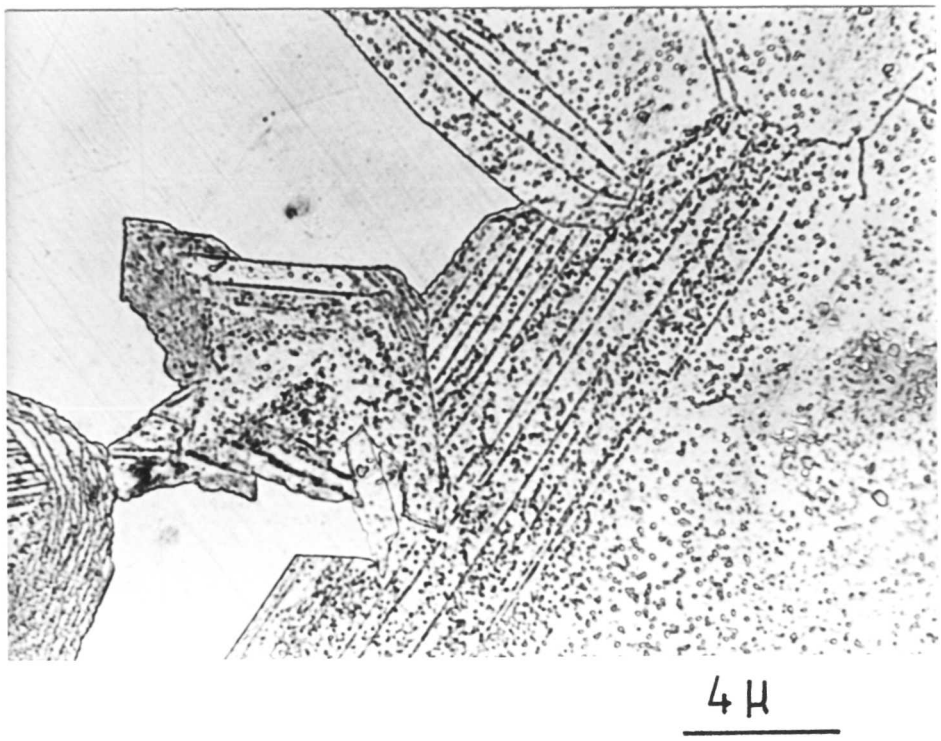

Figure 6.7a - Showing evidence of interphase precipitation at 850°C for 20 minutes.

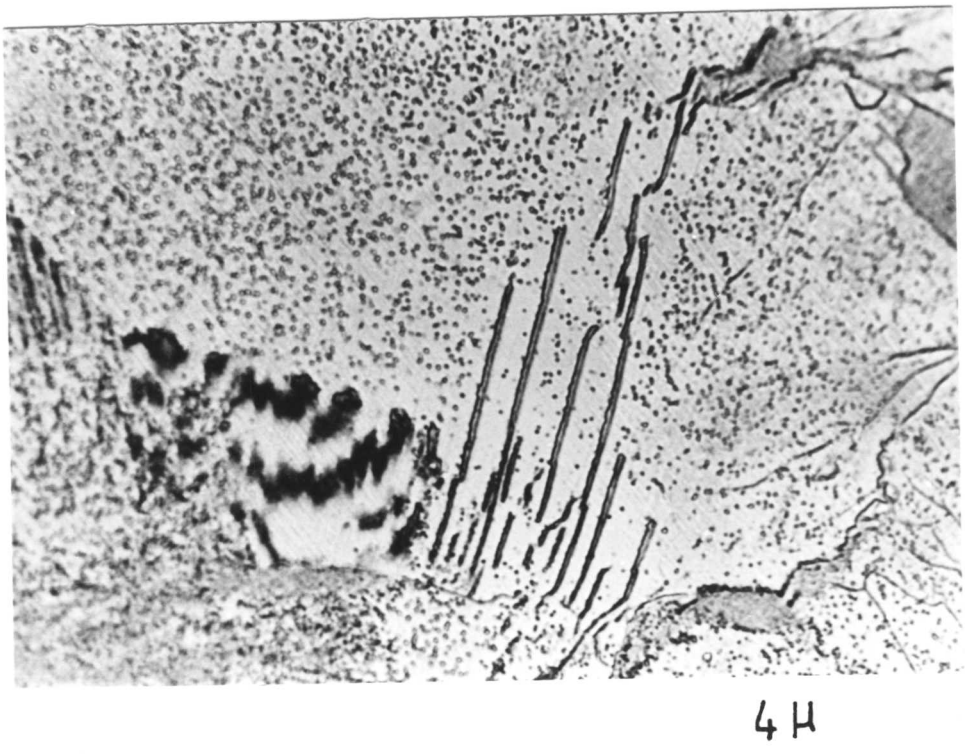

Figure 6.7b - Showing fibrous carbides as well as random dispersions of carbides. (Isothermally transformed at 850°C for 20 minutes.)

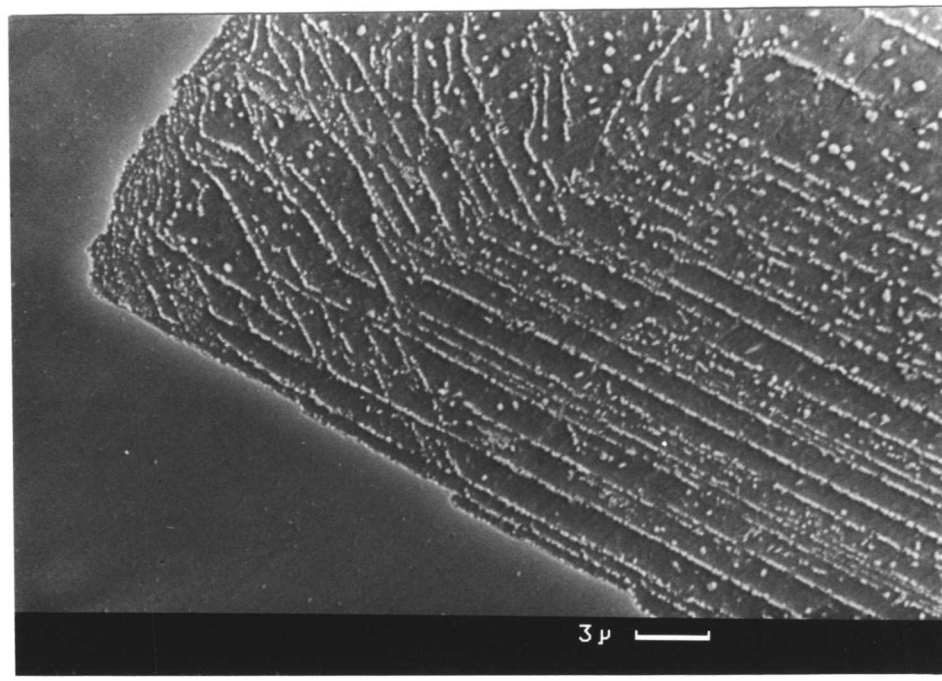

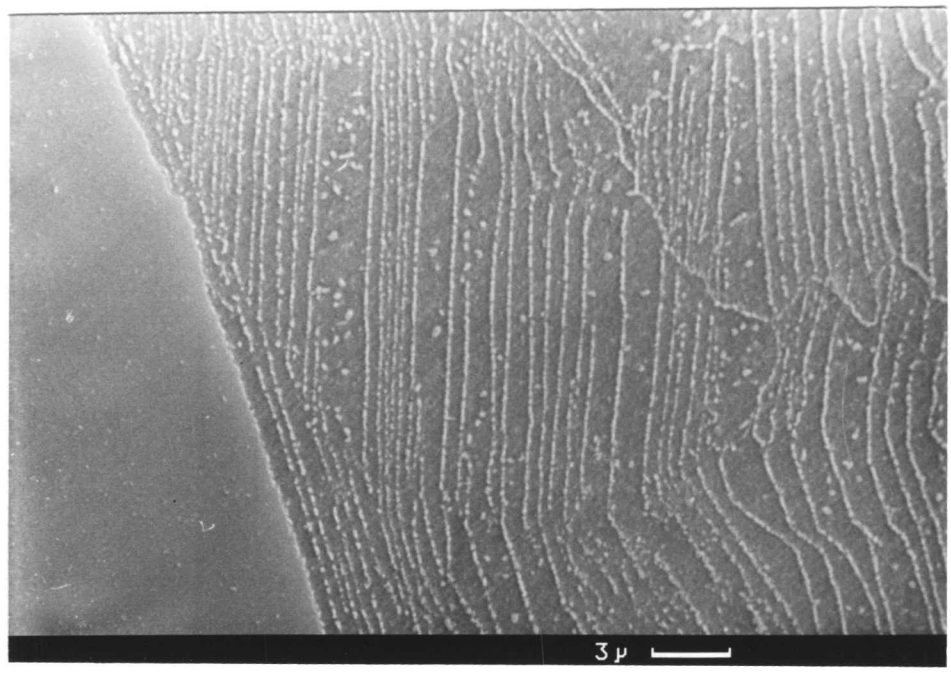

Figure 6.8a and b - Scanning micrographs showing interphase precipitation.

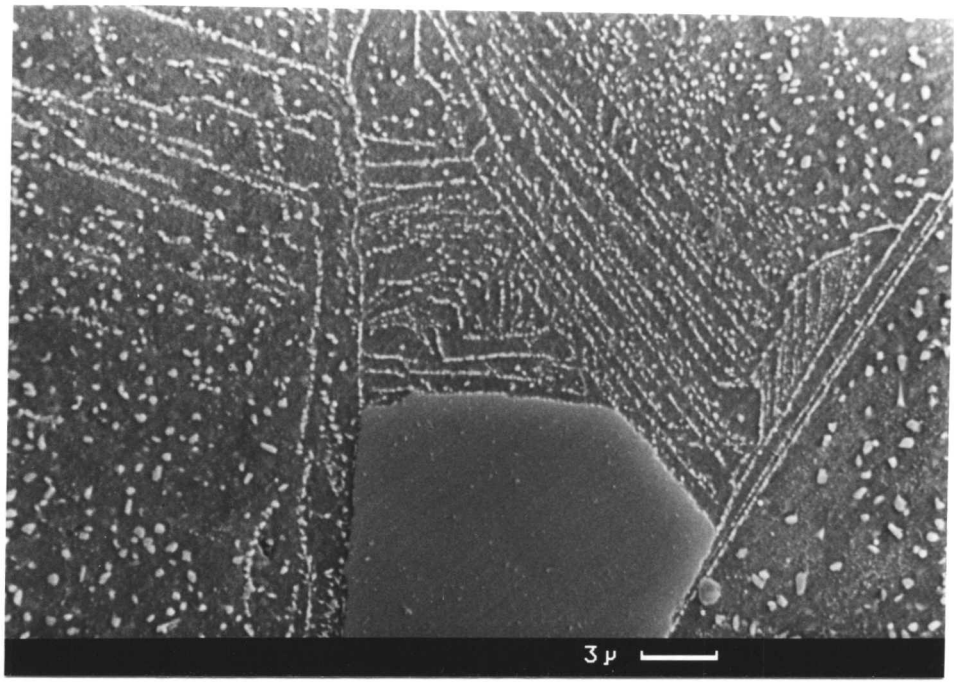

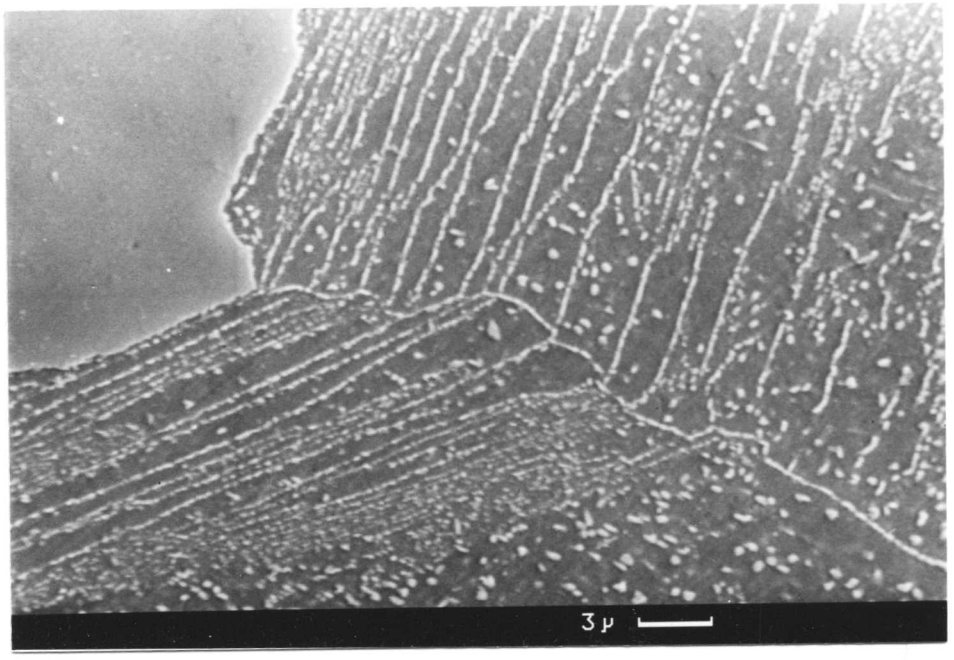

Figure 6.8c and d - Scanning micrographs showing interphase precipitation.

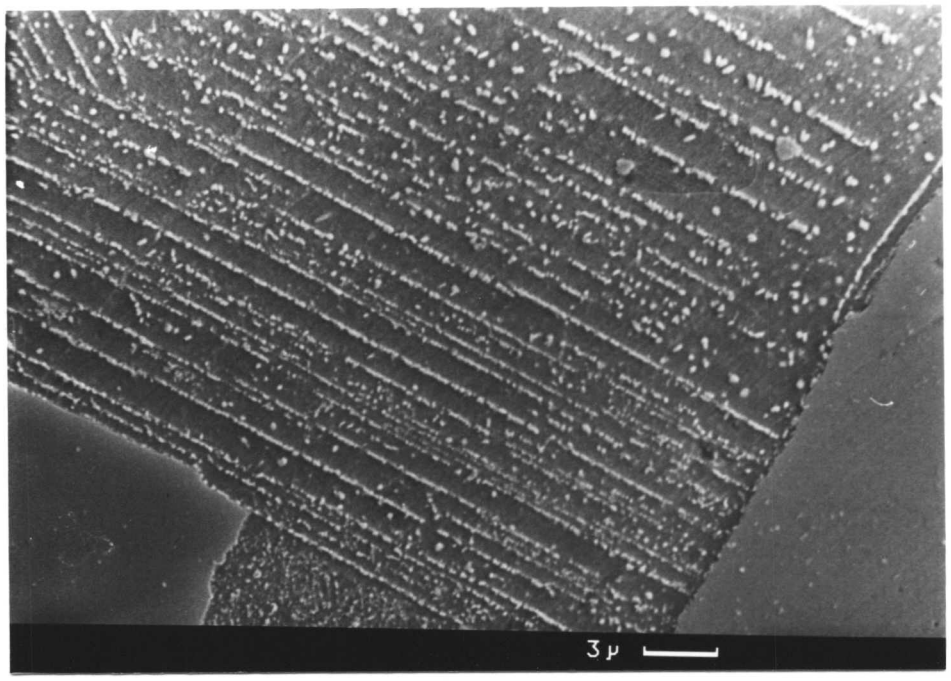

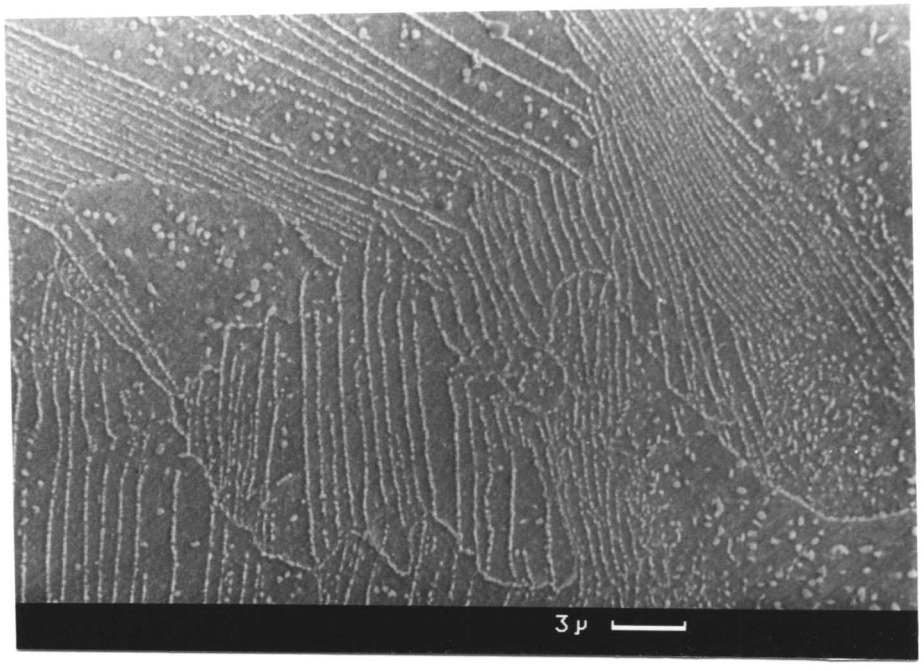

Figure 6.8e and f - Scanning micrographs showing interphase precipitation.

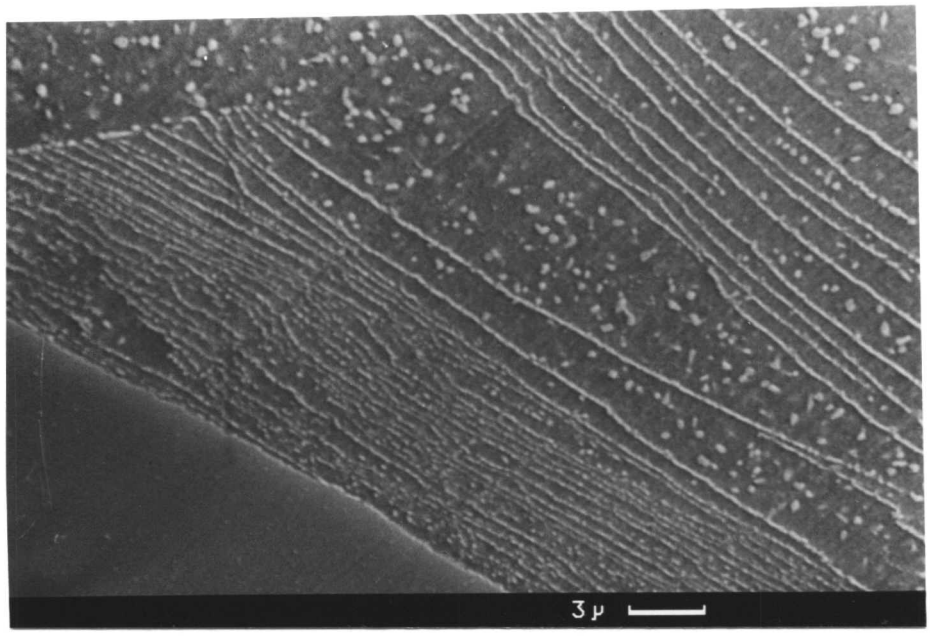

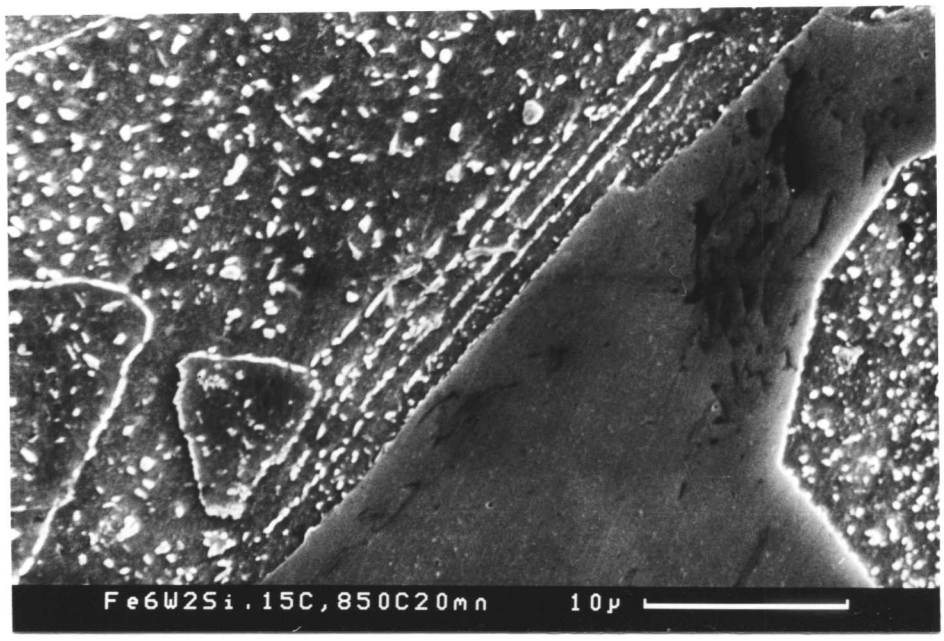

Figure 6.8g and h - Scanning micrographs showing interphase precipitation.

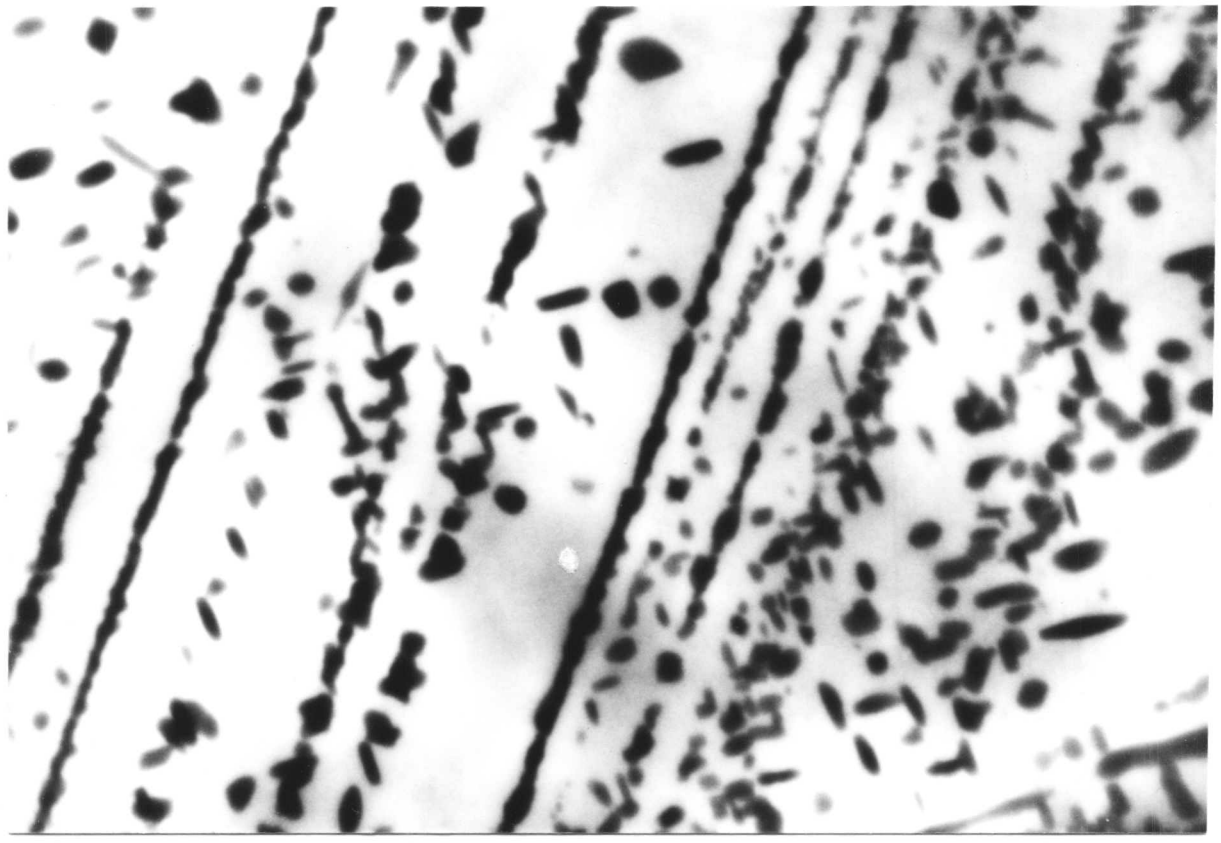

Figure 6.9 Variable band spacing is apparent in this micrograph. (TEM).

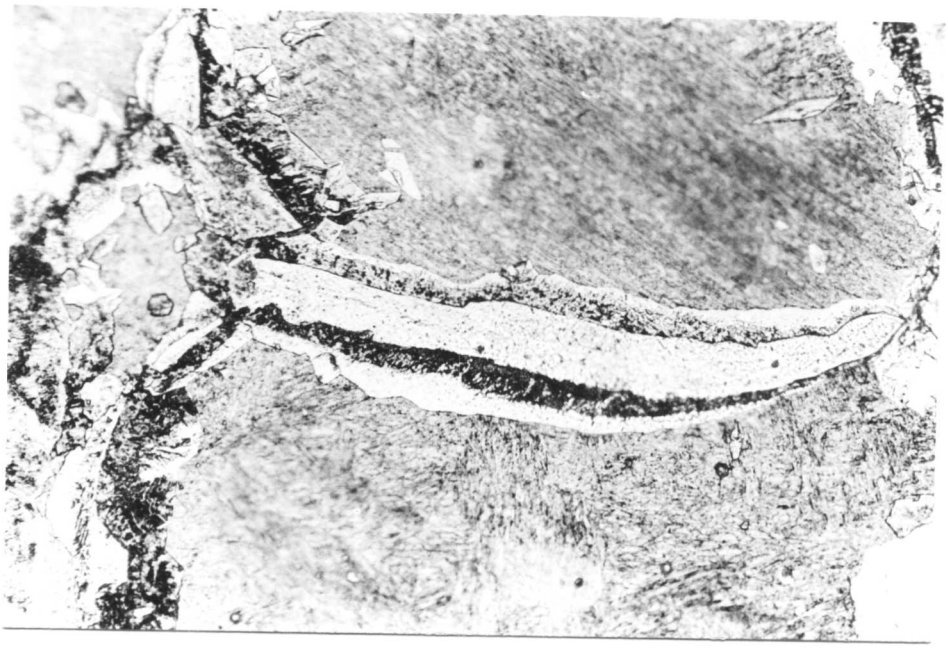

Figure 6.10 - Isothermal transformation at 700°C for 20 minutes followed by upquenching at 800°C for 3.5 minutes.

CHAPTER VII

THE INFLUENCE OF CARBIDE PRECIPITATION ON THE NUCLEATION OF ALLOTRIOMORPHIC FERRITE IN Fe5.8W-0.5C (wt%) ALLOY.

7.1 Introduction: Strong carbide forming substitutional alloying elements such as niobium sometimes significantly increase the hardenability of steels even when used at concentrations well below 0.1 wt%[1-4]. The increase in hardenability is unexpected, since the formation of niobium carbide (NbC) at austenite grain boundaries restricts grain growth during austenitization. The resulting fine grained structure should provide a larger number density of grain-boundary sites for the heterogeneous nucleation of ferrite, an effect which should accelerate the $\gamma \rightarrow \alpha$ transformation and hence reduce hardenability. In spite of this, Nb is known to retard the nucleation of α ferrite, although the mechanism by which it does so is not clear. Niobium carbide forms very thin plate-like particles which grow along the austenite grain boundaries; these particles are in general difficult to detect, especially if their presence has to be related to some coarse feature of the microstructure (such as ferrite grains during the early stages of their growth).

In this work, we used an Fe-W-C alloy to examine the influence of carbide precipitation on the heterogeneous nucleation of ferrite at austenite grain boundaries. In this alloy, tungsten carbide (WC/M_6C) can preferentially precipitate at the austenite grain boundaries (in the form of coarse, globular particles as well as lamellar rod like particles) which can easily be resolved using optical microscopy. The kinetics of the $\gamma \rightarrow \alpha$ change have been studied over a range of isothermal transformation temperatures under two circumstances: firstly, in the presence of copious WC/M_6C precipitation at the austenite grain-boundaries, and when such carbide precipitation has occurred to an extent which covers only a small proportion of the austenite grain boundaries. At low undercooling (i.e. at temperature close to Ae_3) the kinetics of transformation have been expressed both in terms of the rate of nucleation as well as with respect to volume fraction transformed. But at higher under coolings, the kinetics have been only expressed in terms of volume fraction as it became extremely difficult to recognise individual ferrite due to rapid impingement even during the early stages of transformation.

7.2 Experimental Procedure: The Fe-W-C alloy used was prepared as a 65g Argon-Arc melt using high-purity constituents and was homogenised at 1300°C (± 5) for 2 days in a quartz tube under a partial pressure of argon; the composition of the alloy (analysis carried out after homogenisation) was found to be Fe-5.8W-0.5C(wt%);the high alloy content was chosen to ensure sufficient hardenability for the heat-treatments discussed below, even when some of the W and C was tied up as carbide. The alloy was swaged down to 3mm diameter rod and cut into 10mm lengths for further heat-treatment. Specimens were all electrolytically plated with Ni, to a thickness of about 75 μm, prior to heat-treatment, in order to prevent surface degradation and surface nucleation. The heat treatments used were as follows:

A. After sealing in a quartz tube under a partial pressure of argon, the alloy was heated in the (γ + WC/M_6C) phase field at 1200°C (± 5) for 30 minutes; this avoided the development of any coarse-grained structure which might exhibit strong orientation texture not typical of normal practice. It was then transferred into a furnace at 900°C (± 5) (i.e. γ + WC) where it was held for 5 hours to induce the formation of WC at the austenite grain boundaries. The quartz tube was then transferred to a fluidized bed maintained at a pre-specified isothermal temperature (i.e. 800°C, 750°C and 700°C) to promote the formation of ferrite and at the end of a specified interval of time, the quartz tube was rapidly broken and the specimen quenched into water to prevent further reaction. To fully explore the transformation characteristics, three distinct isothermal transformation temperatures were selected. The first one was 800°C which is just below Ae_3 of the alloy. This isothermal transformation temperature was selected to induce a slow rate of nucleation and growth of ferrite to ensure a small equilibrium volume fraction of ferrite and to avoid nucleation site saturation and problems with impingement between adjacent growing particles. The second isothermal temperature was 750°C near the nose of the TTT diagram and the third one was at 700°C a temperature well below Ae_3. These two temperatures were selected to see the effect of increasing driving force (i.e. change in free energy per unit volume, ΔG_v) on the transformation characteristics.

B. As above, but with the alloy held at 900°C ± 5 for only 5 minutes before the isothermal treatment. This heat-treatment was designed to permit the formation of only a small amount of carbide-phase so that much of the ferrite could then nucleate from the γ/γ grain boundaries. The alloy could, after austenitisation, have directly been transferred to the fluidized bed at

isothermal temperature but there would then have been uncertainties about the time taken for the specimen to reach the isothermal temperature.

All the stereological measurements were performed on light optical images using a Quantimet 720 image analysing system. Nucleation was characterised by counting the number of ferrite grains per unit area of plane section; we note that this cannot be converted into nuclei per unit volume without making specific assumptions about the ferrite particle shapes.

7.3 Results and Discussion: Fig. 7.1 (a) and (b) illustrate the microstructures obtained when the specimens were subjected to isothermal treatment at 800°C under the two different conditions of pre-precipitation in the (γ + WC) phase field. These micrographs clearly indicate the marked difference in the transformation kinetics under these two conditions of heat-treatment. SEM pictures Fig. 7.2 (a) and (b) taken using a CamScan 4 give an idea about the percentage of grain-boundary area occupied by the carbide (WC/M_6C). While about 65-70% of grain-boundaries are covered with carbide in the heavily pre-precipitated alloy, only about 10% of these are covered when the time of pre-precipitation was reduced to 5 minutes from 5 hours. TEM (Fig. 7.3) clearly shows the shape of the carbides formed on the grain-boundaries. These carbides precipitate at the grain-boundaries in the form of coarse globular particles as well as rod-like carbides.

The nucleation counts presented in Fig. 7.4 demonstrate the drastic drop in the nucleation rate of ferrite in the presence of WC at the grain-boundaries when the isothermal temperature was close to Ae_3 i.e. 800°C ($\pm$ 2). Similarly it also shows the difference in the volume fraction of ferrite obtained at this isothermal temperature. These results are contrary to the fact that WC formation leads to a depletion of solute in the matrix resulting in increased driving force for the $\gamma \rightarrow \alpha$ transformation. It seems that the nucleation of ferrite at carbide-austenite interfaces is less favourable compared to nucleation at austenite grain boundaries.

Fig. 7.5 (a) and (b) show the volume fraction (V_α) transformed at the isothermal temperature of 750°C and 700°C respectively. The plots show that the volume fraction (V_α) transformed in case of heavily pre-precipitated alloys is much higher at these isothermal temperatures. It can be anticipated that with increasing undercooling, the driving force per unit volume (ΔG_v) increases and eventually it exceeds a value required for nucleation on the austenite/carbide interface. Some workers[4,5,6] have shown that coarse grain-boundary carbides can be potent nucleation site for the formation of ferrite. They argued that these coarse carbide increase the lattice mismatch with respect to austenite resulting in high energy

interfaces conducive for nucleation of ferrite. It also locally reduces the C concentration which assists ferrite formation.

In majority of the cases, it was observed that the α is growing only one side of the boundary (Fig. 7.6). This may be due to the fact that the mobility of the carbide/ferrite interface is very restricted and hence the growth of α occurs via movement of the more mobile γ/α interface.

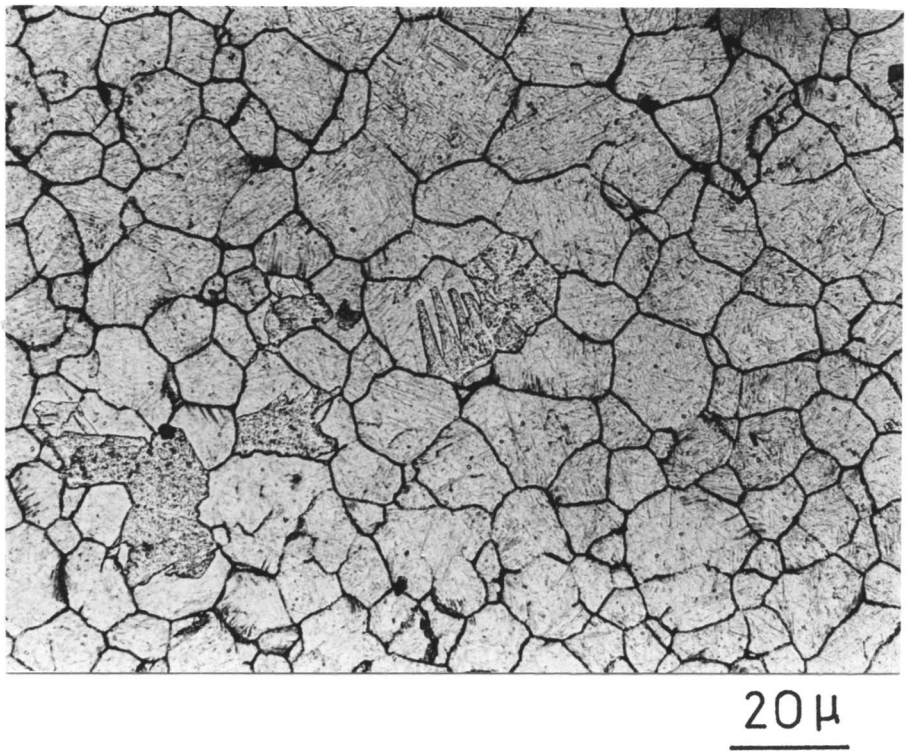

Figure 7.1a: Low volume fraction of α in heavily pre-precipitated (900°C/5 hours) specimen.

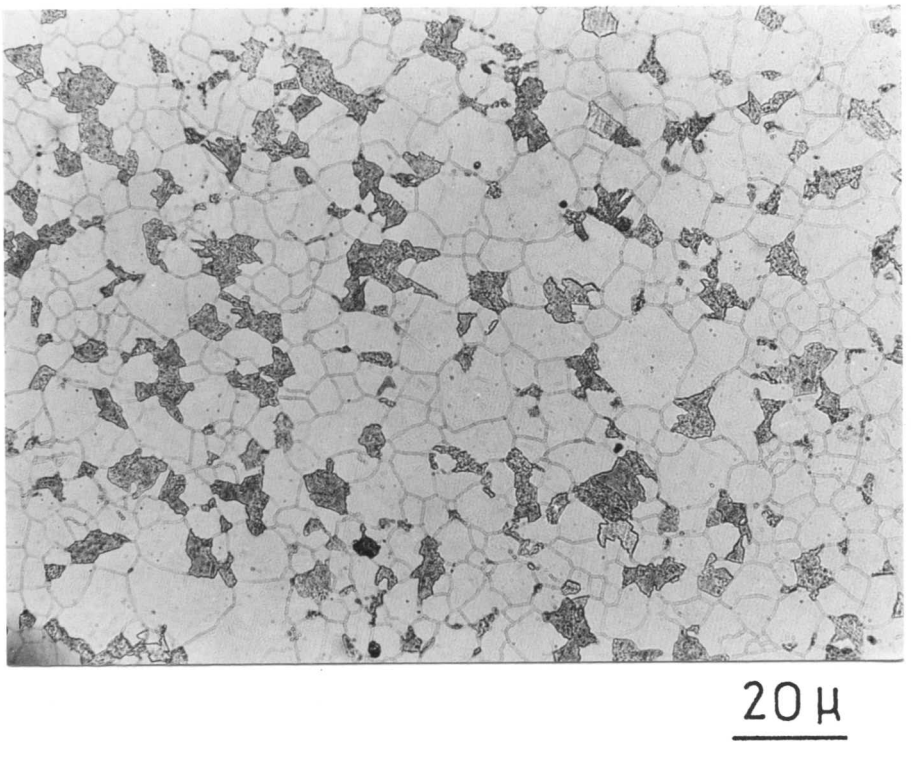

Figure 7.1b: High volume fraction of α in specimen prepreipitated for very small time (900°C/5 min).

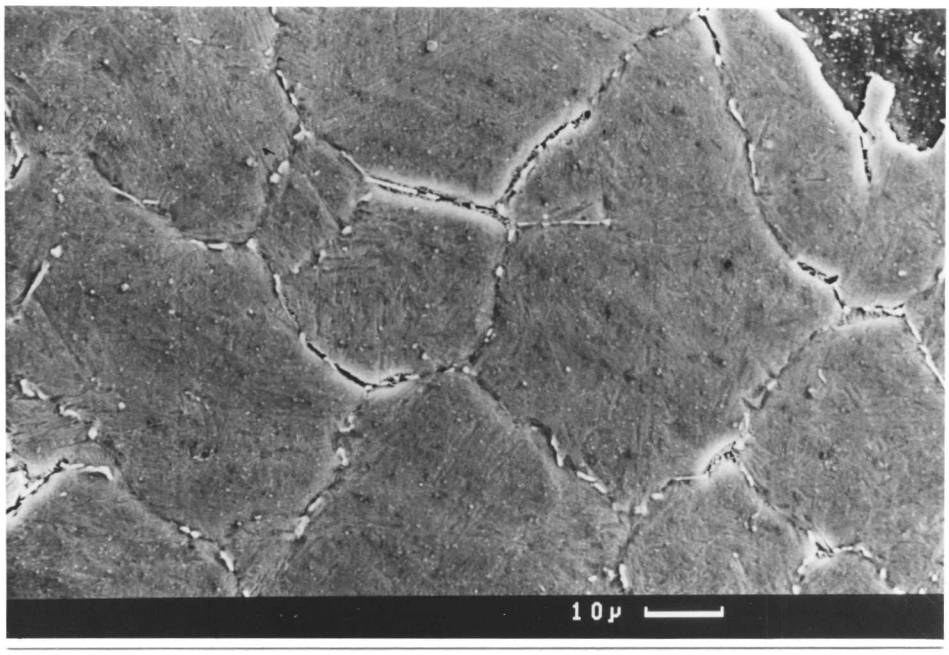

Figure 7.2a: Approximately 65 to 70% austenite grain-boundary area are covered by tungsten carbide (WC/M_6C) in heavily pre-precipitated alloy.

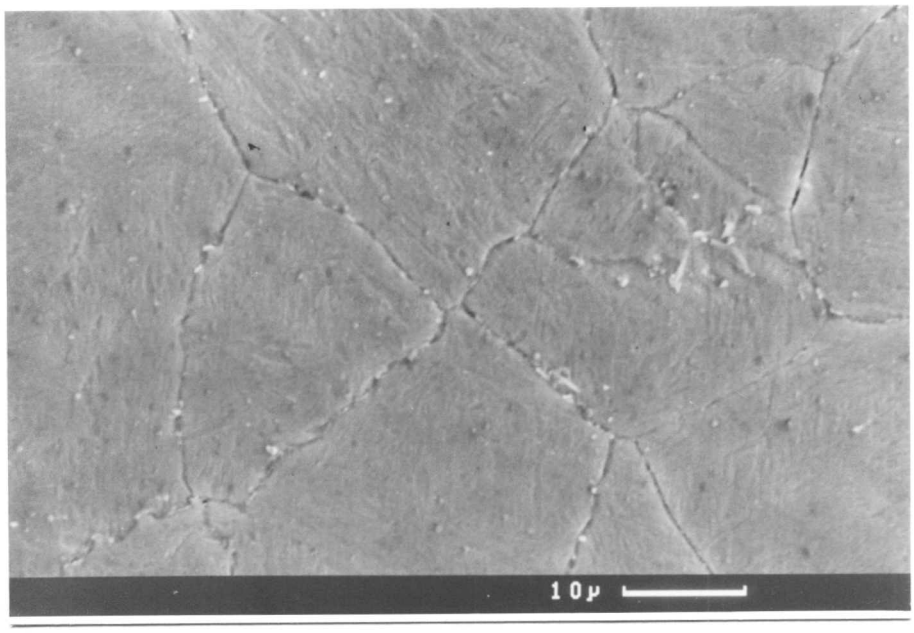

Figure 7.2b: Less than 10% austenite grain-boundary area are occupied by tungsten carbide when specimen was pre-precipitated for small time (i.e. 900°C/5 minutes).

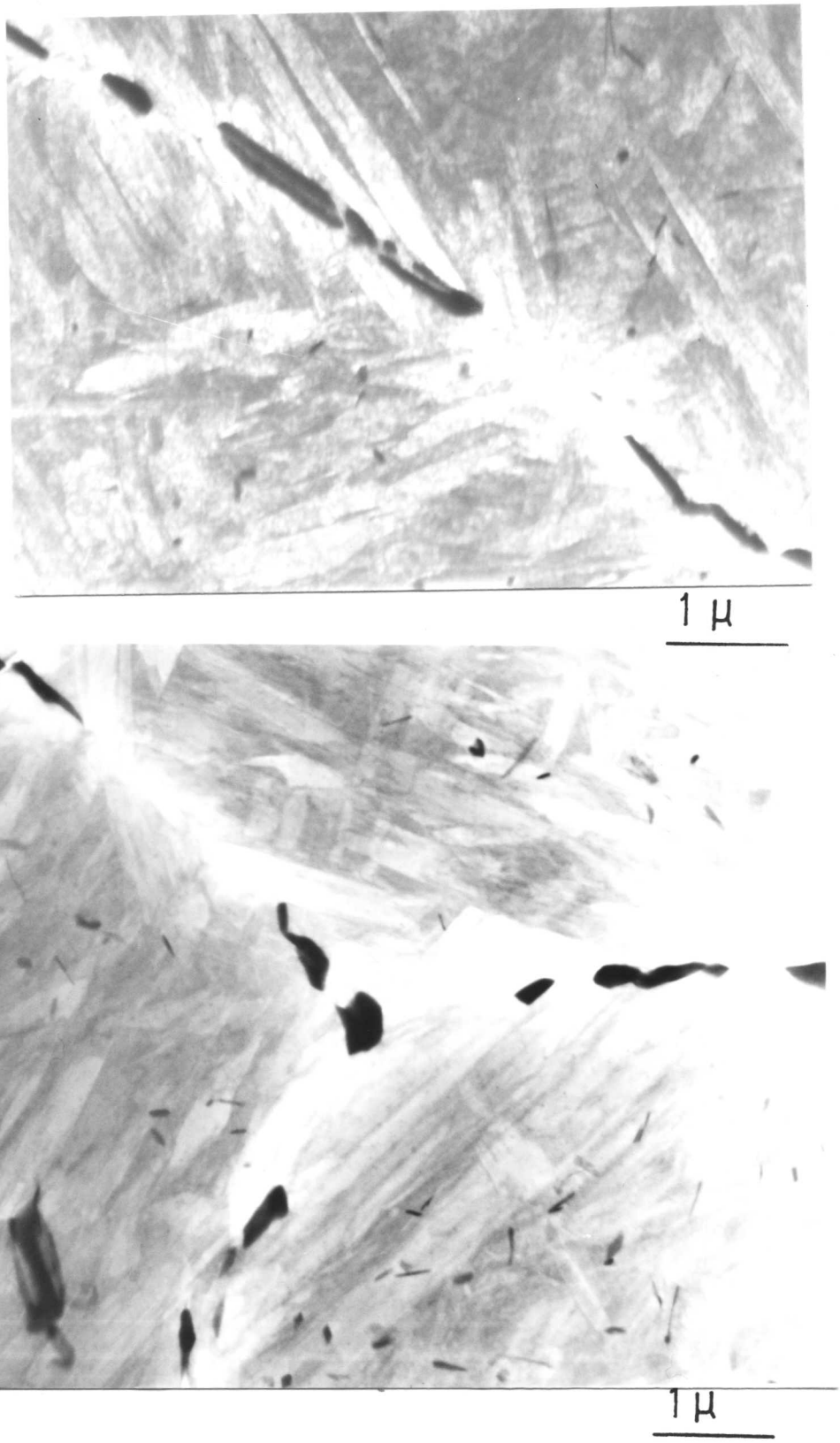

Figure 7.3a and b: Morphology of tungsten carbide varied from coarse globular to the rod like in appearance.

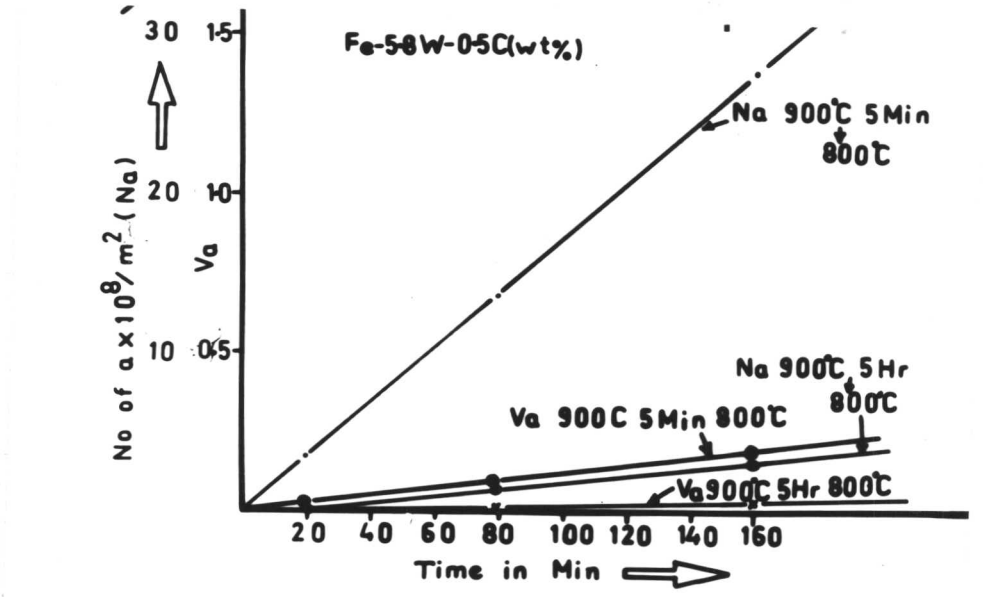

Figure 7.4: Curve showing number of α (N_α) vrs time as well as volume fraction (V_α) vrs time obtained under two different heat-treatments.

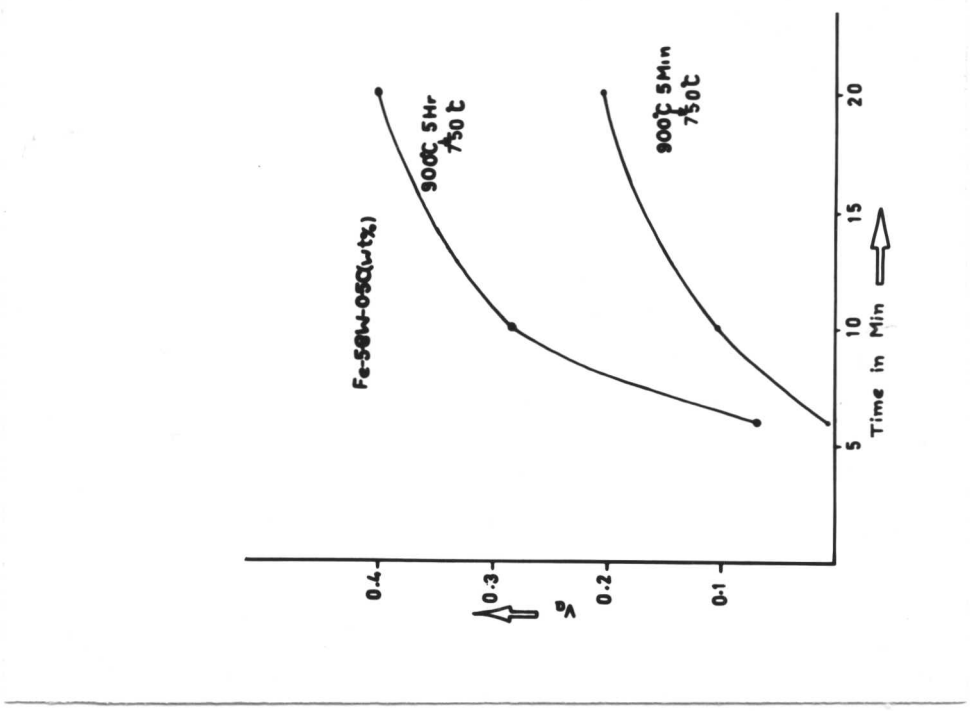

Figure 7.5a: Plot of volume fraction (V_α) vrs time for specimens isothermally transformed at 750°C under two different conditions of pre-precipitation.

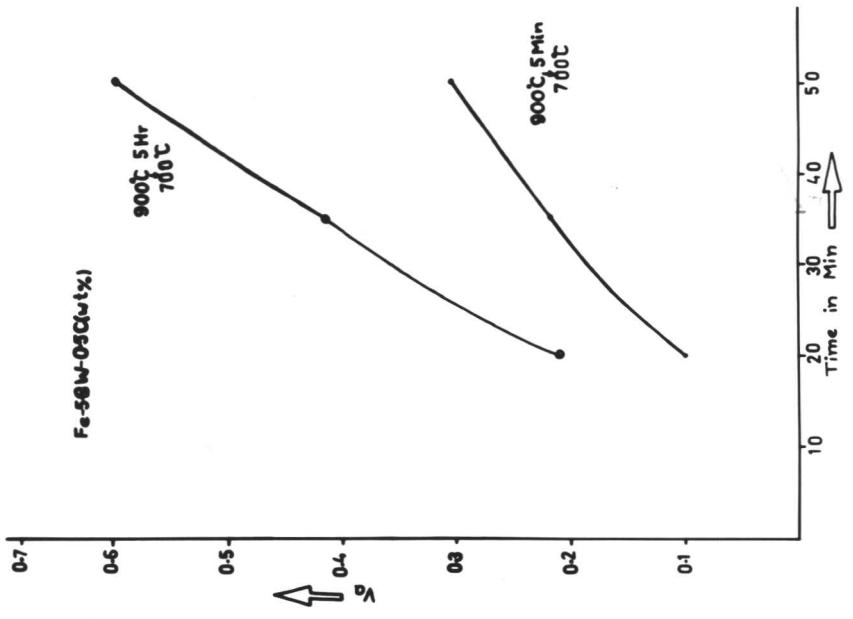

Figure 7.5b: Plot of V_α vrs time for specimens isothermally transformed at 700°C under two different conditions of pre-precipitation.

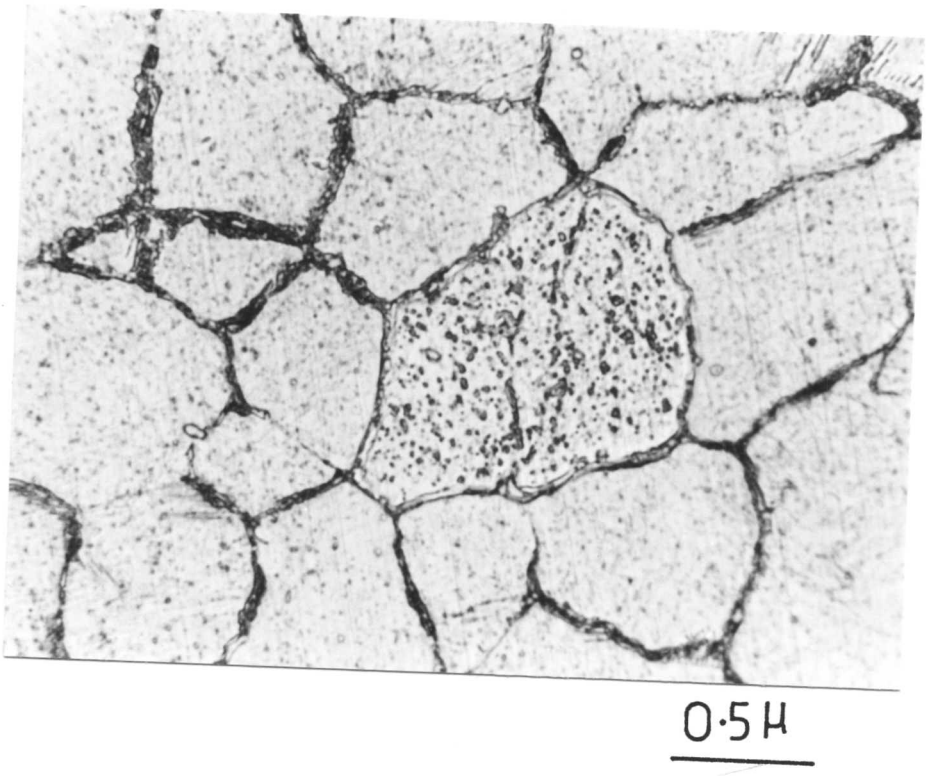

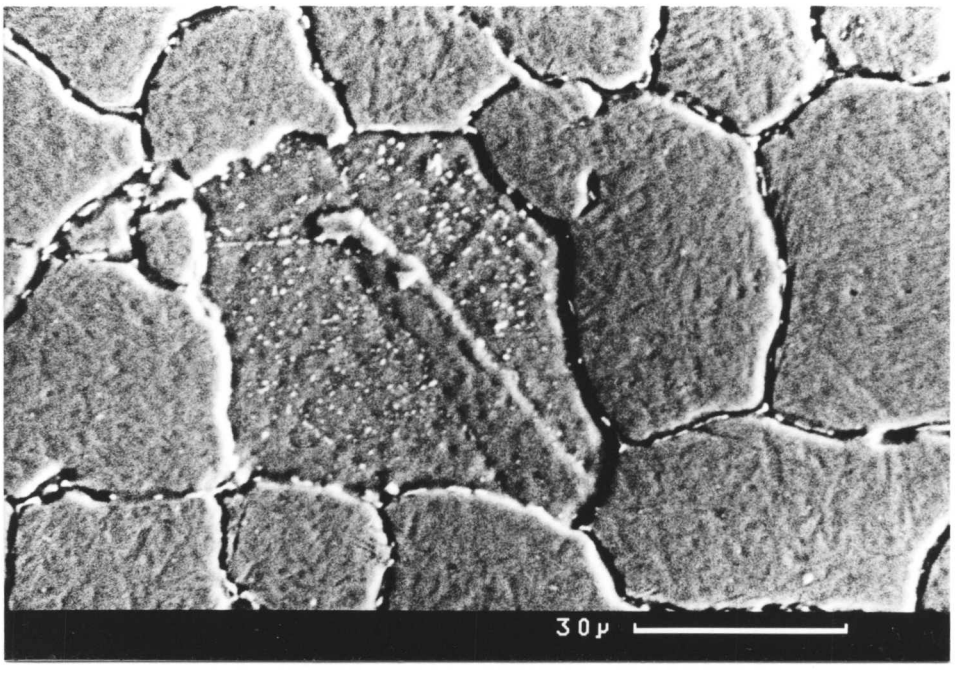

Figure 7.6a and b: Ferrite growing within one grain only.

CHAPTER VIII

THE STUDY OF GROWTH KINETICS IN Fe-2.99Cr-0.11C (wt%).

8.1 INTRODUCTION: The study of the growth kinetics of allotriomorphic ferrite in Fe-C-X ternary system has provoked considerable interest in the past two decades. Various models have been developed to predict the diffusion limited growth rate of allotriomorphic ferrite over a wide range of temperature and composition (Fig. 8.1). Diffusion limited growth refers to a situation in which the rate of growth of ferrite depends on the rate at which both carbon and substitutional alloying element (X) diffuse away from the γ/α interface and does not depend upon the nature of the processes at the interface by which atoms are incorporated in the allotriomorphic ferrite[1]. The transport or flux these atoms across the γ/α interface must be fast enough to maintain an equilibrium density of carbon and substitutional atoms in solution at the interface. The term "diffusion limited growth" has been modified and commonly used under the generic term "volume diffusion control (VDC) growth". Volume diffusion control growth means that a precipitate crystal grows in volume diffusion controlled manner as long as the growth kinetics resulting from volume diffusion in the matrix phase away from or towards the growing crystal are slower than those derived from transport across the interface boundary[2]. However, this modified definition of volume diffusion controlled growth can no longer be regarded as a unique and complete description of precipitate growth kinetics and that considerable additional information may be required in order to furnish such a description.

In recent years the growth scenario in binary and ternary systems has been examined via two different models :

(i) No partition local equilibrium (NPLE).

(ii) Para-equilibrium (PE).

8.2 Local equilibrium at the γ/α interface: The existence of local equilibrium during the growth of ferrite (α) implies that the compositions of the α and γ phases at the interface are connected by a tie line of the ($\alpha+\gamma$) phase-field in the equilibrium Fe-C-X phase diagram. This tie-line which defines the interface composition does not in general pass through the point in the ($\alpha + \gamma$) phase field which identifies the alloy composition. This is because the diffusivities of interstitial (C) and substitutional alloying elements (X) in the γ are significatly different. The appropriate tie line must be chosen to satisfy mass conservation

conditions at the moving interface and must be consistent with the partitioning behaviour of the alloying elements. Hence, the tie line corresponding to low supersaturation may lead to partitioning and long range diffusion of substitutional alloying elements. During this period, the driving force for carbon diffusion is reduced to a level which allows the substitutional element (X) flux to keep pace with the carbon flux at the interface. This situation is referred to as partitioning with local-equilibrium (PLE). The tie line for an alloy transforming at high super-saturation is such that there is virtually no partitioning of substitutional alloying elements between the γ and α and the transformation rate is controlled by volume diffusion of carbon in γ ahead of the moving interface. This situation is referred to as no partitioning with local equilibrium (NPLE).

The problem of diffusional growth of isolated α-precipitate particles in an infinite γ-matrix has been investigated in detail by Coates[3]. He assumed that local equilibrium is maintained at the $\gamma \rightarrow \alpha$ interface and then developed expressions to evaluate the interface velocity and interface composition contours. Refering to Fig. 8.2a and b $C_i^{\alpha\gamma}$ and $C_i^{\gamma\alpha}$ (i = 1, 2) are, respectively, molar concentrations in the α-precipitate and the γ-matrix at the α-γ interface. The points ($C_1^{\alpha\gamma}$, $C_2^{\alpha\gamma}$) and ($C_1^{\gamma\alpha}$, $C_2^{\gamma\alpha}$) define a unique tie line which corresponds to the α-γ interface. The tie line does not pass through the bulk composition $\bar{C}_1$, $\bar{C}_2$ because the diffusion coefficient for C (i.e. 1) and X(i.e. 2) in Fe-C-X is quite different. Coates[4] solved the problem of locating the interface tie line corresponding to a given bulk composition. and subsequently derived an expression for interface velocity as follows: Let us consider that a specimen of bulk composition ($\bar{C}_1$, $\bar{C}_2$) has been quenched from the austenite (γ) phase field into the austenite plus ferrite ($\gamma + \alpha$) phase field at a temperature T_1. Schematic T_1 ternary isotherms are shown in Fig. 8.2a where X is an α-stablizer and a γ-stablizer respectively. The equation for mass conservation at the α-γ interface under local equilibrium conditions is represented by:

$$(C_i^{\alpha\gamma} - C_i^{\gamma\alpha}) \frac{ds^*}{ds} = - J_i \Big|_{s = s^*} \quad (i = 1, 2) \qquad \ldots\ldots (8.1)$$

where J_1 = The molar fluxes of the solutes in a volume-fixed reference frame.

$$= - D_{11} \nabla C_1 - D_{12} \nabla C_2 \qquad \ldots\ldots (8.2)$$

and

$$J_2 = - D_{22} \nabla C_2 \qquad \ldots\ldots (8.3)$$

where D_{ij} (i = 1, 2; j = 1, 2) are empirical chemical diffusion coefficients and the concentrations C_i (i = 1, 2) are in moles per unit volume.

s refers to appropriate distance co-ordinate and s* is the position of the α-γ interface.

$$S^* = n_1 \sqrt{D_{11} t_1} = n_2 \sqrt{D_{22} t} \quad .. \quad .. \quad .. \quad .. \quad .. \quad .. \quad .. \quad .. \quad .. \quad (8.4)$$

where n_1 and n_2 are the growth rate constants. These growth rate constants are related by the following equations[3].

For carbon (C):-

$$f_1^k = f^k(n_1) - m\frac{D_{12}}{D_{11}}\left[f^k(n_2) - f^k(n_1)\right] \quad .. \quad .. \quad .. \quad .. \quad .. \quad .. \quad .. \quad (8.5)$$

and for X

$$f_2^k = f^k(n_2) \quad .. \quad .. \quad .. \quad .. \quad .. \quad .. \quad .. \quad .. \quad .. \quad .. \quad .. \quad .. \quad (8.6)$$

where k $\equiv$ p, c, and s for planar, cylindrical and spherical growth respectively.

f_i^k is referred to as the fractional compositions or relative supersaturations and represented by

$$f_i^k = \frac{C_i^{\gamma\alpha} - \bar{C}_i}{C_i^{\gamma\alpha} - C_i^{\alpha\gamma}} \quad (i = 1, 2) \quad .. \quad .. \quad .. \quad .. \quad .. \quad .. \quad .. \quad .. \quad .. \quad (8.7)$$

schematically it is shown in Fig. 8.3.

The functions $f^k(n_i)$ (i = 1, 2) are shown graphically in Figure 8.4.

Finally m represents the slope of the α-γ interface and given by

$$m = \frac{(C_2^{\gamma\alpha} - C_2^{\alpha\gamma})}{(C_1^{\gamma\alpha} - C_1^{\alpha\gamma})} \quad .. \quad .. \quad .. \quad .. \quad .. \quad .. \quad .. \quad .. \quad .. \quad .. \quad .. \quad .. \quad (8.8)$$

Equations (8.5) and (8.6) , can be solved to determine the growth velocity and the tie line governing interface compositions during growth since they contain only two unknown (for instance n_1 and $C_1^{\gamma\alpha}$) and the rest being determined by equation (8.4) and ternary isotherm phase-boundaries and tie lines.

The above theory for diffusion controlled growth is based on the assumption that the diffusion coefficients D_{ij} are independent of concentration. However theoretical studies[5, 6] show that the growth kinetics are influenced by the ternary diffusion interaction. It has been suggested that the weighted average diffusion coefficient is most appropriate value to use in growth rate equation i.e.

$$\bar{D}_{11} = (C - C^{\gamma\alpha})^{-1} \int_{C_1^{\gamma\alpha}}^{C_1} D_{11}(C_1)\, dC_1 \quad \ldots\ldots\ldots\ldots\ldots\ldots\ldots (8.9)$$

where C_1 represents mole fraction of carbon. The ratio D_{12}/D_{11} is also concentration dependent but Bolze et al[7], suggested that the use of a constant D_{12}/D_{11}, evaluated at the composition $\bar{C} = C_1^{\gamma\alpha}$ gives an adequate approximation to the problem.

The theory of diffusion controlled growth of α under local equilibrium conditions needs further justification to explain how can a ternary system accommodate two independent mass balances when one component (carbon) diffuses many orders of magnitude (10^4 to 10^6) faster than the other (X) Hillert[8] first realised the gravity of this situation and tried to resolve it in a rather simple way. He showed that either the fast diffuser (C) is forced to keep pace with the slow diffuser (X) by former's driving force for transformation being reduced to esentially zero or the slow diffuser is allowed to keep pace with the fast diffuser by the former's driving force for transport being raised to essentially infinity. The same concept was proposed independently by Kirkaldy[9] and co-workers[10]. To elaborate the same problem, let us consider Fig. 8.5a for low supersaturation (e.g. point A). The transformation rate is controlled by slow diffuser X. The bulk composition corresponding to this situation lies on the extrapolation of the γ-phase-isoactivity line through ($C_1^{\gamma\alpha}$, $C_2^{\gamma\alpha}$). It implies that $a_1^{\gamma\alpha} = \bar{a}_1$, where a_1 is activity of carbon. This leads to condition where driving force for fast diffuser (C) is eliminated. The amount of partitioning of X is given by $C_2^{\gamma\alpha} - \bar{C}_2$.

Let us choose a bulk composition corresponding to high supersaturation (e.g. point B) as shown in Fig. 8.5b. In this region, the transformation rate is controlled by fast diffuser C and there is effectively no partitioning of X between the precipitate and the matrix (driving force for X is infinity.) It implies that $C_2^{\alpha\gamma} \simeq \bar{C}_2$ and bulk compositions which satisfy this condition must lie on the horizontal line passing through the point ($C_1^{\alpha\gamma}$, $C_2^{\alpha\gamma}$).

In summary, the bulk composition lying on two dotted lines in Fig. 8.5a and 8.5b utilizes the same tie line. The intersection of these lines refere to a situation where transition occurs. The locus of such intersections for various tie lines generates a transition line as shown in Fig. 8.6a and b. Clearly the transition line define the two-phase field into two regions: one representing PLE (partitioning under local equilibrium) and the other NPLE (negligible partition under local equilibrium).

The growth velocity in P-LE regime is expressed from equation (8.4)

$$\frac{ds^*}{dt} = \frac{1}{2} n_2 \sqrt{D_{22}}\, t^{-\frac{1}{2}} \quad .. \quad .. \quad .. \quad .. \quad .. \quad .. \quad .. \quad .. \quad .. \quad .. \quad (8.10)$$

and in the NP-LE regime, it is given by

$$\frac{ds^*}{dt} = \frac{1}{2} n_1 \sqrt{D_{11}}\, t^{-\frac{1}{2}} \quad .. \quad .. \quad .. \quad .. \quad .. \quad .. \quad .. \quad .. \quad .. \quad .. \quad (8.11)$$

Interface composition (IC) contours: Interface contours provide a very compact means of illustrating the influences of the diffusivity ratio D_{11}/D_{22} and the precipitate morphology. (i.e. planar, cylindrical or spherical growth). Fig 8.7 shows a IC contour. The method for constructing such IC contours are discussed in details by Coates. Each bulk composition lying on this contours utilizes the same interface tie line. Every point on the IC contour represent a bulk composition which transfers with the same interface composition. As one moves along IC contour from $(C_1^{\gamma\alpha}, C_2^{\gamma\alpha})$ to $(C_1^{\alpha\gamma}, C_2^{\alpha\gamma})$ the fractional compositions f_1 and f_2 go from zero to unity.

The fractional composition ie. relative supersaturation is represented by

$$f_i^k = \frac{(\bar{C}_i - C_i^{\gamma\alpha})}{(C_i^{\alpha\gamma} - C_i^{\gamma\alpha})} = \frac{(\bar{C}_i - C_i^{\gamma\alpha})}{(C_i^{\alpha\gamma} - \bar{C}_i) + (\bar{C}_i - C_i^{\gamma\alpha})} \quad .. \quad .. \quad .. \quad .. \quad .. \quad .. \quad (8.12)$$

Fig. 8.8 shows the IC contours for various D_{11}/D_{22} ratio. As the D_{11}/D_{22} ratio increases the IC contours bulges more and more away from the tie line and finally breaks up into two straight lines $f_1 = 0$ and $f_2 = 1$ when D_{11}/D_{22} approaches infinity. In the region of $f_1 = 0$, the driving force $(\bar{C}_1 - C_1^{\gamma\alpha})$

for diffusion of the fast diffuser (C), component, is negligible (referring to equation (8.12) and hence it keeps pace with the slow diffuser, component 2 (i.e. X). Accordingly in this region transformation is controlled by slow diffuser (X). The amount of partitioning of component (i.e. X) is given by $C_2^{\gamma\alpha} - \bar{C}_2$. In the region where $f_2 \simeq 1$, $C_2^{\alpha\gamma} - \bar{C}_2 \simeq 0$ from equation (8.12) and hence the slow diffuser, component 2 (X), is keeping pace with the fast diffuser, component, by virtually eliminating the partitioning of the slow diffuser. Accordingly in this region, the transformation rate is determined by the fast diffuser, component (i.e. C).

The intersections of two straight lines $f_1 = 1$ and $f_2 = 0$ defines a transition from growth rate control by component 2 (X) to control by component (C). The locus of such intersections for various tie lines in the given two-phase field generates a transition line which is referred to as "envelop of zero-partition". The two regions of two-phase field thus defined are designated as the PLE (i.e. partioning under local equilibrium conditions) and NPLE (negligible partitioning under local equilibrium condition) regimes as shown in Fig. 8.6.

Interface velocity (IV) contours: Interface velocity contours provide a very powerful means of understanding the growth kinetics in Fe-C-X system. The effect of substitutional alloying element (X) as well as the relative supersaturation f_i^k on kinetics can be explained on the basis of this diagram.

An interface velocity contour is a line in the two-phase field of a ternary isotherm every point of which defines a bulk composition which transforms at the same rate for an assumed precipitate morphology. Fig. 8.9 show contours corresponding to various tie line in the given two-phase field. The interface velocity increases from zero to infinity as one move along IC from $f_i^k = 0$ to $f_i^k = 1$. The points corresponding to identical velocity on the various IC contours are joined to generate IV contours. The construction of IV contours is shown schematically in Fig. 8.9. The construction clearly shows that in PLE region the IV contours radiate from the Fe-C $(\gamma+\alpha)/\gamma$ phase boundary while in the NPLE region, they emerge from the Fe-X $\alpha/(\gamma+\alpha)$ phase boundary. This disposition of the IV contours results from a direct consequence of the system accommodating the two mass conservation conditions either forcing C to keep pace with X(PLE) or allowing X to keep pace with C (NPLE).

In Figs. 8.10a and b are shown schematic IV contours on Fe-C-X ternary isotherms in which X is a γ- and α- stablizer respectively. If X is a γ-stablizer, the vertical arrow in Fig. 8.10a indicates that progressive additions of X, holding the C constant, should continuously reduce the ferrite growth. It can be anticipated that well known enhancement of

hardenability induced by γ-stablizer (e.g. Mn, Ni, etc) is in part due to a reduction in proeutectoid growth rate. In the case X is α stabilizer (e.g. Si, Al), then its progressive additions at constant C level will result in increased growth rate of ferrite as shown in Fig. 8.10b.

8.3 Para-Equilibrium: Hultgren[11] introduced the term "Para-Equilibrium" to describe the kinematically constrained local equilibrium where the two adjoining phases are in local equilibrium with respect to the carbon only, the iron and the alloying element (X) being too sluggish to redistribute. In other words the ratio of the alloying element (X) and the solvent (Fe) remain constant across the α/γ interface and hence the tie lines in para-equilibrium region exists as "component rays" of the mobile species. The growth rate of the ferrite is exclusively controlled by volume diffusion of carbon ahead of the α/γ interface in the austenite matrix. Hillert[12] and Rudberg[13] introduced the same concept of unique kinetic state which deviates strongly from the true local equilibrium and the transformation proceeds under pure carbon diffusion control, local equilibrium being maintained across the interface with respect to carbon only. Aaronson, Domain and Pound[14] discussed the same concept under designation "No partition Equilibrium".

Hillert,[12] Rudberg,[13] Aaronson et al,[19] Gilmore et al[15] and Bhadeshia[16] treat the situation of para-equilibrium condition in a clear and concise way and developed the thermodynamic expression to calculate the para-equilibrium phase boundaries as follows:-

Thermodynamic condition for para-equilibrium:-

$$G_1^{-\alpha} = G_1^{-\gamma} \quad \ldots\ldots (8.13)$$

And

$$G_2^{-\gamma} - G_2^{-\alpha} = -(G_0^{-\gamma} - G_0^{-\alpha})\frac{C_0}{C_2} \quad \ldots\ldots (8.14)$$

$$G_i^{\gamma} = G_i^{\circ\gamma} + RT \ln \alpha_i^{\gamma} \quad \ldots\ldots (8.15)$$

where $\frac{C_0}{C_2}$ = Ratio of the solvent mole fraction to the immobile solute mole fraction along the component ray in question.

G_i = Partial molar free energy of respective component in the phase concerned. $G_i^{o\gamma}$ is the free energy of the i in its standard state.

Substitation of eqn. (8.15) into equ. (8.13) and equ. (8.14) yields the follow two expressions between the four composition variables which in turn define one tie line of the para-equilibrium diagram.

$$\frac{{}^{o\alpha\rightarrow\gamma}\Delta G_1}{RT} = \ln \frac{C_1^{\alpha}}{C_1^{\gamma}} + \ln \frac{x_1^{\alpha}}{x_1^{\gamma}} \quad .. \quad .. \quad .. \quad .. \quad .. \quad .. \quad .. \quad .. \quad .. \quad .. \quad (8.16)$$

or

$$\frac{{}^{o\alpha\rightarrow\gamma}\Delta G_2}{RT} - \ln\frac{C_2^{\alpha}}{C_2} - \ln\frac{{}^{\alpha}_{2}}{{}^{\gamma}_{2}} = -\frac{C_0}{C_2}\frac{G_0^{\alpha\rightarrow\gamma}}{RT} - \ln \frac{C_0^{\alpha}}{C_0^{\gamma}} - \ln \frac{x_0^{\alpha}}{x_0^{\alpha}} \quad (8.17)$$

where x represents activity coefficient in the phase concerned.

The third condition necessary to solve for the four unknown concentrations corresponding to the requirement that C_0/C_2 be a constant along the carbon component ray. Hillert showed the PE phase boundaries lies inside equo-phase diagram as shown in Fig. 8.11. The activity coefficients for dilute solutions may be explained[17] as

$$\ln\gamma_1 = e_{11} C_1 + e_{12} C_2 \quad .. \quad .. \quad .. \quad .. \quad .. \quad .. \quad .. \quad .. \quad .. \quad .. \quad (8.18)$$

$$\ln\gamma_2 = e_{12} C_1 + e_{22} C_2 \quad .. \quad .. \quad .. \quad .. \quad .. \quad .. \quad .. \quad .. \quad .. \quad .. \quad (8.19)$$

$$\ln\gamma_0 = -\frac{e_{11}}{2} C_1^2 - e_{12}C_1 C_2 - \frac{e_{22}}{2} C_2^2 \quad .. \quad .. \quad .. \quad .. \quad .. \quad .. \quad .. \quad (8.20)$$

where e_{ij} is known as Wagner interaction parameters.

These are two possible ways in which the volume diffusion controlled growth of allotriomorphic ferrite may occur. e.g. (NPLE) and (PE). Purdy and Kirkaldy[18] designed an elegant experiment to continuously monitor the movement of the γ/α interface by use of a diffusion couple. They found the interface position to vary in proportion to the square root of time indicating diffusion controlled interface motion. Furthermore, their experimentally determined parabolic growth rate constant (i.e. slope of maximum half thickness vrs square root of time) matched accurately with the theoretically calculated value based on local equilibrium model (NPLE) in Fe-Mn-C alloys. Those are important and accurate results and support the for growth mechanism by NPLE. Except these two results, all other reported data on parabolic rate constant differ

significantly from the theoretical value[20, 21, 22, 23]. The reasons for such discrepancies are explained on the basis of facetting, solute-drag like effect, interphase-carbide precipitation, stereological error and interaction of clusters with moving interfaces.

The transition from local-equilibrium to para-equilibrium:-

In the NPLE region of the two-phase field, the distribution of X involves a narrow zone of enrichment (viz γ stabliser) or depletion (α stablizer).

This narrow zone is generally referred to as spike or diffusion zone. This diffusion zone or spike must be pushed ahead of the α-γ interface as the transformation proceeds. Currently, considerable discussion[10, 14, 24, 25] is centered about the question of whether or not this diffusion zone exists for transformations in the system Fe-C-X. It is conceivable that at very high growth rates the diffusion zone becomes so thin as to exist only mathematically and in reality disappears completely.

For situation in which a narrow diffusion zone is involved in the growth of ppt particle, the Zener[26] approximation is a useful means of estimating the diffusion zone thickness. The diffusion zone is approximated by a triangle of height $(\bar{C}_1^{\gamma\alpha} - C_1^{\gamma\alpha})$ and width ΔS is determined by an overall mass balance of the form

$$V_p (C_1^{\alpha\gamma} - \bar{C}_1^{\alpha\gamma}) = \tfrac{1}{2} A_p \Delta S (\bar{C}_1^{\gamma\alpha} - C_1^{\gamma\alpha}) \quad \ldots\ldots\ldots\ldots\ldots\ldots\ldots\ldots (8.21)$$

where A_p = Ppt area

V_p = Ppt volume

ΔS = Average diffusion zone thickness.

$$V = \frac{2D_{22}}{\Delta S} \qquad \text{where } \frac{ds}{dt} = V$$

$$\text{or } \Delta S = \frac{2D_{22}}{V} \quad \ldots\ldots\ldots\ldots\ldots\ldots\ldots\ldots\ldots\ldots (8.22)$$

The criteria to distinguish between NPLE and PE is based on the value of ΔS. If ΔS is more than 50 A^0, the precipitate (i.e. α) grows under no-partition local equilibrium condition. Local equilibrium is no longer established at the interface if the concentration profile (i.e. ΔS) in the parent phase ahead of an advancing interface becomes less than 10 A^0. Under such circumstances, the growth of α is believed to occur by para-equilibrium mechanism. Hence it is conceivable that at high supersaturation, the thickness of the diffusion zone becomes thin enough to lose its physical

existence and the growth will occur under para-equilibrium mechanism.

8.4 Calculation of Parabolic Growth Rate using para-equilibrium model: The position of the α/γ interface as a function of time, under carbon diffusion-controlled mechanism, can be described by the equation[5, 27].

$$q = \alpha_1 t^{\frac{1}{2}} \quad .. \quad .. \quad .. \quad .. \quad .. \quad .. \quad .. \quad .. \quad .. \quad .. \quad .. \quad (8.23)$$

where q = Half thickness of the allotriomorphic ferrite

t = Time in seconds

α_1 = Parabolic growth rate constant for one dimensional growth.

α_1 is obtained by solving the following equation:-

$$\left\{2\,(C^{\gamma\alpha} - \bar{C})/(C^{\gamma\alpha} - C^{\alpha\gamma})\right\}\left\{(\underline{D}/\pi)^{\frac{1}{2}}\right\} = \alpha_1\left\{\exp \alpha_1^2/(4\underline{D})\right\}\left\{1 - \mathrm{erf}\left[\alpha_1/(2\underline{D}^{\frac{1}{2}})\right]\right\} \quad (8.24)$$

where $C^{\gamma\alpha}$ = Para-equilibrium carbon content in the austenite (γ) which is obtained from the line Ae_3' are given in Appendix II (Ref[28-30]) The Ae_3' line represents $\gamma/(\gamma+\alpha)$ para-equilibrium-phase-boundary.

$C^{\alpha\gamma}$ = Para-equilibrium carbon content in the ferrite (α). Since 'C' content in α is too small it is obtained by the line Ae_1 of the Fe-C diagram.

$\bar{C}$ = Average carbon content of the alloy.

The term $\underline{D}$ is a weighted average diffusivity of carbon in α and it is given by [15, 27].

$$\underline{D} = \int_{C^{\gamma\alpha}}^{\bar{C}} D\,dx/(\bar{C} - C^{\gamma\alpha}) \quad .. \quad .. \quad .. \quad .. \quad .. \quad .. \quad .. \quad .. \quad .. \quad (8.25)$$

where D is the diffusivity of carbon in γ. The value of D depends upon the amount of carbon in austenite as well as the substitutional alloying concentration[31].

Bhadeshia[32] developed a successful computer program to calculate parabolic growth rate constant under para-equilibrium condition. The program

has been extensively used in the present investigation to calculate parabolic growth rate constant under PE mechanism for Fe-C-X alloys.

8.5 Experimental Results on Fe-3.05Cr-0.11C (wt%) alloy: The details of the heat treatment are given in chapter 2 section 3.3.

Isothermal transformation at 750°C showed that the nucleation of α started heterogeneously at prior austenite grain boundaries with subsequent growth occurring rapidly along the grain-boundaries, resulting in a thin layer (Fig 8.12). This morphology of the ferrite is referred to as allotriomorphic ferrite. Optical microscopy revealed that the observable nucleation of α at 750°C started only after 40 seconds. However, dilatometry experiments were done at several isothermal temperatures to determine the exact incubation period and the time taken to achieve 95% of equilibrium volume fraction of the transformation. The results from the dilatometry experiments will be discussed later on in this section. The α/γ interface of the allotriomorphic ferrite appeared ragged in some cases Fig. 8.13. Allotriomorphic ferrite which formed at grain boundary triple junctions appeared more or less triangular in the plane of observation Fig 8.14. Two out of the three interfaces appeared planar (i.e. semi-coherent) in such allotriomorphs. During the early stages of transformation no carbide was detected even using TEM. Prolonged transformation, (i.e. 750°C/3 min) showed the precipitation of carbide. (Fig. 8.15.) In order to determine the parabolic growth rate the maximum half-thickness (t/2) of the allotriomorphic ferrite was measured at successive intervals of time. The parabolic growth rate constant at 750°C was 0.8 $\mu m/\sqrt{sec}$ (see Fig. 8.16).

Isothermal transformation at 700°C again showed heteregeneous nucleation of α at the prior austenite grain-boundaries with subsequent allotriomorphic growth Fig. 8.17. Evidence of interface pinning was also noticed (Fig 8.18) frequently along the interface at this temperature. Occasionally evidence of Widmanstätten ferrite was noticed along highly curved grain boundaries (Fig 8.19.) Fig. 8.16 shows the plot of maximum half thickness (t/2) vrs square root of time. From the slope of this curve the parabolic growth rate constant was determined as 0.3 $\mu m/\sqrt{sec}$. TEM showed that the allotriomorphs formed during the early stages of transformation were free of carbide (Fig. 8.20)

With further decrease in isothermal temperature (i.e. 650°C) a slight decrease in the parabolic growth rate was observed as shown in Fig. 8.16. Parabolic growth rate constant (α) estimated in this case was 0.225 $\mu m/\sqrt{sec}$. Optical micrographs taken at successive intervals of time are shown in Fig. 8.21 to Fig. 8.22. Fig. 8.20 shows faceted allotriomorphs while Fig. 8.21 serrated interface. Along some highly curved grain-boundaries Widmanstätten ferrite was observed Fig. 8.23. The Widmanstätten ferrite plates appeared

to grow along the martensite trace direction. No evidence of carbide precipitation was recorded during the early stage of transformation Fig. 8.24. However the allotriomorph appeared to be highly faceted in some cases.

When the specimens were isothermally transformed at 610°C, they showed an increasing tendency to form Widmanstätten ferrite. However, the Widmanstätten ferrite always showed a tendency to form on highly curved grain boundaries. (Fig. 8.25 and Fig. 8.26.) The plates appeared to grow in martensitic trace direction. Evidence of faceting on the planar γ/α interface was noticed in many cases Fig. 8.27. TEM shows again carbide free ferrite Fig. 8.28. Evidence of interface pinning is shown in Fig. 8.29. Again the curve was plotted between maximum half-thickness vrs square root of time to determine the parabolic growth rate constant. The value thus obtained was 0.28 $\mu m/\sqrt{sec}$.

The value of the parabolic growth rate constant determined at each temperature was plotted against temperature and compared with the theoretically calculated values based on the paraequilibrium model. The plot is shown in Fig. 8.30.

The volume fraction (V_α) at each isothermal temperature was measured and plotted against time Fig. 8.31. The volume fraction was measured by image analysis on a Quantimet 720 machine. In order to reduce the statistical errors 10 fields were measured from each specimen.

In order to construct a TTT diagram, dilatometry experiments were conducted in the temperature range of 600°C to 800°C. The graph was plotted between relative length change ($\frac{\Delta L}{L}$) vrs time for each isothermal temperature (Figs. 8.32a to d). From this graph, the times for start of transformation (Ts) and termination of transformation were obtained and used for construction of the TTT diagram (Figure 8.33). The TTT diagram thus constructed was compared with the calculated TTT diagram. (Fig. 8.34.) The details for calculations of TTT have been discussed in the Appendix I. The partitioning behaviours of the substitutional alloying element (Cr) over a range of isothermal transformation temperatures was studied using the ISI (Scanning electron microscopy with microanalysis facilities). ZAF-4/ FLS program was used to determine quantitatively the partitioning of Cr in α and γ More than 5 readings were taken from each specimen. Practically no evidence of bulk-partitioning was observed. Micro-analysis results are shown in Table 8.1.

In order to obtain a measure of the nucleation rate, the number of ferrite allotriomorphs observed per unit area (N_α) was plotted against time for a range of isothermal temperatures (i.e.750°C to 610°C). The plot is shown in Fig. 8.35. The slope of this curve gives a measure of the nucleation rate $(\frac{dN}{dt})$.

8.6 Discussion: The parabolic growth rate of grain boundary allotriomorphic ferrite over a range of temperature was calculated on the basis of the paraequilibrium model. The details of the calculations are explained in the introduction of this chapter. The calculated growth constants are compared with those experimentally determined (see Fig. 8.30) The plot clearly shows significant discrepancies between calculated and measured parabolic growth rate constants, particularly at lower temperatures (610°C to 700°C). Kinsman and Aaronson,[33, 34] Atkinson et al,[35] and Bradley et al,[36] have similarly found that the growth constants of ferrite allotriomorphs are significantly less than those calculated for control by the volume diffusion of carbon in austenite. It is essential to examine in detail the sources of discrepancies in the light of the experimental observations available. Sources of discrepancies may be listed as follows:-

(i) Presence of planar facets (i.e. semi-coherent interface) over a sufficient proportion of the interfacial area of the allotriomorphs: the growth rate constant was calculated with the assumption that the allotriomorphic ferrite is entirely consisted of high energy incoherent γ/α interface which moves normal to itself under diffusion control of carbon in austenite. In the present investigation the allotriomorphic ferrites observed by optical and electron microscopy showed a tendency to develop planar facets (Figs. 8.14, 8.20, 8.24, 8.27). The presence of partially coherent facets at interphase-interfaces between crystals differing in crystal structure. has already been observed and reported[37-40]. These partially coherent boundaries are displaced solely by a ledge mechanism[41, 42]. This means that the interface is stepped and atoms are transferred from one phase to the other only at these steps. Consequently the macroscopic growth of the interface results from the motion of steps such that an element of the interface remains stationary until a step passes over it, after which the interface advances through a distance equal to the step height. For these interfaces, the growth of the ferrite will be controlled by the rate of step motion as well as the ability to nucleate steps which in turn may be controlled by the volume diffusion process. Except sometimes during early stages of growth, facets migrate less rapidly than disordered-boundaries under given conditions of alloy composition and reaction temperature.[42] The presence of planar facets over a sufficient proportion of the interfacial area of the allotriomorphic ferrite is believed to be one of the reasons responsible for discrepancies.

(ii) Pinning of the γ/α interface by carbide precipitation:- "Interphase-interface precipitation" is now a well established mode of precipitation during the $\gamma \rightarrow \alpha$ transformation of alloy steels[43]. It is believed that these interphase-carbides locally pin the γ/α interface and hence restrict its mobility[44, 45, 46]. However, interphase precipitation may not have any significant effect on the mobility of the semi-coherent planar interfaces because such interfaces are solely displaced by a ledge mechanism and ledges themselves remain unaffected by carbide precipitation due to their high mobility[47]. In the case of interphase precipitation at incoherent γ/α interfaces significant retarding effect on their mobility is expected due to the pinning action of the carbides on these interfaces.

The mobility of the γ/α interface is similarly restricted by the presence of a fine dispersion of carbide in the austenite[44]. By keeping the specimen in the austenite + carbide phase field, fine dispersions of carbide in the austenite can easily be achieved. On subsequently holding the specimen in the $\gamma+\alpha$ phase field, these carbides would be expected to restrict the mobility of the γ/α interface through a pinning action.

Evidence of interface pinning was noticed (Figs. 8.18, 8.21, 8.29) over the entire range of temperature. It can be anticipated that either interphase precipitation at incoherent γ/α interfaces or the fine dispersion of carbide in the matrix (i.e. austenite) is responsible for pinning. TEM investigation did not reveal any interphase-precipitation during the early stages of transformation throughout the temperature range. Some carbides, probably Cr_7C_3[48] (which is h.c.p) were observed during the later stages of transformation Fig. 8.15. These carbides have formed by a mechanism of co-operative growth. Any effect of interphase precipitation on the mobility of γ/α interfaces is thus ruled-out in the present case. The protuberances/ serrations observed are mainly due to pinning by a fine dispersion of alloy carbides in the matrix. The restricted mobility of the γ/α interface due to the pinning action is considered as one of the major factors responsible for slower growth rate than the predicted one.

(iii) Solute-drag-like effect: Another suggestion for slower than the anticipated growth rate is solute drag like effect.[33,42,49] The substitutional alloying element 'Cr' is believed to segregate to austenite/ferrite interfaces during growth, through a "sweeping up" of Cr- atoms, and not by its diffusion through austenite. The segregated 'Cr'-atoms alter the activity of carbon in the austenite which is in contact with these interfaces[50], thereby altering the carbon concentration profile in the austenite ahead of the interface. The interface migration rate is affected by a change in the carbon concentration profile due to presence of 'Cr'-atoms at the

interface. If the substitutional solute atom (such as Mn, Cr i.e. say X in Fe-C-X alloy) reduces the activity of carbon in austenite at the interface, the carbon concentration gradient in the austenite will reduce which in turn will result in a slow growth rate. On the other hand, the opposite effect on growth kinetics is expected if the activity of carbon in the austenite is increased due to alloy (e.g. Si) segregation at the interface. This is referred to as the inverse "solute-drag-like effect",[51] the change in carbon-activity at the two-phase boundary can be estimated from the equilibrium partition coefficient $K^{\gamma/\alpha}$ of the element between the two phases[52].

$$\ln a_C^1/a_C^0 = - \frac{K^{\gamma/\alpha}\left(X_{Fe}^{\alpha} - X_{Fe}^{\gamma}\right)}{X_C^{\gamma} - X_C^{\alpha}} X_M^{\alpha} \quad \ldots\ldots\ldots\ldots\ldots\ldots\ldots\ldots (8.26)$$

where a_C^0 = Activity of carbon without alloy content.

a_C^1 = Activity of carbon with alloy content.

X_M^{α} = Bulk alloy content.

The amount of solute segregating at the interface can be estimated from the modified McLean adsorption[47] expression:-

$$C_{Cr}^{\gamma/\alpha} = \frac{C_{Cr} e^{\Delta G_b/RT}}{1 - C_{Cr} + C_{Cr} e^{\Delta G_b/RT}} \quad \ldots\ldots\ldots\ldots\ldots\ldots\ldots\ldots (8.27)$$

where $C_{Cr}^{\gamma/\alpha}$ = Concentration of Cr at the γ/α interface

C_{Cr} = Bulk concentration of 'Cr'.

ΔG_b = Absorption free-energy of Cr to the γ/α interface.

Bhadeshia[16] in his recent review on "Diffusional Formation of Ferrite in Iron and its Alloys" has raised doubts about the solute-drag-like effect on growth kinetics of ferrite. He pointed out the segregation profile of 'X' solely confined within the interface is an unrealistic assumption particularly when the interface is moving. He supported his view using Cahn's[53] theoretical work which suggests that the solute profile in the vicinity of the moving interface always extends into the region beyond the interface. Secondly, even though the concentration of X in the interface may be different than in the bulk of the austenite, its influence on the activity of carbon in austenite should be identical to that of the X-atoms present

in the bulk of the austenite due to identical partial molar free energy of X-atoms in both the interface as well as in the austenite. Otherwise, the concentration of carbon at the interface must increase to maintain this equality of partial molar free energies. This hypothesis contradicts the one proposed by Kinsman and Aaronson[33].

(iv) Interaction of clusters with interfaces:-

Sharma and Purdy[54] proposed that the formation X-C clusters in the austenite may be responsible for special solute-drag effects. Additional driving force will be needed to strip these clusters from their carbon atmospheres as the interface moves across them. They proposed that the formation of clusters would be difficult at lower temperatures since the ability to form clusters depends on the volume diffusion in the austenite. But at the same time they also proposed that these clusters would have a significant drag effect at low temperatures which is contradictory to the fact that cluster formation is difficult at lower temperatures. Activity coefficient also plays an important role in formation of clusters. In case of 'Cr' or Mo, the activity coefficient is less than unity, implying that these elements do not tend to form clusters in austenite[55].

(v) Error due to the stereology of grain-boundary allotriomorphs:-

To minimize the stereological error, the specimens were austenitized at 1250°C for one hour and fifteen minutes to develop a very large austenite grain size in which austenite boundaries lie normal to the broad faces of the specimens. This technique was suggested by Boswell et al[56]. It is most likely that the γ/α interface formed during transformation lies parallel to the original austenite boundaries. Under such circumstances, the broad face of the allotriomorphic ferrite would represent its true thickness.

However this method (i.e. optical metallography) prevents the recording of the progress of an individual allotriomorphic ferrite during isothermal transformation since measurements are taken on different specimens isothermally transformed for different time periods. In each case, the thickest allotriomorphs were measured. This could lead to significant errors if the incubation period for the nucleation of α is relatively large. The incubation periods of this alloy over a range of temperature were relatively small (Fig 8.33) to have any significant effect.

Micro-analysis: Micro-analysis did not reveal any bulk-partitioning of alloying element 'Cr' over the entire range of investigation (i.e. 750°C to 610°C) between the austenite and ferrite (Table 8.1). This result ruled out the possibility of the $\gamma \rightarrow \alpha$ transformation taking place under equilibrium conditions. But it is thermodynamically possible to achieve the equilibrium conditions at the temperatures very close to the Ae_3 temperature. The alloying element may undergo partitioning towards the equilibrium tie line even at high supersaturations but perhaps at a very late stage of transformation.[15] The partitioning of a substitutional alloying element such as 'Cr' at relatively low supersaturation occurs at a rate-controlled by the diffusivity of the alloying element and hence it is extremely slow.[3,4,10] The methods for calculating growth rate under equilibrium conditions have been discussed by several workers.

The absence of bulk-partitioning between ferrite and austenite points out two mechanisms by which the high supersaturation no-partition reaction may occur.[3,4,9,49,52] These are the no-partition local equilibrium (NPLE) mechanism and the para-equilibrium (PE) mechanism. Both mechanisms have been examined in detail in section 8.2 and 8.3. Briefly, the PE reaction refers to a situation where the alloying element, 'X' remains uniform on both sides of the growing γ/α interface and the reaction occurs by pure diffusion control. In NPLE mechanism, there is essentially no redistribution of the alloying element between the α and the γ-phase but local equilibrium at the γ/α interface is maintained according to a certain tie line in the $(\alpha + \gamma)$ two-phase field.

From the micro-analysis results, it is rather difficult to decide whether the transformation occurred by the PE mechanism or NPLE. It has been suggested that during the early stages of growth period following the nucleation event, local equilibrium does not exist at the α/γ interface and the growth is entirely interface controlled. This initial period is presumably of short duration and soon the paraequilibrium condition is follwoed by local equilibrium at the interface. As the ferrite grows in size with increasing time at the transformation temperature the PE state passes through an infinity of thermodynamically undefined non-equilibrium states and finally gives way to the local equilibrium state.[3]

Aaronson and Domain[57] studied the partitioning behaviour of the substitutional alloying element 'X' during $\gamma \rightarrow \alpha$ transformation in Fe-C-X alloys (where X = Si, Mn, Ni, Cr, Mo, Co, Al, Cu, or Pt). They could not detect the bulk-partitioning of alloying element X during the early stage at high undercooling which indicates the growth of α either by NPLE or PE mechanism.

Recently Bradley and Aaronson[47] studied the growth kinetics in Fe-C-X alloys (where X = Ni, Cr, Mn, Si). The parabolic growth-rate constant of all the alloys studied, except Si-containing steel, showed similar disagreement between the experimentally determined value and the theoretically calculated one assuming paraequilibrium model or NPLE. However, their calculations of parabolic growth constants are incorrect since they intersect at a certain temperature giving the same value by two different mechanisms. This seems to be thermodynamically inconsistent because it contradicts the facet that the PE and NPLE modes are mutually exclusive and PE growth always occurs at a slower rate compared with NPLE growth.

The nucleation of allotriomorphic ferrite predominantly occurred at grain corners, edges and faces over a range of temperatures (i.e. from 750^{o}C down to 600^{o}C) because of reduction in the overall increase in surface energy by eliminating part of the grain boundary surface area.[58] The mis-orientation of the grain-boundary also affects the sequence of nucleation events. The ferrite allotriomorphs are nucleated first on high energy grain-boundaries,[59] while the other relatively low energy boundaries are favoured for nucleation during subsequent stages of transformation. The absence of allotriomorphic ferrite on many grain-boundaries during the early stage of transformation is attributed to this kind of effect. Soon after nucleation the allotriomorphs showed a tendency for rapid growth along the austenite grain-boundaries but thickened very slowly. The high rate of lengthening, compared with that of thickening, is mainly due to enhanced diffusion due to the point effect at the tip of the allotriomorphic ferrite. At a temperature close to Ae_3 both the rate of lengthening and thickening are reduced as expected due to a low driving force With decreasing isothermal temperature, the allotriomorphs showed an enhanced tendency for lengthening compared to that of thickening. In other words, the aspect ratio (i.e. thickness to length) of the allotriomorph is found to decrease with decreasing temperature. Due to rapid lengthening, these allotriomorphs soon impinge with each other and form networks of varying completeness about the austenite grains. Since no α/α boundaries are observed on these networks of ferrite, it is anticipated that either a single ferrite nuclei forms and grows to cover the entire boundary (which is an extreme and rare case), or similarly oriented nuclei link up to form continuous grain boundary layers.[44] The limiting interfaces of the ferrite are not regular and are strongly influenced by the presence of the boundary. The symmetry of its internal structure may be quite different from that of the outer limiting interface.[16] The various morphologies which develop over a range of temperature follow the trend described by Dubé[60] and extended by Aaronson.[41] The details of the Dubé s[60] morphological classifications are discussed in the Chapter II.

Our experimental results show a constant rate of nucleation during early stage of transformation at each isothermal temperature. In order to explain the transformation kinetics it is essential to consider the well known Avrami[67] equation.

$$N = N_o \exp(-v_1 t) \quad \ldots\ldots\ldots\ldots\ldots\ldots\ldots\ldots\ldots\ldots \quad (8.30)$$

and the nucleation rate

$$\frac{dN}{dt} = N_o v_1 \exp(-v_1 t) \quad \ldots\ldots\ldots\ldots\ldots\ldots\ldots\ldots\ldots\ldots \quad (8.31)$$

where N_o = No of the nucleation sites (g.b) per unit volume present initially.

N = No of the nucleation sites available after time 't'.

v_1 = Frequency factor which gives the rate at which an individual site becomes a nucleus.

In the our case N is constant in all the cases (i.e. no of austenite grain boundaries/volume is constant since the austenitizing conditions are same. Hence there must be a significant difference in the values of v_1 i.e. rate at which an individual site becomes a nucleus. Thus it is anticipated that the value of v_1 is gradually reduced with increasing temperature due to decreased driving force (i.e. with decreasing undercooling, the driving force for transformation is also decreased).

The value of $\frac{dN}{dt}$ need not be constant throughout the isothermal reaction period. During the latter stage of transformation the value of $\frac{dN}{dt}$ may drop down primarily due to consumption of nucleation site by allotriomorphic growth[68] and secondly due to mutual impingement of regions transforming from separate nuclei[69]. Gradual drop in $\frac{dN}{dt}$ has been recorded during the later stage of transformation at each temperature (Fig. 8.35).

Figure 8.31 shows plot of V_α vrs time (t). The plot shows again that $\frac{dN_\alpha}{dt}$ may decrease during the latter stage of transformation due to mutual impingement of regions transforming from separate nuclei and also due to gradual exhaustion of available nucleation site[69].

4.7 Conclusions:

1. Thickening of ferrite allotriomorphs occurred at a rate which is approximately proportional to the reciprocal of the square root of time, even when the temperature was as low as 610°C. This indicates that interface motion is diffusion controlled and does not seem to be significantly limited by interface process for temperature range of 750°C to 610°C.

2. Discrepancies between the experimentally determined value of parabolic growth rate constants and theoretically determined value based on the PE mechanism have been attributed to the presence of facetting, pinning of the γ/α interface by carbide, the possibility of growth by NPLE and perhaps a drag, interaction of clusters with interfaces and stereological error.

3. On the basis of micro-analysis results, it is not possible to prove conclusively whether the growth occurred by paraequilibrium or no partition local equilibrium mechanism. In principle it is possible to distinguish between these two on the basis of thickness of the diffusion zone. If it is less than 10 A^{o}, para-equilibrium mechanism governs the growth rate. However if it exceeds 50 A^{o}, no-partition local equilibrium mechanism controls the growth rate. These criteria are ad hoc, and need to be supported by experimental evidence.

TABLE 8.1 (cont.)

Temp °C/ Time	Cr in α (wt%)	FI	Cr in γ (wt%)	FI
700 °C/ 80 sec	2.805	0.66	2.441	0.41
	3.73	0.93	2.825	0.38
	3.617	0.78	2.416	0.74
	3.394	0.74	2.92	0.68
	3.293	0.54	2.86	0.76
650 °C/ 40 sec	3.409 (wt%)	1.10	2.898	0.56
	3.489 "	1.05	3.127	1.17
	3.289 "	0.92	3.075	0.86
	3.459 "	0.99	3.174	0.98
	3.048 "	1.36	3.013	0.93
	3.071 "	0.86	2.953	0.77
	3.221	0.96	3.219	1.26
	3.059	0.52	2.939	0.38
	3.087	0.44	2.926	1.62
	2.934	0.69	3.133	1.75
	2.88	1.12		
650 °C/ 60 sec	3.228	2.08	3.728	0.75
	3.146	1.94	3.459	1.29
	2.996	2.34	3.349	2.20
	3.211	2.25	3.369	1.6
	3.104	1.23	3.161	1.03
	2.795	1.31	3.301	1.93
	3.314	4.46	3.3032	1.83
	3.289	5.71	3.384	11.21
	3.423	2.24	3.246	13.94
	3.327	0.79	3.044	15.
	3.209	1.26	3.361	13.10
	3.531	0.55	3.077	5.69
	3.3	2.36	3.288	13.61
	3.433	9.56		
	3.597	8.59		
650 °C/ 120 sec	3.326	1.35	3.202	1.19
	3.359	1.22	3.074	2.11
	3.110	0.89	3.364	1.92
	3.056	1.11	3.578	0.85
	3.098	1.27	3.552	0.68
	3.131	1.11	3.538	0.58
	2.989	0.81	3.154	0.91
	3.115	0.97	2.948	1.31
	3.336	0.65	3.196	0.74
	2.920	0.60	3.009	1.0
			2.986	0.63

TABLE 8.1 (cont.)

Temp °C/ Time	Cr in α (wt%)	FI	Cr in γ (wt%)	FI
650 °C/ 5 min	3.167	2.16	3.034	1.6
	3.288	3.18	3.144	1.15
	3.274	3.03	3.081	2.81
	3.154	2.54	3.755	2.35
	3.210	3.23	2.914	2.30
	3.025	2.31	2.953	2.53
			3.095	2.45
610 °C/ 75 sec	3.13	0.67	2.805	1.85
	3.09	1.19	3.037	1.90
	2.532	1.01	2.575	1.37
	3.03	1.04	2.958	1.05

TABLE 8.2

610°C/ Time	No of α X $10^8/m^2$	650°C/ Time	No of α X $10^8/m^2$
40 sec	0.11 X $10^8/m^2$	20 sec	0.7789 X $10^8/m^2$
50 sec	134.4 X $10^8/m^2$	40 sec	143 X $10^8/m^2$
60 sec	209 X $10^8/m^2$	60 sec	128.2 X $10^8/m^2$
75 sec	185.8 X $10^8/m^2$	2 min	118.2 X $10^8/m^2$
90 sec	238.4 X $10^8/m^2$	5 min	372 X $10^8/m^2$
120 sec	260 X $10^8/m^2$		
700°C/ Time		750°C/ Time	
20 sec	0.667 X $10^8/m^2$	40 sec	0.4145 X $10^8/m^2$
60 sec	137 X $10^8/m^2$	60 sec	137.3 X $10^8/m^2$
80 sec	267 X $10^8/m^2$	80 sec	125.87 X $10^8/m^2$
		45 sec	0.733 X $10^8/m^2$

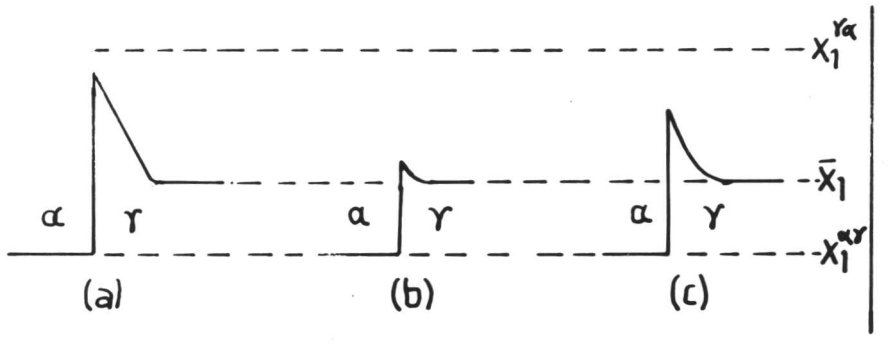

Figure 8.1: Carbon concentration profile at αγ interface moving under (a) diffusion control; (b) interface control; and (c) mixed control.

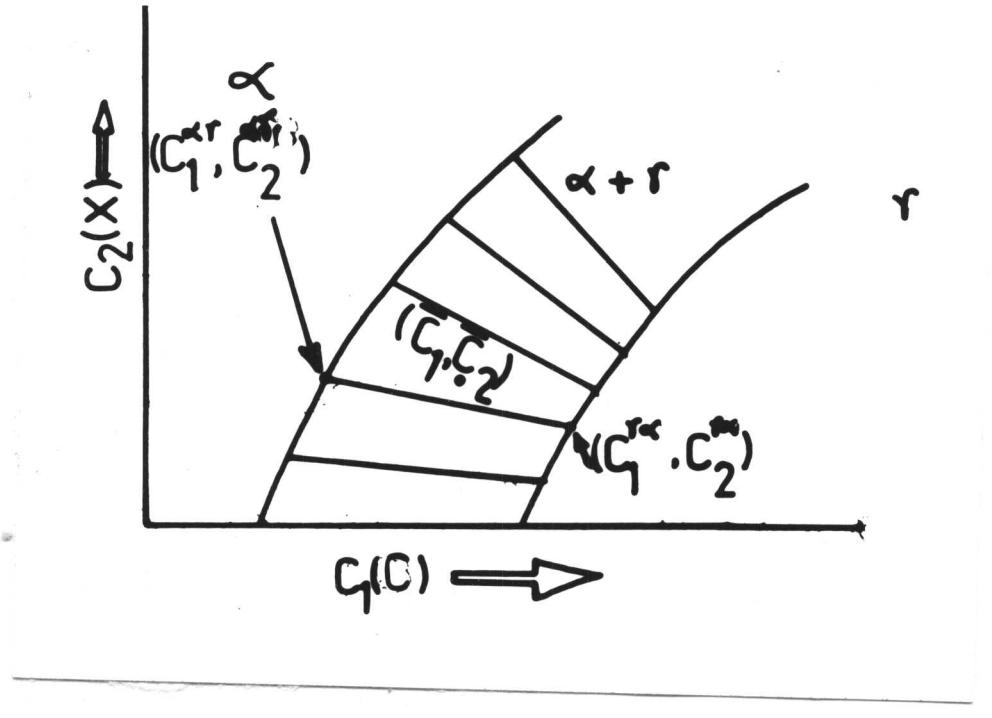

(b)

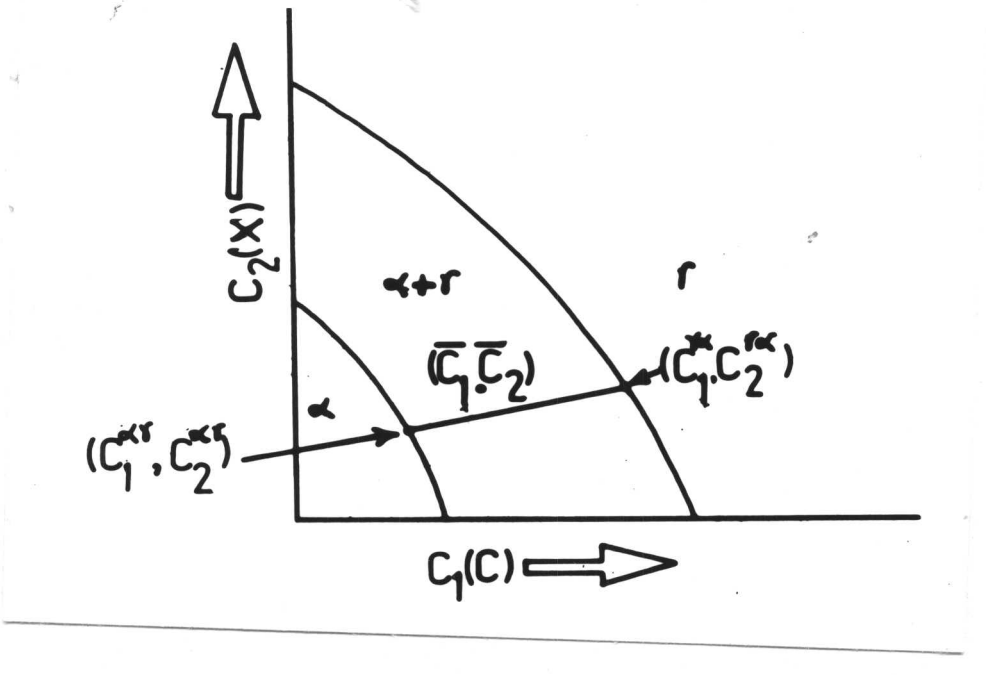

(a)

Figure 8.2: Schematic Fe-C-X isotherms showing (a) X is a γ-stabilizer (b) X is an α-stabilizer.

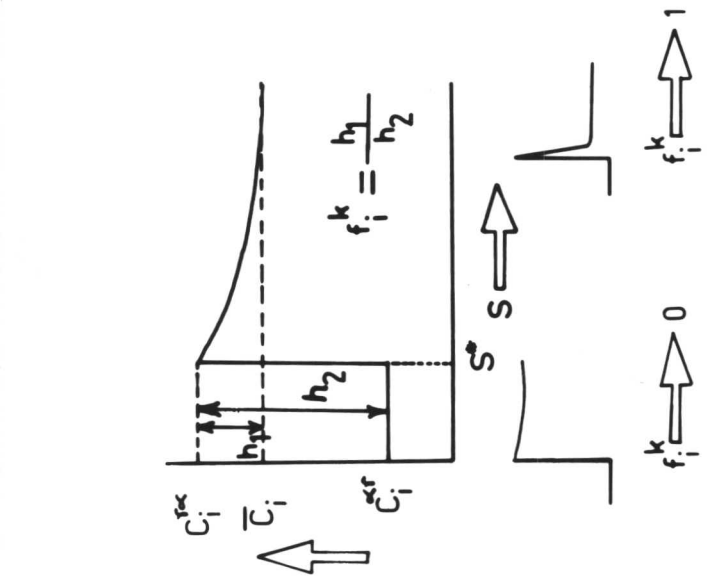

Figure 8.3: Schematic representation of the fractional composition of component i, f_2^k. The concentration distribution corresponds to $f_2^k \to 0$ or 1 are also shown.

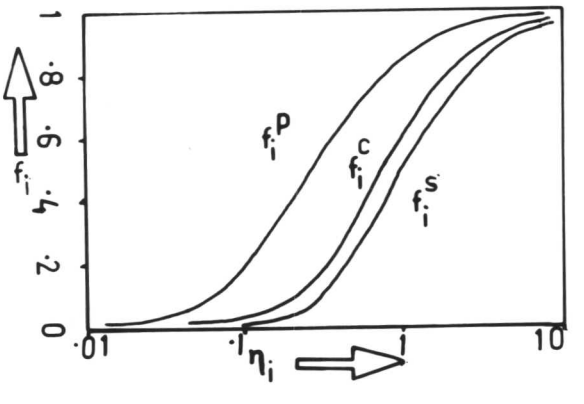

Figure 8.4: The functions f^k (n_i) vs growth rate constant n_i for planar, cylindrical and spherical growth.

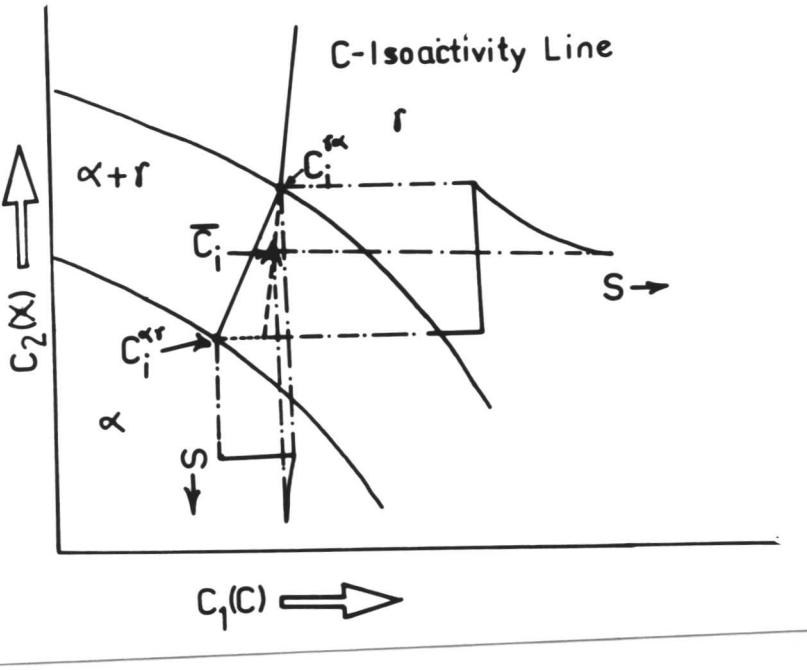

(a)

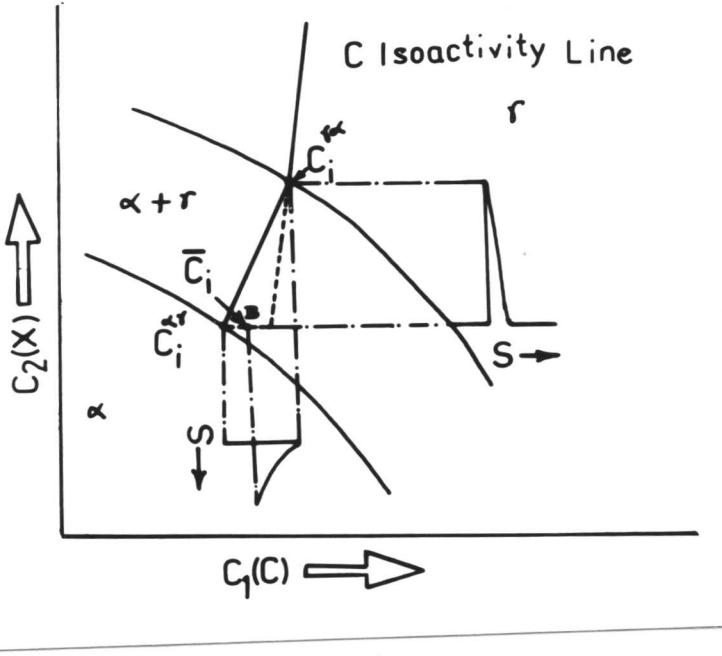

(b)

Figure 8.5: Schematic isotherm and concentration distributions depicting proeutectiod ferrite under local equilibrium at the γ/α interface, uniform C activity in the γ, partition of X between α and γ and (a) growth rate controlled by X i.e. growth via PLE mode. (b) growth rate controlled by C i.e. via NPLE mode.

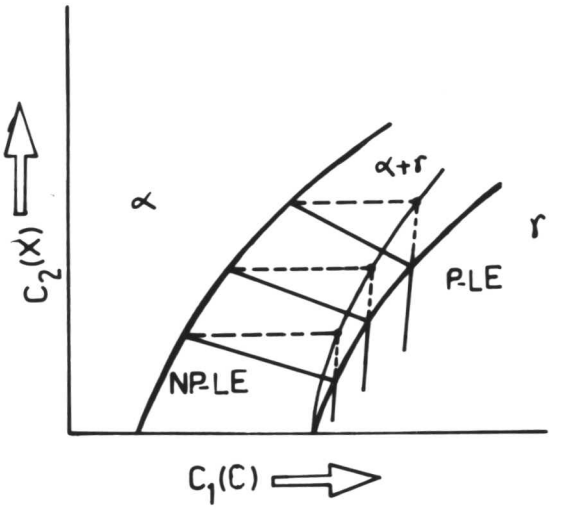

(b)

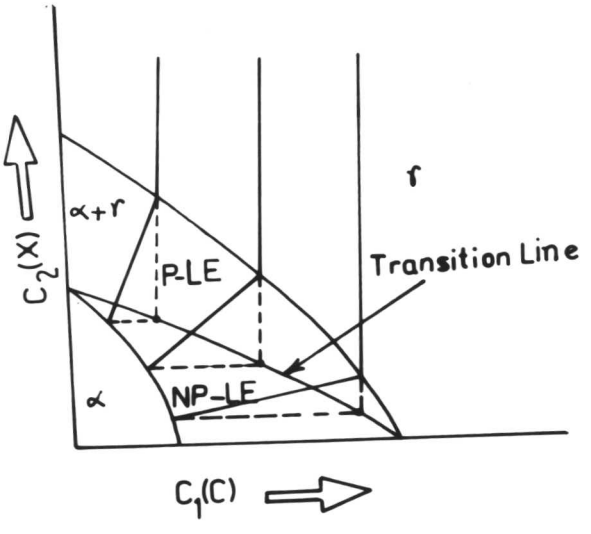

(a)

Figure 8.6: Schematic F-C-X isotherms showing NPLE and PLE regions (a) X is a γ-stablizer (b) X is an α-stablizer.

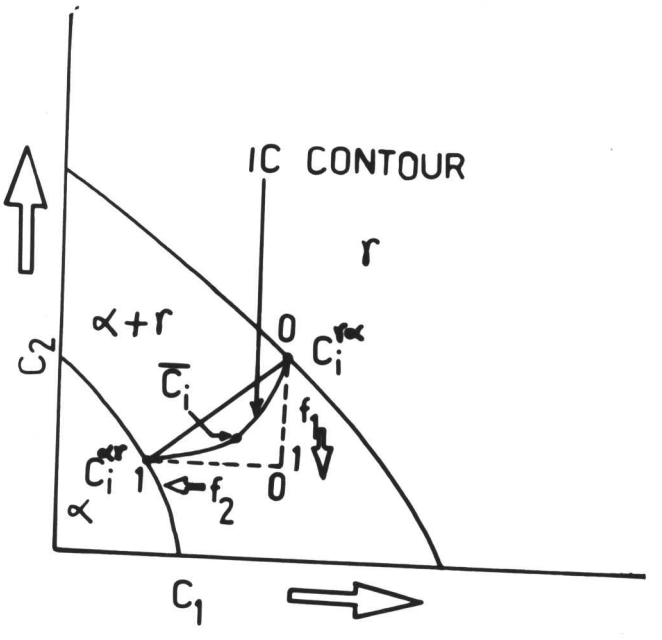

Figure 8.7: Schematic showing IC contour corresponding to a particular tie line.

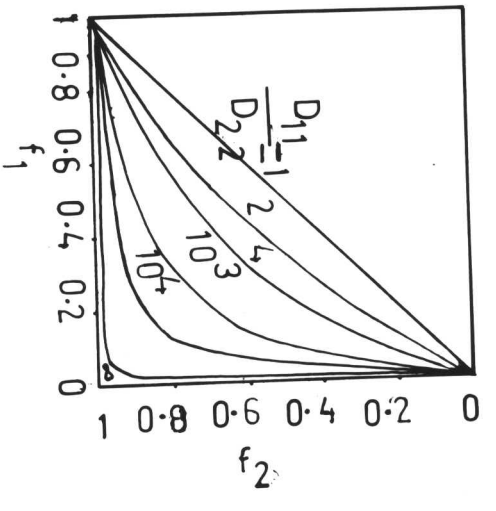

Figure 8.8: IC contours for planar growth with D_{22}/D_{11} = 1, 2, 10^3, 10^4 and ∞.

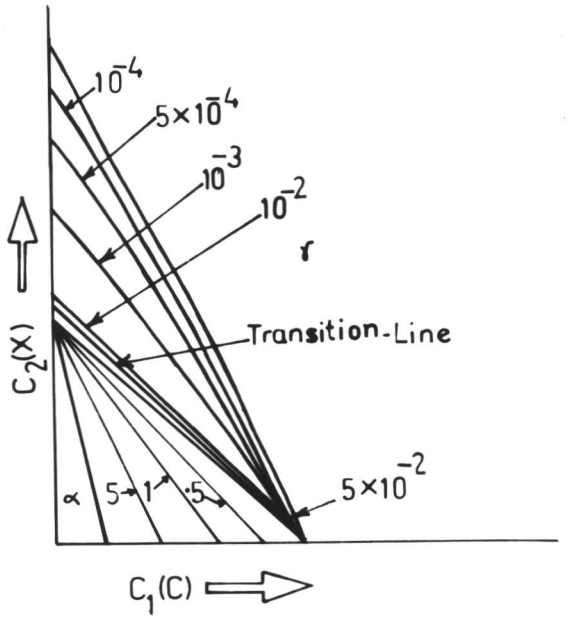

Figure 8.9: Interface velocity (IV) contours for planar precipitate growth in ($\gamma+\alpha$) field. The value of n_i corresponding to each contour is also shown.

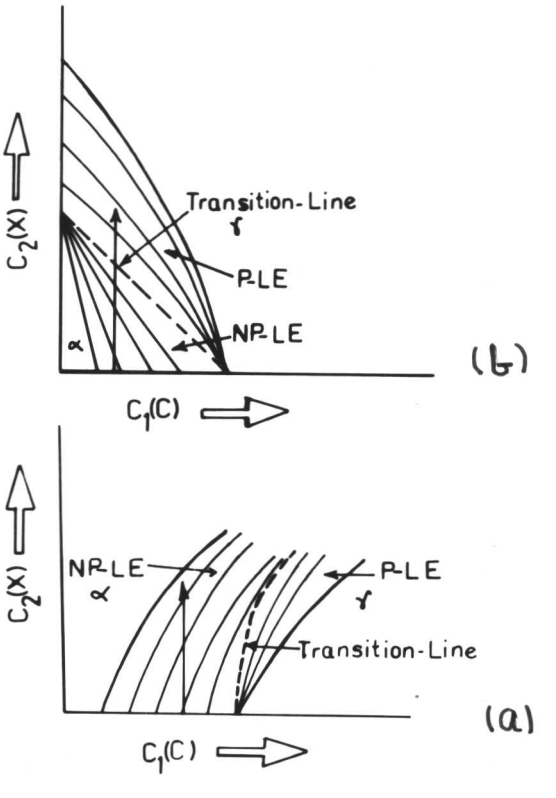

Figure 8.10: Schematic Fe-C-X isotherms showing the transition line (dotted) between NPLE and PLE growth modes and a system of IV contours. (a) X is a γ-stablizer (b) X is a α-stablizer.

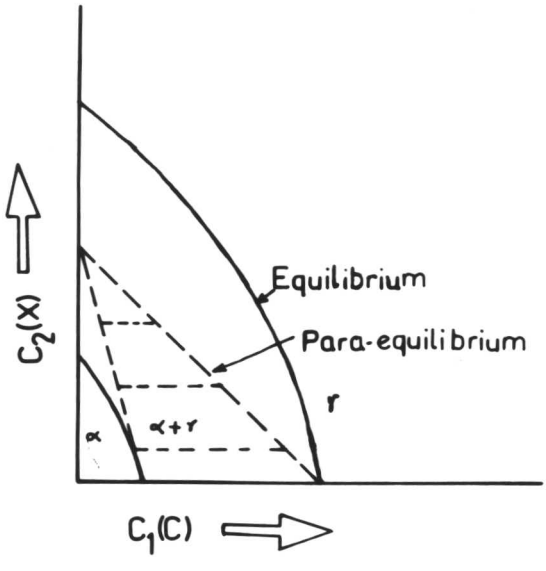

Figure 8.11: Isotherm of ternary phase - diagram. Broken line represents para-equilibrium phase boundary.

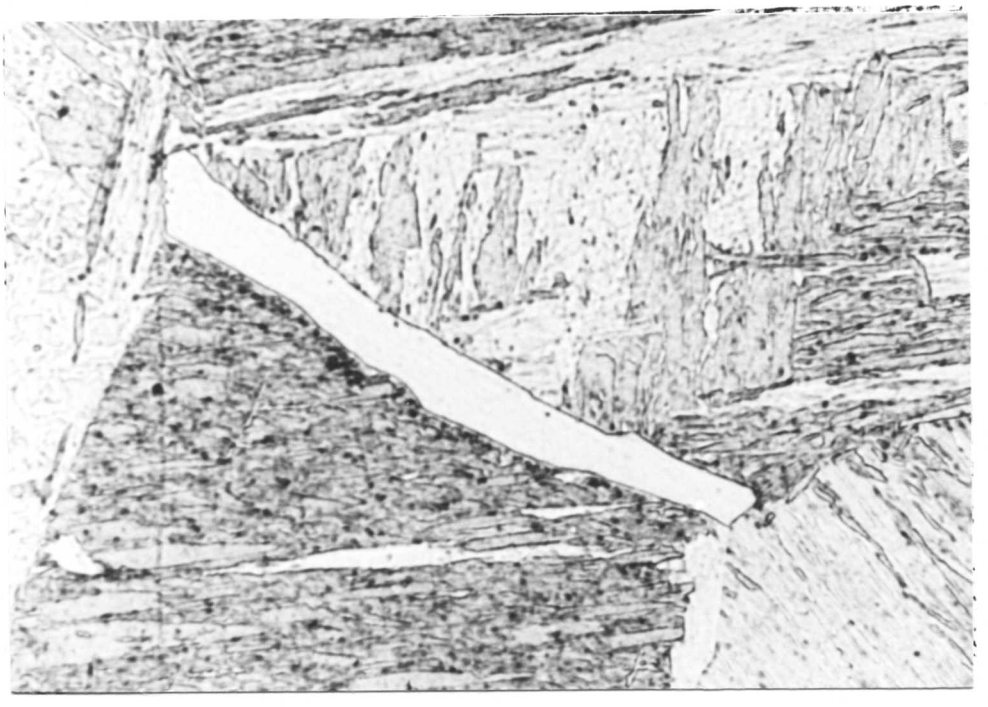

Figure 8.12: Grain-boundary allotriomorphic ferrite growing along the prior austenite grain-boundary. (750°C/40 sec).

Figure 8.13: Allotriomorphic ferrite with ragged interface. (750°C/60 sec).

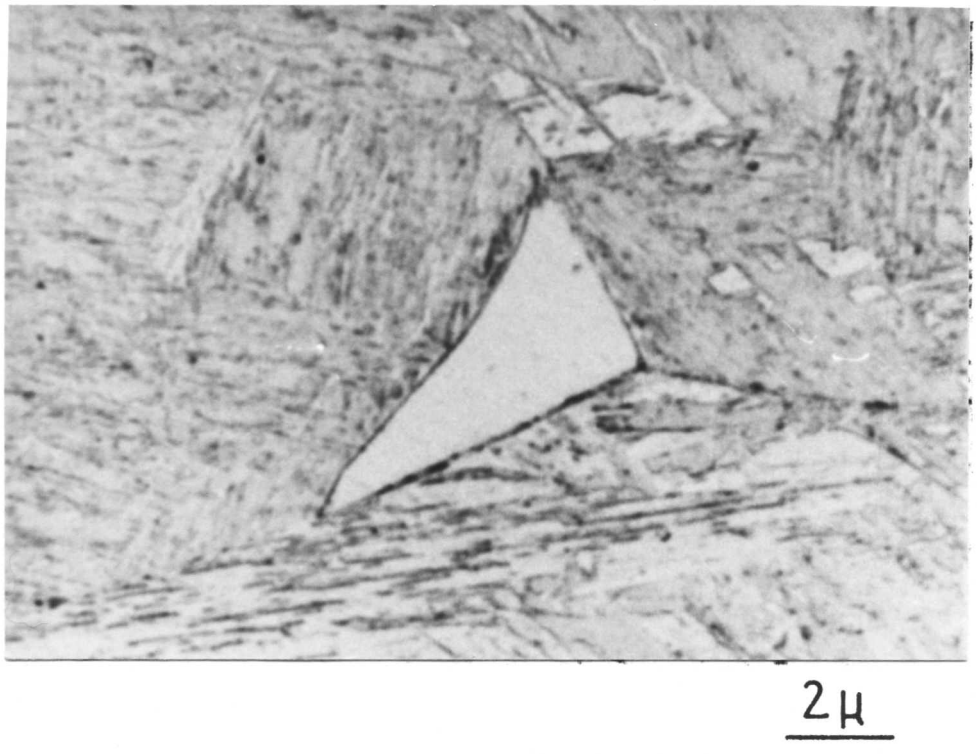

Figure 8.14: Nucleation of α at triple junction of austenite grain boundaries. (750°C/60 sec).

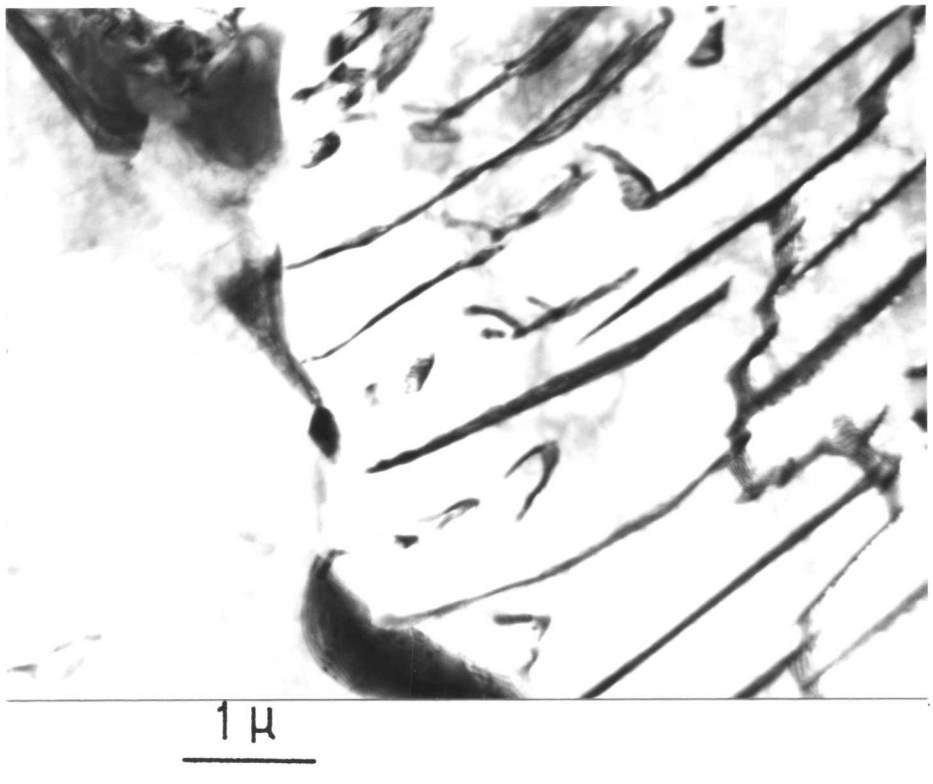

Figure 8.15: Carbide precipitation during latter stage of transformation at 750°C.

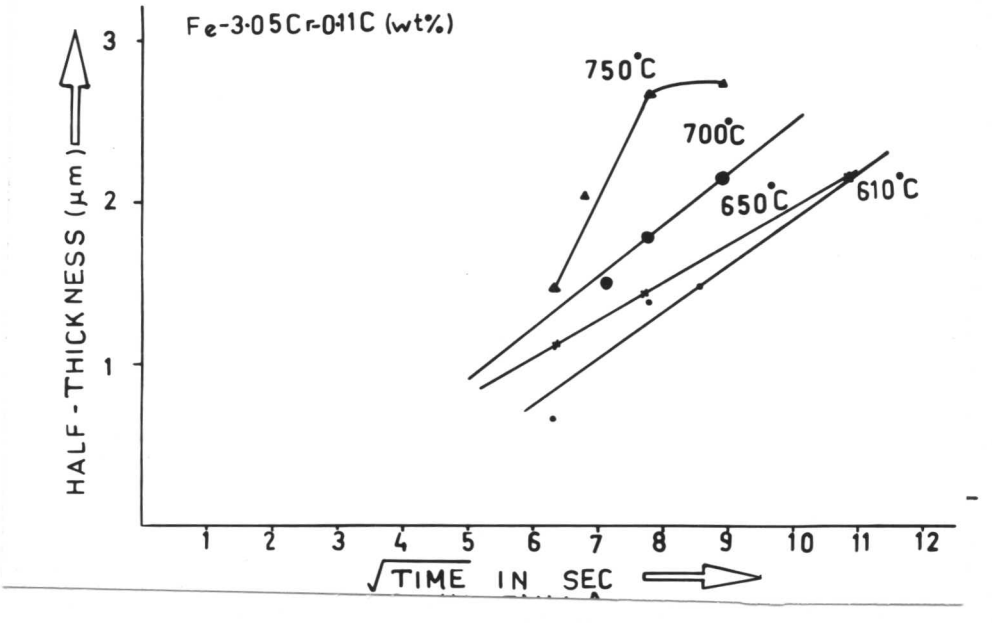

Figure 8.16: Showing a plot between maximum half thickness vs square root of time.

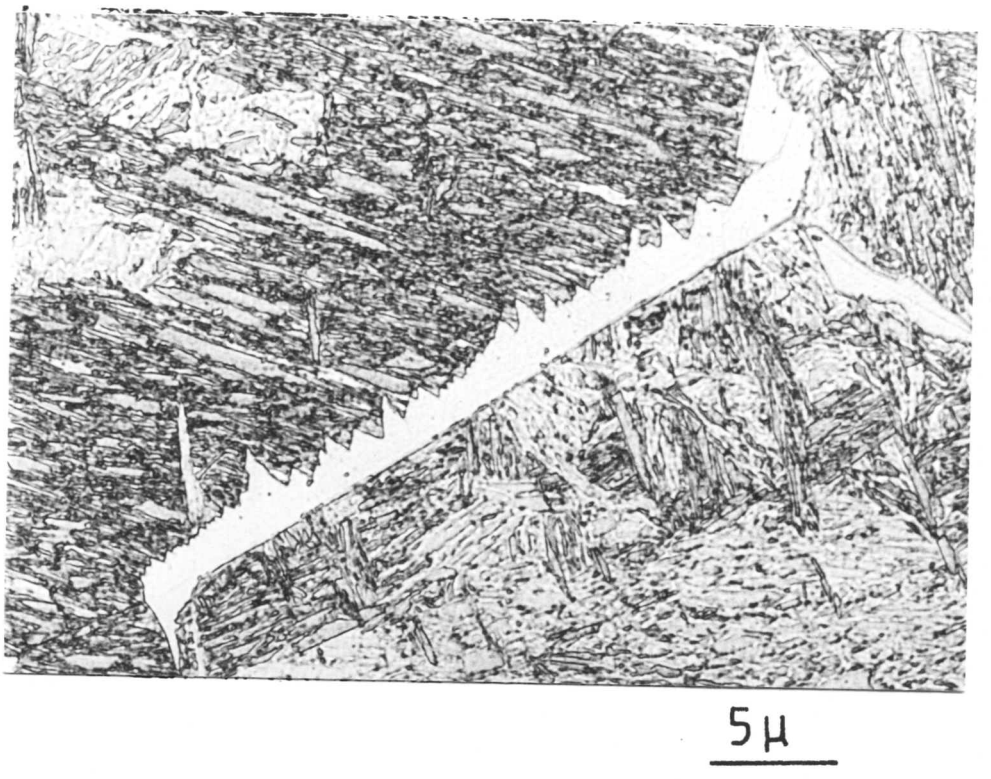

Figure 8.17: Allotriomorphic ferrite along the prior austenite grain-boundaries. (700°C/60 sec).

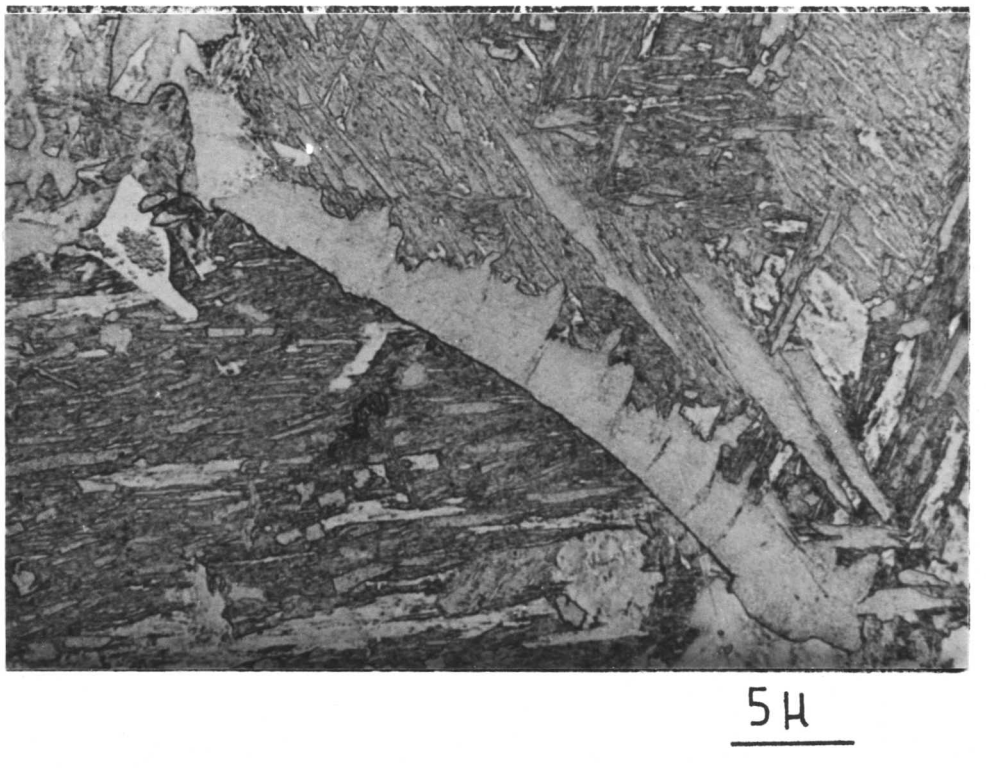

Figure 8.18: Ragged interface developed as a result of pinning by chromium carbides. (700°C/80 sec).

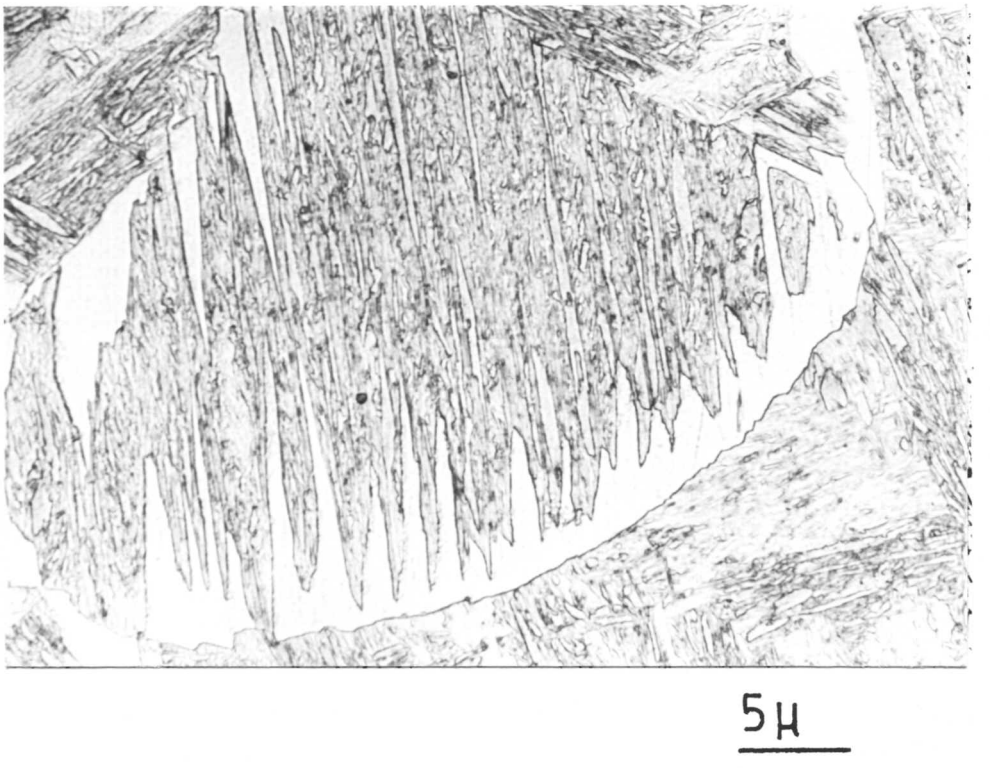

Figure 8.19: Nucleation of Widmanstätten ferrite along highly curved γ-grain-boundary. (700°C/80 sec).

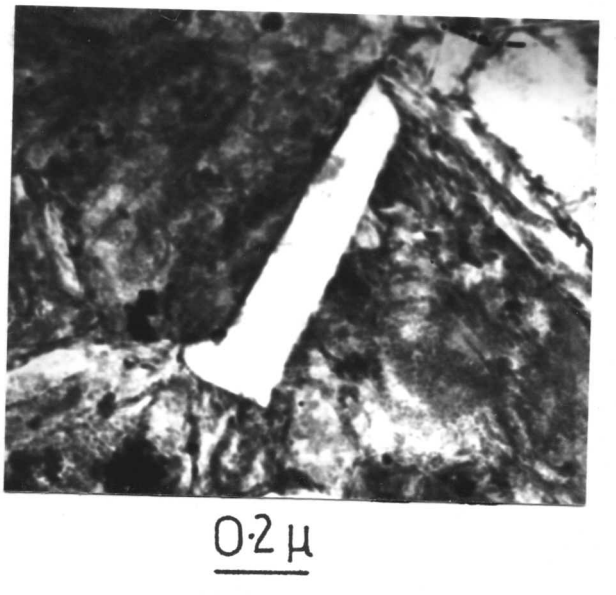

Figure 8.20: Carbide free allotriomorphic ferrite which is highly facetted. (700°C/25 sec).

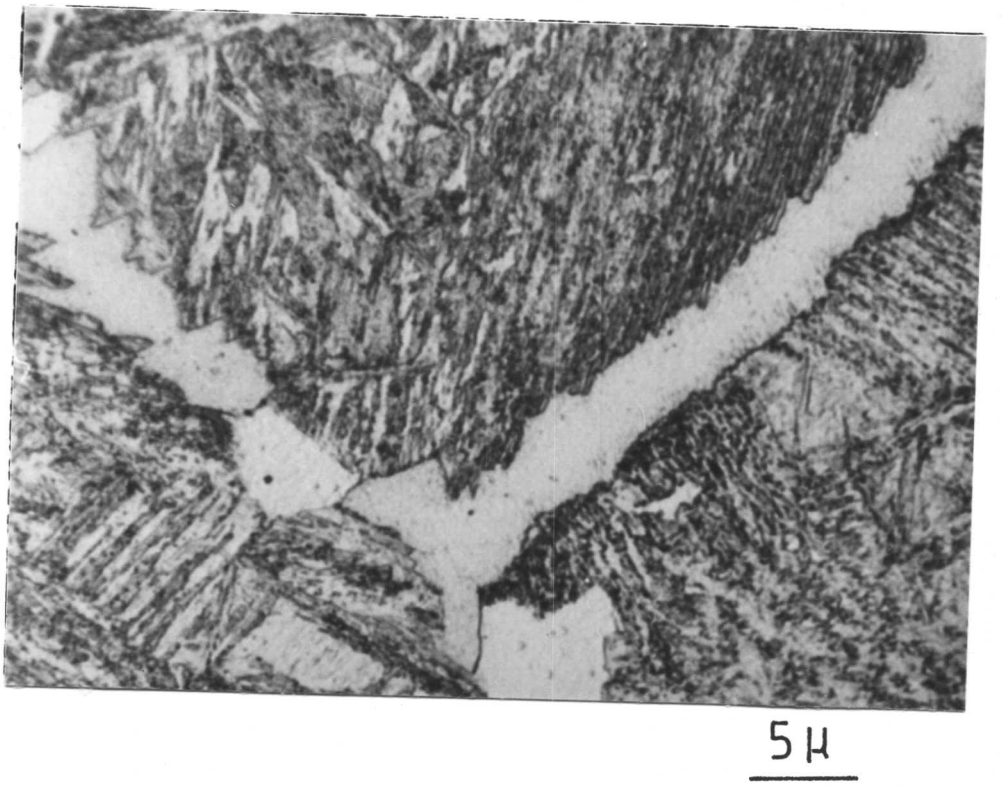

Figure 8.21: Allotriomorphic ferrite with serrated γ/α interfaces. (650°C/ 120 sec).

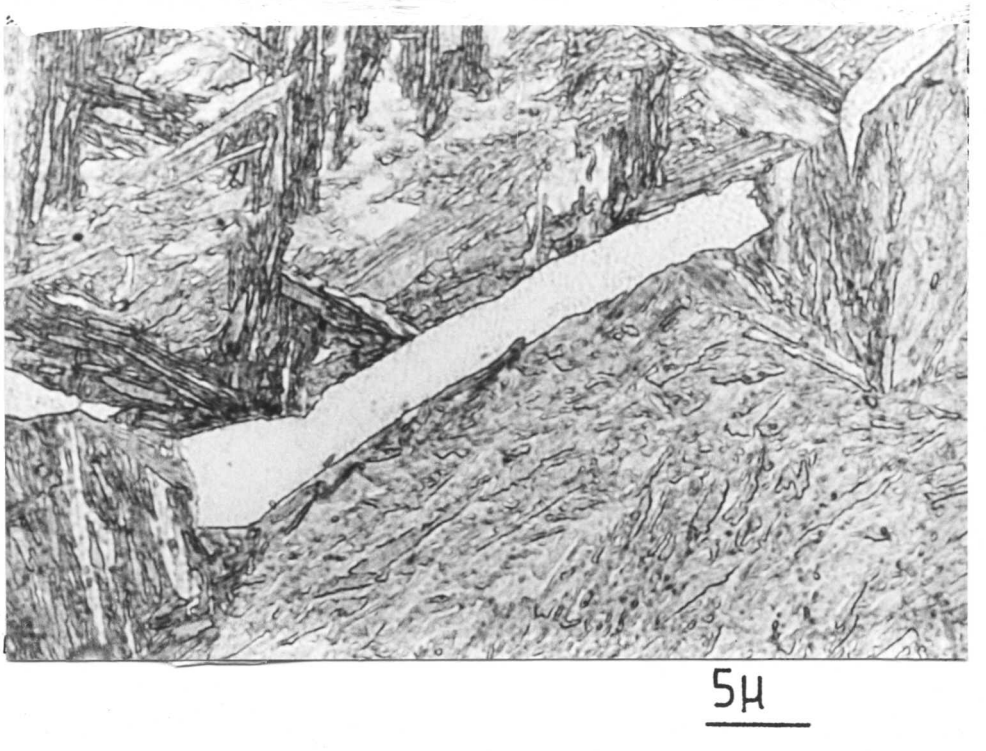

Figure 8.22: Showing facetted allotriomorphic ferrite. (650°C/40 sec).

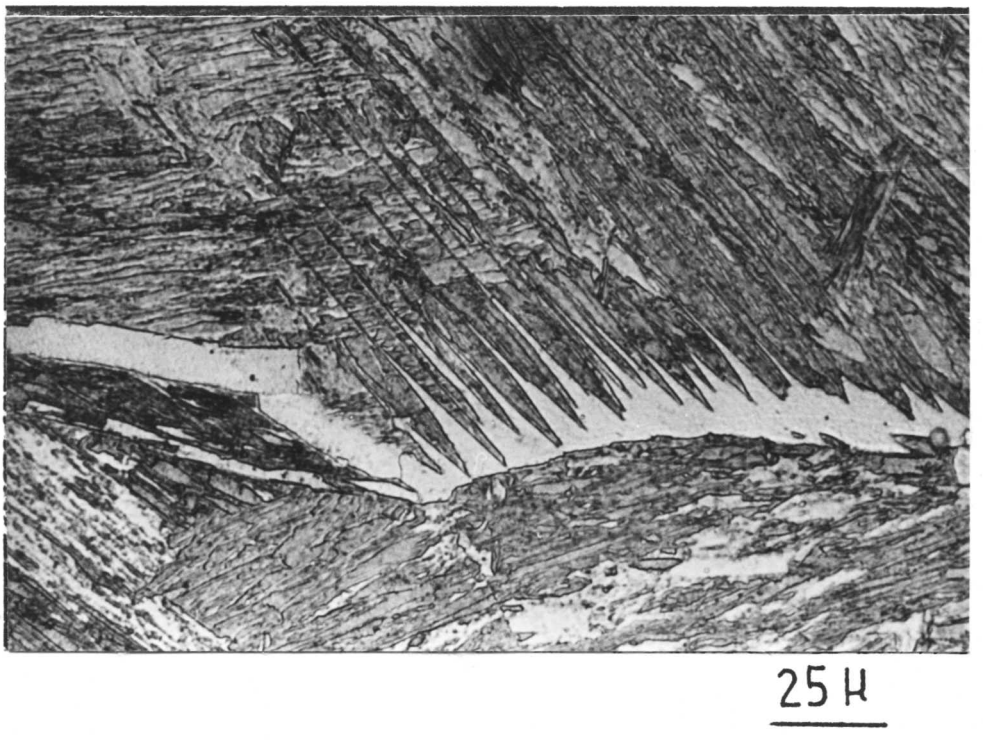

Figure 8.23: Formation of Widmanstätten along highly curved γ-grain-boundary. (650°C/40 sec).

Figure 8.24: Transmission electron micrograph showing carbide free facetted ferrite. (650°C/10 sec).

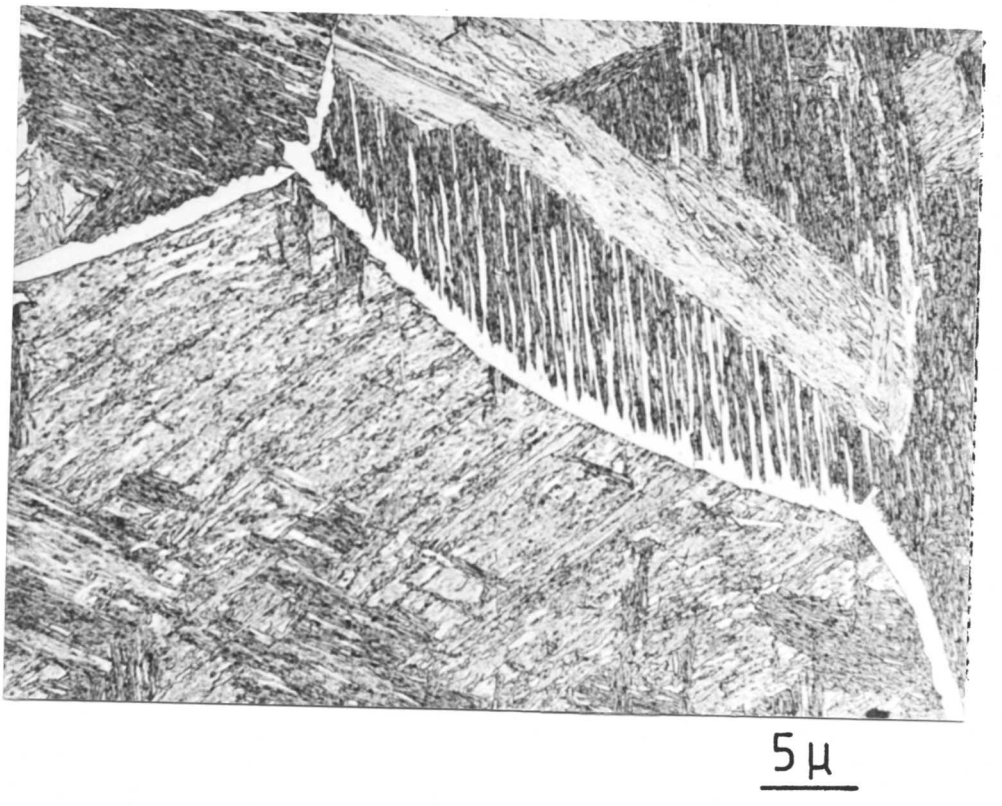

Figure 8.25: Formation of Widmanstätten ferrite along highly curved grain-boundaries. (610°C/60 sec).

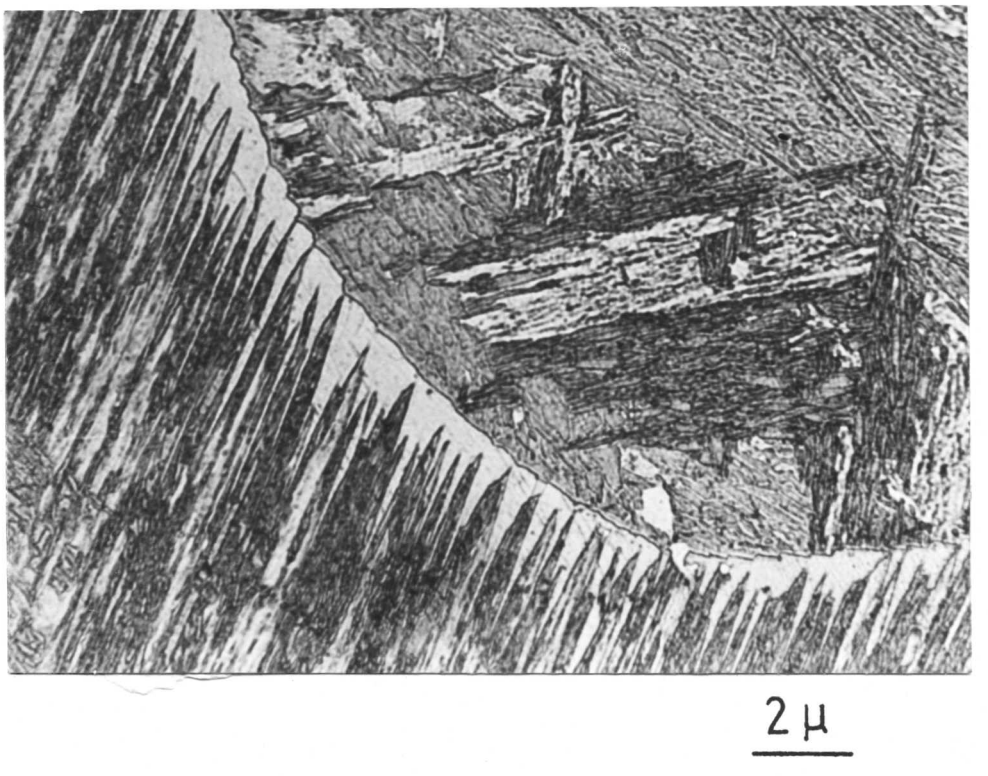

Figure 8.26: Formation of Widmanstätten ferrite along highly curved grain-boundaries. (650°C/50 sec).

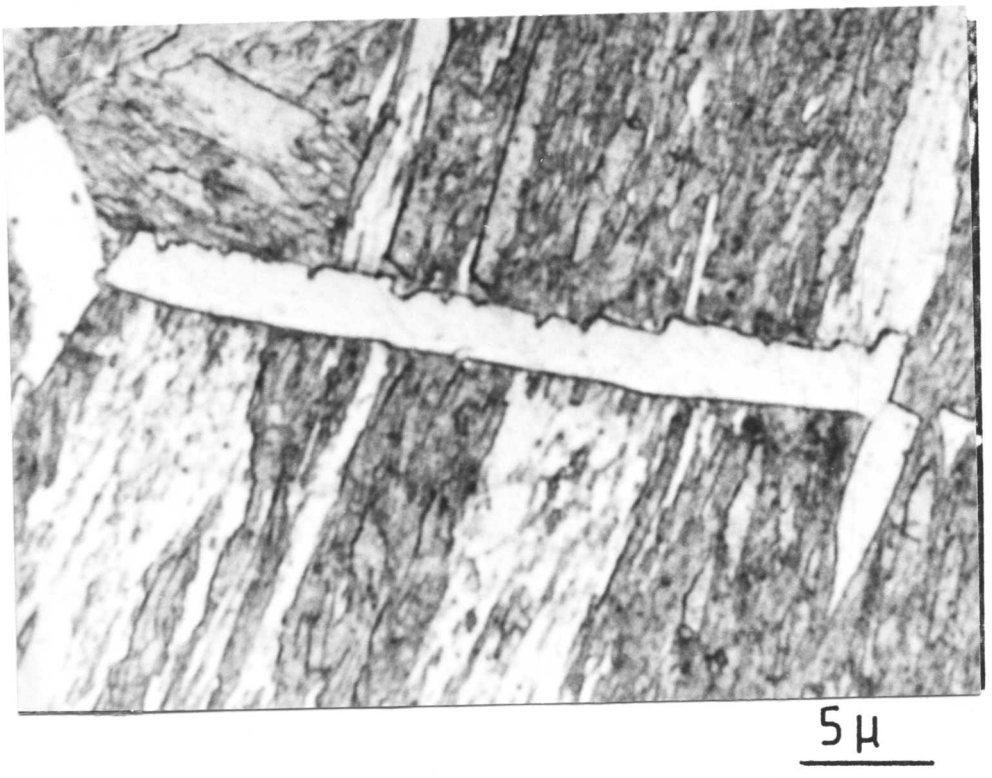

Figure 8.27: Showing evidence of interface pinning (610°C/50 sec).

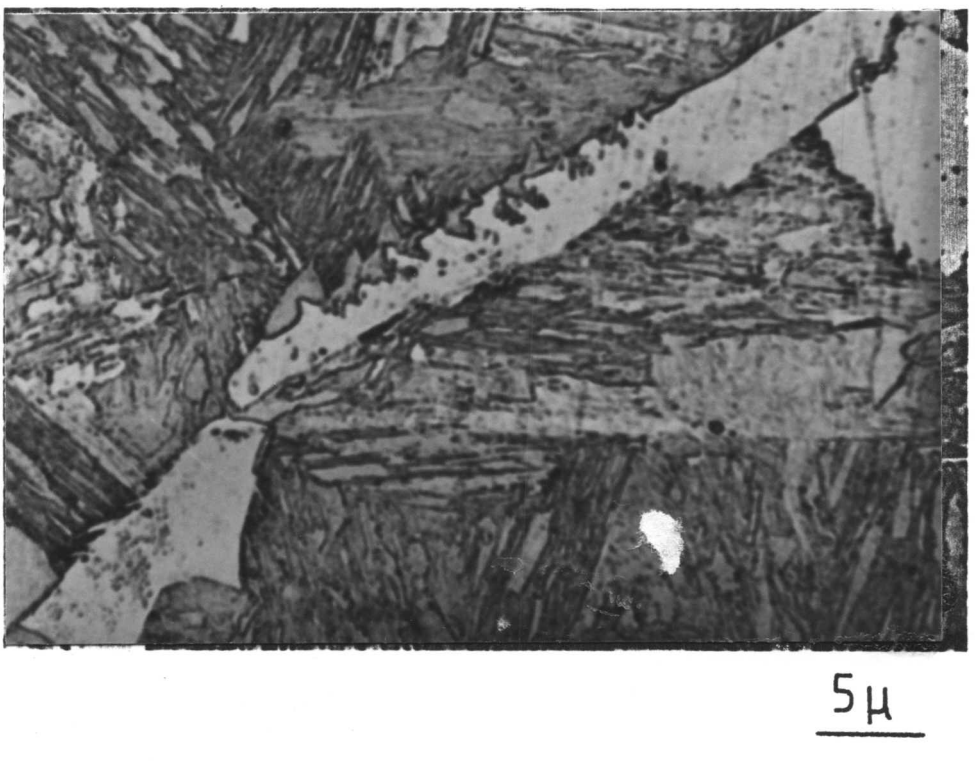

Figure 8.28: Showing evidence of interface pinning. (610°C/20 min).

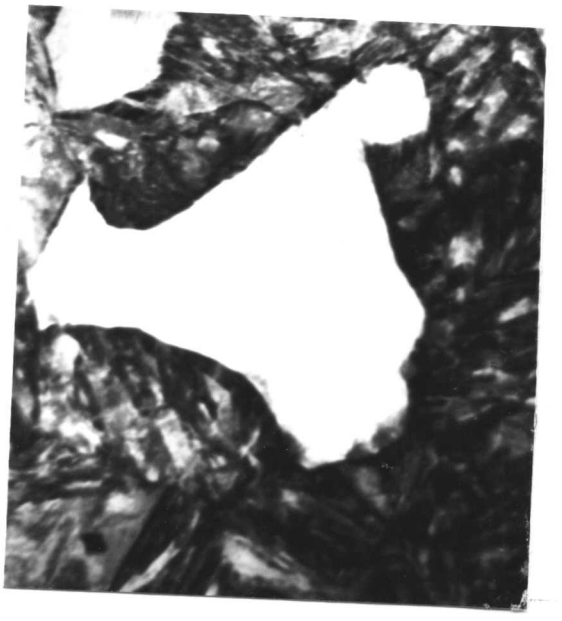

Figure 8.29: Carbide free ferrite formed during the early stages of transformation (610°C/15 sec).

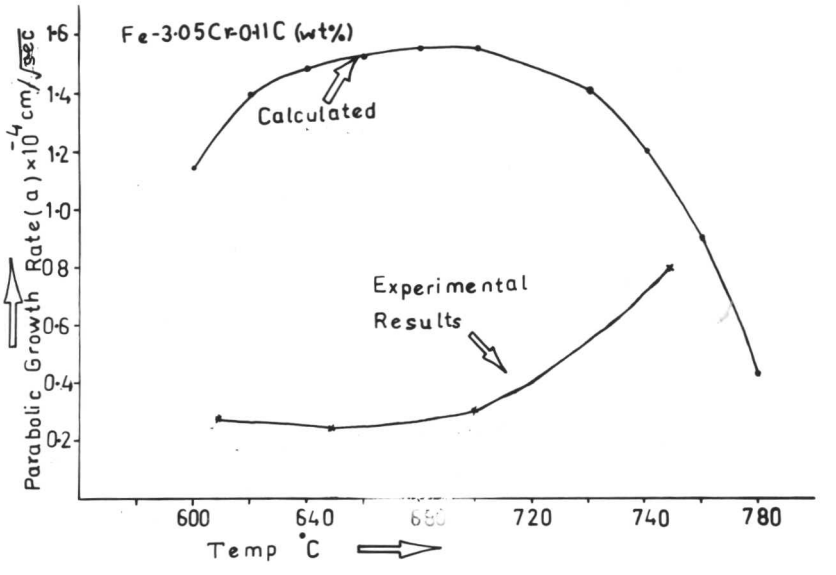

Figure 8.30: Plot of parabolic rate constant vrs temperature.

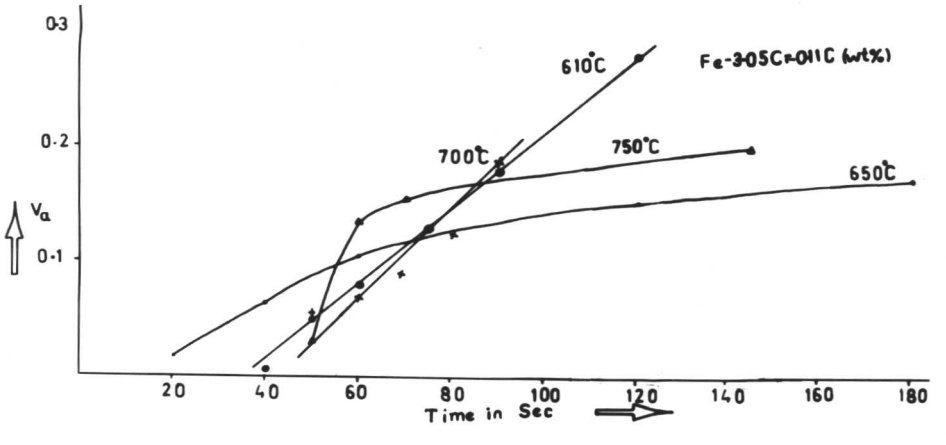

Figure 8.31: Plot of volume fraction vs temperature.